

1 **A Review of the Interactions between Tropical Cyclones and Environmental**
2 **Vertical Wind Shear**

3 Rosimar Rios-Berrios,^a Peter M. Finocchio^b, Joshua J. Alland^{c,d}, Xiaomin Chen^{e,f}, Michael S.
4 Fischer^{g,f}, Stephanie N. Stevenson^d, and Dandan Tao^h

5 ^a *National Center for Atmospheric Research, Boulder, Colorado*

6 ^b *Naval Research Laboratory, Monterey, California*

7 ^c *University Corporation for Atmospheric Research, Boulder, Colorado*

8 ^d *NOAA National Hurricane Center, Miami, Florida*

9 ^e *Department of Atmospheric and Earth Science, University of Alabama in Huntsville, Huntsville,*
10 *Alabama*

11 ^f *NOAA/OAR/Atlantic Oceanographic and Meteorological Laboratory, Miami, Florida*

12 ^g *Cooperative Institute For Marine And Atmospheric Studies, University of Miami, Miami, Florida*

13 ^h *Geophysical Institute, University of Bergen, Bergen, Norway*

14 *Corresponding author: Rosimar Rios-Berrios, rberrios@ucar.edu*

15 ABSTRACT: Tropical cyclone (TC) structure and intensity are strongly modulated by interactions
16 with deep-layer vertical wind shear (VWS)—the vector difference between horizontal winds at 200
17 and 850 hPa. This paper presents a comprehensive review of more than a century of research on
18 TC-VWS interactions. The literature broadly agrees that a TC vortex becomes vertically tilted,
19 precipitation organizes into a wavenumber-one asymmetric pattern, and thermal and kinematic
20 asymmetries emerge when a TC encounters an environmental sheared flow. However, these
21 responses depend on other factors, including the magnitude and direction of horizontal winds at
22 other vertical levels between 200 and 850 hPa, the amount and location of dry environmental air,
23 and the underlying sea-surface temperature. While early studies investigated how VWS weakens
24 TCs, an emerging line of research has focused on understanding how TCs intensify under moderate
25 and strong VWS (i.e., shear magnitudes greater than 5 m s^{-1}). Modeling and observational
26 studies have identified four pathways to intensification: vortex tilt reduction, vortex reformation,
27 axisymmetrization of precipitation, and outflow blocking. These pathways may not be uniquely
28 different because convection and vortex asymmetries are strongly coupled to each other. Besides
29 discussing these topics, this review presents open questions and recommendations for future
30 research on TC-VWS interactions.

31 **1. Background**

32 Meteorologists started to notice that the vertical profile of horizontal winds influences tropical
33 cyclone (TC) formation and intensification even before the advent of weather satellites. Based on
34 observations of different types of clouds, Weightman (1919) argued that deep easterlies through the
35 troposphere were conducive for the formation of the 1919 West India TC. This argument was also
36 supported by Riehl and Shafer (1944), who performed an analysis of balloon-based wind charts at
37 the Institute of Tropical Meteorology in Puerto Rico. They found that deep easterlies to the north
38 of tropical disturbances were most favorable for TC development, but that a vertical profile with
39 easterlies at the surface and westerlies at 14,000 ft (approximately 4.3 km) “prevented development
40 of strong rotating vortices” in the North Atlantic. Fifteen years later, Ramage (1959) analyzed
41 balloon-based wind charts and found that large changes in the horizontal winds with height also
42 prevented TC development over the South China Sea and the Bay of Bengal. These early studies
43 using cloud motions and sparse sounding observations provided some of the first evidence that
44 TCs are most likely to form where the horizontal winds have small variations with height.

45 As aircraft and satellite observations became available later in the 20th century, more detailed
46 studies were conducted to explore the effects of the wind profile on TC development and inten-
47 sification. Simpson and Riehl (1958) introduced the concept of “ventilation”, where dry air is
48 imported from the environment into the TC inner core by the vertically sheared flow. López (1968)
49 combined flight-level observations with satellite data to compare a disturbance that developed
50 into Hurricane Carla (1961) with a disturbance that did not develop into a TC. This comparison
51 showed that the disturbance that did not evolve into a TC was embedded in an environment with
52 stronger vertical wind shear (VWS) than the disturbance that later became Hurricane Carla (López
53 1968). This result was later generalized with composites of satellite observations of upper- and
54 lower-tropospheric winds for developing and non-developing disturbances around the world (Gray
55 1968). These composites showed that TC development occurred where the VWS was “a minimum
56 or zero” —a finding that was later supported by the composites of McBride and Zehr (1981). The
57 composite approach was also employed by Merrill (1988), except this study compared intensifying
58 and non-intensifying TCs. Consistent with previous studies, intensifying TCs were characterized
59 by weaker VWS than non-intensifying TCs.

60 Due to limited wind observations within the middle troposphere, Gray (1968) and others defined
61 VWS as the wind vector difference between 200 and 850 hPa. The shear calculated between these
62 two pressure levels is commonly referred to as the “deep-layer” VWS. In calculating the deep-layer
63 VWS around a TC, early studies such as Gray (1968) considered the full vector difference—that
64 is, including both the environment and the TC winds—between the observed winds at these two
65 levels. Gray (1968) and others did not account for the VWS that is induced by the TC itself given
66 that the strongest winds in TCs are located in the lower troposphere and that the winds turn from
67 cyclonic to anticyclonic with height. Subsequent studies developed various methods to estimate the
68 VWS primarily contributed by the environmental winds (e.g., Kurihara et al. 1993; DeMaria and
69 Kaplan 1994; Galarneau and Davis 2013; Wang et al. 2015). These methods have been re-evaluated
70 and challenged over the past decades due to limitations and uncertainties in their estimations of
71 *environmental* VWS (Velden and Sears 2014; Ryglicki et al. 2020; Dai et al. 2021; Ryglicki et al.
72 2021).

73 The strong influence of deep-layer VWS magnitude on TC intensity motivated the inclusion
74 of this variable in statistical models for intensity prediction. One of the first models to include
75 VWS was the Statistical Hurricane Intensity Prediction Scheme (SHIPS) model (DeMaria and
76 Kaplan 1994), in which deep-layer VWS magnitude was ranked as the second most important
77 predictor of TC intensity (only behind the maximum potential intensity). The deep-layer VWS
78 is a key predictor in more recent versions of the SHIPS model and other statistical models for
79 intensity prediction (DeMaria and Kaplan 1999; Emanuel et al. 2004; DeMaria et al. 2005). New
80 shear-related predictors quantifying shear in shallower layers have also been incorporated into these
81 models. Deep-layer VWS is routinely estimated from real-time satellite products (see, for example,
82 <https://tropic.ssec.wisc.edu/>), and it is one of the key variables routinely examined by
83 hurricane forecasters.

84 The important relationship between 200–850 hPa VWS and TC intensity has inspired a plethora
85 of studies since the 1990s aimed at understanding the effects of VWS on TC formation, intensity,
86 and structure. Jones (1995) and DeMaria (1996) were amongst the first studies to show that a TC
87 vortex is tilted in the presence of VWS. These studies, which relied on simple computer models of
88 TC-like vortices, also found that the tilted vortex resulted in asymmetric patterns of upward and
89 downward motions around the TC center. Several years later, observational studies confirmed these

90 findings by documenting that TCs under VWS exhibited enhanced precipitation in their downshear
91 quadrants, and suppressed precipitation in their upshear quadrants (Black et al. 2002; Corbosiero
92 and Molinari 2002; Chen et al. 2006; Cecil 2007; Hence and Houze 2011; Reasor et al. 2013;
93 DeHart et al. 2014). Detailed observations, including those taken during field campaigns, enabled
94 detailed case studies (Molinari et al. 2006; Shelton and Molinari 2009; Molinari and Vollaro 2010;
95 Stevenson et al. 2014; Bukunt and Barnes 2015; Rogers et al. 2015; Zawislak et al. 2016; Rogers
96 et al. 2016; Nguyen et al. 2017; Ryglicki et al. 2021; Wadler et al. 2021b; Alvey et al. 2022) and
97 multi-case composite analyses (Rogers et al. 2013; Reasor et al. 2013; DeHart et al. 2014; Wadler
98 et al. 2018; Fischer et al. 2022) of TC-VWS interactions. The recent theoretical and modeling
99 developments of the concept of “ventilation”, which was originally coined by Simpson and Riehl
100 (1958), has led to further advancement in our understanding of the thermodynamic impacts of
101 VWS on TC structure and intensity (Tang and Emanuel 2010; Riemer et al. 2010). While much
102 of the focus of early work on TC-VWS interactions centered around how TCs weakened under the
103 influence of VWS, a new line of research has emerged focusing on how certain TCs can intensify
104 while interacting with moderate-to-strong shear.

105 This review article provides a comprehensive summary of the scientific literature on TC-VWS¹
106 interactions and their effects on TC structure and intensity changes. While other review articles
107 have broadly summarized the existing knowledge about TCs (Emanuel 2003; Wang and Wu 2004;
108 Smith and Montgomery 2015; Montgomery and Smith 2017; Emanuel 2018), those articles only
109 provide brief discussions about TC-VWS interactions owing to their broad scope. Their limited
110 discussions together with a more than doubling of peer-reviewed manuscripts on the topic during
111 the last decade motivated this synthesis solely focused on TC-VWS interactions. Recent advances
112 in modeling and analysis techniques, including artificial intelligence/machine learning, and the
113 proliferation of novel observing platforms offer several new avenues for research on sheared TCs.
114 By summarizing the rapidly growing body of research and identifying key knowledge gaps, this
115 review can serve as a starting point for future research utilizing new tools, techniques, and datasets
116 to better understand and predict sheared TCs.

117 We begin our review by discussing how VWS, both by itself and in combination with other
118 environmental factors, influences TC structure and intensity (Sections 2 and 3). This discussion
119 sets the stage for a review of knowledge about how TCs can intensify—sometimes rapidly—under

¹Hereafter, the acronym “VWS” will refer to deep-layer (200–850 hPa) *environmental* shear of the horizontal wind.

120 moderate-to-strong VWS (Section 4). The intricate multi-scale nature of processes associated
121 with TC-VWS interactions challenge their prediction, and we summarize the work on this topic
122 in Section 5. Lastly, we present our conclusions, open questions, and recommendations for future
123 research in Section 6.

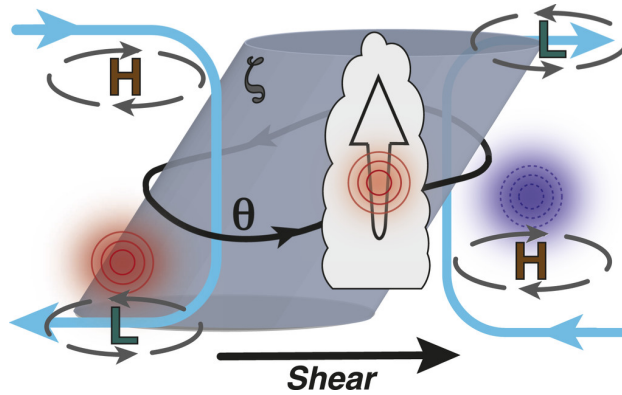
124 **2. Effects of VWS on TC Structure and Intensity**

125 A central focus of TC research is understanding how a storm responds to both external and
126 internal factors (Emanuel 2018). The literature on TC-VWS interactions offers plenty of evidence
127 that VWS is one of the most influential external factors of TC structure. This section will describe
128 the main effects of VWS on TC structure and how those effects can modulate TC intensity changes
129 under environmental sheared flow.

130 *a. Vortex tilt*

141 If a TC is represented by a column of potential vorticity, a vertically sheared flow will differentially
142 advect the vortex column. This process results in a vertically tilted vortex as illustrated in Fig. 1.
143 The earliest work on TC vortex tilt focused on dry dynamics. Jones (1995) was amongst the first
144 to document in detail the dynamics of vortex tilt using dry, adiabatic, and nonhydrostatic models.
145 Her seminal work showed that vortex tilt magnitude is largely dependent on VWS magnitude and
146 on properties of the TC vortex (e.g., size, strength, etc.). The dynamics of vortex tilt evolution
147 have been described by two different paradigms: (1) potential vorticity anomalies and (2) vortex
148 Rossby waves.

149 The first paradigm relies on “potential vorticity” thinking to describe how the winds associated
150 with the tilted vortex modulate both the direction and magnitude of vortex tilt (Jones 1995, 2000a,b).
151 In this view, the winds associated with an upper-tropospheric vorticity anomaly due to the tilted
152 vortex can advect the lower-tropospheric vorticity anomaly and vice versa (Jones 1995). Provided
153 the environmental vertical wind shear is not strong enough to irreversibly shear apart the TC (e.g.,
154 Smith et al. 2000; Reasor et al. 2004), the upper and lower portions of a tilted vortex will begin
155 to co-rotate, or precess, cyclonically about one another (Jones 1995; Wang and Holland 1996;
156 Jones 2000a; Reasor and Montgomery 2001; Reasor et al. 2004). In a quiescent environment, the
157 upper and lower portions of the tilted TC vortex may continue to orbit around one another multiple



131 FIG. 1. Summary schematic of the kinematic and thermodynamic structure of Hurricane Rita (2005). The
 132 gray cylinder represents the vortex tower of the eyewall, which is tilted by the environmental wind shear (black
 133 vector). Green “L” symbols and vectors denote cyclonic low pressure anomalies, and brown “H” symbols denote
 134 anticyclonic high pressure anomalies. Thermal anomalies are denoted by blue (cold) and red (warm) circles and
 135 shading associated with slanted isentropic surfaces. Blue arrows show the modified secondary circulation. The
 136 thick black contour denotes a representative potential temperature surface, with arrows illustrating the cyclonic
 137 vortex flow around the eyewall. In the downshear-right quadrant, air parcels move cyclonically downstream and
 138 adiabatically upward along the potential temperature surface resulting in individual convective motions denoted
 139 by the cumulus cloud and upward arrow. A warm anomaly is shown in the convective cloud to denote the release
 140 of latent heat associated with the buoyant updraft. From Fig. 15 in Boehm and Bell (2021).

158 times; however, in the presence of a sheared background flow, dry idealized modeling studies have
 159 discovered a preferred tilt orientation along—and to the left of—the VWS vector (Jones 1995;
 160 Wang and Holland 1996; Reasor et al. 2004). When the vortex tilt is directed downshear-left,
 161 the projection of the cyclonic flow associated with the storm’s lower-tropospheric circulation onto
 162 the displaced mid–upper-tropospheric circulation acts to oppose the environmental vertical wind
 163 shear, which can halt the cyclonic precession of the vortex. This process can also lead to vortex tilt
 164 reduction, which will be discussed in detail in Section 4a.

165 The second paradigm describes vortex tilt evolution as being governed by vortex Rossby waves
 166 (Reasor and Montgomery 2001; Schechter et al. 2002; Schechter and Montgomery 2003; Reasor
 167 et al. 2004; Reasor and Montgomery 2015). These waves, which are excited by a tilted vortex
 168 under VWS, are analogous to midlatitude Rossby waves except their restoring mechanism is the
 169 radial vorticity gradient of the TC vortex. By examining a tilted quasigeostrophic vortex in a dry

170 model, Reasor and Montgomery (2001) found the evolution of vortex tilt was consistent with the
171 projection of the tilted vortex onto a near-discrete VRW, or “quasi mode”, which is similar to an
172 edge wave propagating on a Rankine vortex. In this paradigm, the evolution of vortex tilt is largely
173 described by the azimuthal propagation and, as will be discussed in more detail in Section 4a,
174 inviscid damping of the discrete vortex Rossby waves that are excited by shear.

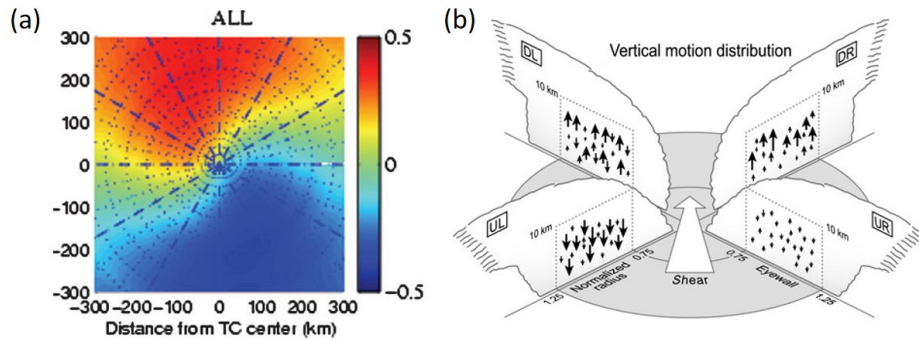
175 In a balanced framework, tilted TC vortices are associated with thermal and convective asym-
176 metries (Jones 1995; DeMaria 1996; Jones 2000a; Xu and Wang 2013; Boehm and Bell 2021), as
177 reflected by the schematic in Fig. 1. More specifically, a cold anomaly is found in the downtilt
178 region of the storm, whereas a warm anomaly is located within the up-tilt portion (Jones 2000a).
179 Observations of tilted, mature TCs corroborate this balanced thermal state (Reasor and Eastin 2012;
180 Boehm and Bell 2021). The structure of a tilted TC vortex also varies vertically, as the direction
181 of vortex tilt and the corresponding vorticity and temperature anomalies rotate anticyclonically
182 with height (Jones 2000a; Reasor and Eastin 2012; Boehm and Bell 2021). These tilt-induced
183 thermal asymmetries impact the TC convective structure, as will be discussed in more detail in
184 the following subsection. As air travels cyclonically around the TC vortex, adiabatic ascent is
185 promoted along upward-slanted isentropes located to the right-of-tilt direction; however, observa-
186 tions indicate convectively-driven diabatic heating maximizes in the downtilt portion of the inner
187 core (Reasor and Eastin 2012; Reasor et al. 2013; Boehm and Bell 2021). The location of peak
188 ascent may be influenced by other factors, such as diabatic lifting, microphysics processes, and
189 frictional convergence (e.g., Frank and Ritchie 2001; Didlake and Kumjian 2018; Feng and Bell
190 2019; Laurencin et al. 2020; Schechter 2022). Additionally, the magnitude of the asymmetric ascent
191 depends on the TC vortex strength, VWS magnitude, amongst other factors (Jones 2000a; Xu and
192 Wang 2013; Finocchio and Rios-Berrios 2021).

193 If a TC is not strong enough to be characterized by a column of potential vorticity, the effects
194 of VWS on the vortex structure differ from those discussed above. Consider, for example, a weak
195 tropical storm. The vortex structure is most likely shallow in comparison to the vortex of a major
196 hurricane (Fischer et al. 2022). The extent to which VWS can “tilt” such a shallow vortex is
197 unclear from the existing literature. Instead, idealized numerical simulations and airborne radar
198 observations suggest that tropical storms and other weak TCs under VWS exhibit displaced centers
199 of circulations in the middle and lower troposphere (Nugent and Rios-Berrios 2018; Rios-Berrios

200 et al. 2018; Ryglicki et al. 2018b; Rogers et al. 2020; Schecter and Menelaou 2020; Chen, X.
201 et al. 2021; Schecter 2022; Fischer et al. 2022). Convective anomalies and their associated outflow
202 co-evolve with the tilted vortex, as demonstrated in satellite observations (Ryglicki et al. 2018a,
203 2019) and idealized simulations (Rios-Berrios et al. 2018; Ryglicki et al. 2018b; Schecter 2022).
204 The corresponding thermodynamic response includes both warm anomalies above the surface
205 circulation and cool anomalies below the middle tropospheric circulation (Tao and Zhang 2019).
206 Vertical motions respond more strongly to buoyant accelerations underneath the midtropospheric
207 vortex (Ryglicki et al. 2018b) and to frictional convergence (Schecter 2020, 2022) than to the
208 adiabatic ascent and descent induced by the temperature anomalies. Consequently, the evolution
209 of vortex misalignment in weak vortices is largely governed by the influences of diabatic processes
210 (Kwon and Frank 2008; Hogsett and Stewart 2013; Nguyen and Molinari 2015; Rios-Berrios et al.
211 2018; Ryglicki et al. 2018b; Tao and Zhang 2019; Rogers et al. 2020; Schecter and Menelaou 2020;
212 Schecter 2022; Stone et al. 2023). However, the literature on vortex tilt of weak TCs is limited,
213 and this is an area of much needed research.

214 *b. Asymmetric precipitation*

215 The asymmetric pattern of vertical motions that results from VWS tilting a mature TC vortex
216 influences the distribution of precipitation around the storm center. Moderate-to-strong VWS (i.e.,
217 magnitudes exceeding 2.5 m s^{-1}) can produce a distinct wavenumber-one precipitation asymmetry,
218 with most precipitation occurring downshear and the maximum precipitation in the inner core
219 located downshear left (Fig. 2a). This relationship is consistent across many observational (e.g.,
220 Corbosiero and Molinari 2002; Chen et al. 2006; Wingo and Cecil 2010; Pei and Jiang 2018;
221 Stevenson et al. 2016) and modeling (e.g., Rogers et al. 2003; Braun et al. 2006) studies using a
222 variety of metrics for measuring convective intensity. The downshear-left quadrant corresponds
223 to the previously-described preferential tilt orientation. Convective initiation is favored within the
224 downshear-right quadrant (Fig. 2b), but the inner-core precipitation maximum occurs downwind
225 in the downshear-left quadrant due to a combination of strong ascent and azimuthal advection of
226 hydrometeors (Hence and Houze 2011; Reasor et al. 2013; DeHart et al. 2014). In the outer region
227 of mature TCs known to contain the outer rainbands, convection is maximized downshear right
228 due to the adiabatic ascent induced by the vortex tilt (Corbosiero and Molinari 2002; Stevenson



231 FIG. 2. (a) Fraction of the wavenumber-1 asymmetry of rainfall rates normalized by the azimuthal mean value
 232 (shading) relative to the 200–850-hPa environmental VWS, with the shear vector pointing to the top [adapted
 233 from Fig. 4a in Chen et al. (2006)]. (b) Schematic of the vertical motion distribution in a sheared environment.
 234 The environmental shear vector is denoted by the white arrow, and quadrants are labeled according to their
 235 direction relative to the shear vector (DR: downshear right, DL: downshear left, UL: upshear left, UR: upshear
 236 right) [adapted from Fig. 15a in DeHart et al. (2014)].

229 et al. 2016). This region exhibits a persistent and nearly stationary region of precipitation, known
 230 as the stationary band complex (Willoughby et al. 1984; Riemer 2016).

237 Asymmetric convection within the downshear-left quadrant of weak-to-moderately sheared TCs
 238 provides a focal point for the formation of concentric eyewalls that can lead to eyewall replacement
 239 cycles (Wang and Tan 2022). Using airborne Doppler radar observations in Hurricane Earl (2010),
 240 Didlake et al. (2018) showed that a descending air stream, originating in the asymmetric stratiform
 241 precipitation, enhanced the boundary-layer convergence outside the eyewall and eventually led to
 242 the formation of a secondary eyewall.

243 While shear is frequently the dominant factor in causing azimuthal precipitation asymmetries
 244 in TCs (Chen et al. 2006), Stevenson et al. (2016) found that rainfall asymmetries were more
 245 closely tied to the storm motion vector for fast-moving TCs. Those TCs exhibited an upshear
 246 lightning maximum, suggesting that shear alone could not explain their convective asymmetries.
 247 Other factors—including frictional convergence, orographic lifting, and the TC circulation—also
 248 contribute to TC rainfall production and organization (Lonfat et al. 2004, 2007; Lu et al. 2018).
 249 Additional research is needed to understand the relative importance of each factor.

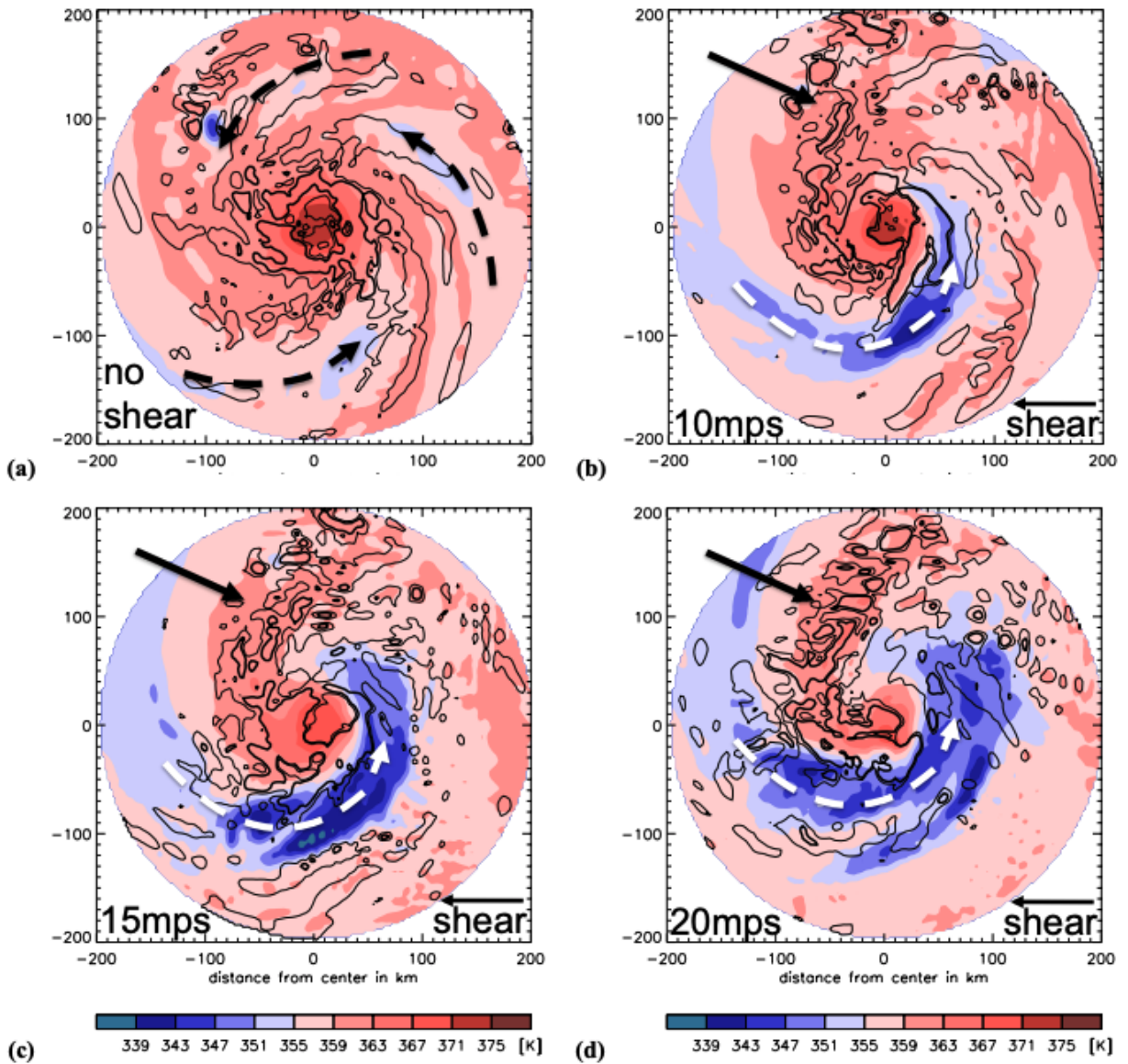
250 *c. Ventilation*

251 VWS can also impact the thermodynamic and convective TC structure through ventilation—or
252 simply, the transport of low-equivalent potential temperature (θ_e) air into the TC inner core.
253 Ventilation occurs through either vertical fluxes of low- θ_e air in downdrafts, radial fluxes of low- θ_e
254 air from the environment, or a combination of both mechanisms. The literature has traditionally
255 labeled ventilation pathways based on their vertical position (i.e., low-level, mid-level, and upper-
256 level ventilation). However, in this review, we adopt the terms downdraft and radial ventilation to
257 establish a clear relationship to the physical mechanism responsible for transporting low- θ_e air into
258 the inner TC circulation (Alland et al. 2021a,b). We recognize that these processes are not fully
259 independent of each other and they can both co-exist at a given time (Riemer et al. 2010).

260 1) DOWNDRAFT VENTILATION

269 Downdraft ventilation refers to downward transport of low- θ_e air. Riemer et al. (2010) identified
270 downdraft ventilation in low to mid levels as being associated with the shear-induced, wavenumber-
271 one precipitation asymmetry and the stationary band complex described in Willoughby et al. (1984).
272 As precipitation from convection downshear is transported cyclonically left-of-shear and upshear,
273 it evaporates into the unsaturated air below to develop downdrafts. The evaporatively-cooled
274 downdraft air within the subcloud layer is generally transported radially outward upshear, which
275 can limit the areal extent of convection there, and radially inward right-of-shear (Riemer et al.
276 2010, 2013; Shu et al. 2014; Molinari et al. 2013; Alland et al. 2021a, see Fig. 4a). The magnitude
277 of downdraft ventilation and the extent to which it limits TC development generally increases as
278 the magnitude of VWS increases, as shown in Fig. 3.

279 The extent to which downdraft ventilation affects TC structure and intensity is sensitive to the
280 ability of surface fluxes to recover the θ_e . The term recovery in this context refers to the process by
281 which enthalpy fluxes from the sea surface fully increase the θ_e of evaporatively-cooled downdraft
282 air in the subcloud layer. In many cases, air parcels are unable to fully recover from the effects
283 of downdraft ventilation (e.g., Riemer et al. (2010)), which makes the boundary layer upshear
284 dynamically (i.e., radial outflow) and thermodynamically (i.e., lower θ_e) less favorable for deep
285 convection. As such, downdraft ventilation tends to suppress convection in the upshear quadrants
286 – the same part of the TC where balanced downward motions (i.e., another form of downdraft



261 FIG. 3. Boundary layer θ_e (color, averaged over the lowest 1 km), and upward motion (thin contour: 0.2 ms^{-1} ,
 262 thick contour: 1 ms^{-1} , averaged between 1.25 and 2 km height) at 5 h. The center of the TC averaged over the
 263 lowest 2 km is in the middle of the domain. The no_shear case is depicted in (a), the 10 ms^{-1} , 15 ms^{-1} , and
 264 20 ms^{-1} case in (b), (c), and (d), respectively. The shear direction is indicated in the lower right corner of each
 265 plot. Solid arrows highlight the quasi-stationary convective asymmetry outside of the eyewall in the shear cases
 266 and dashed white arrows the quasi-stationary region of depressed BL θ_e air. The dashed black arrows indicate
 267 transient bands of less-reduced θ_e values in the no_shear case. The depicted times are representative for the early
 268 part of the experiments. [adapted from Fig. 7 in Riemer et al. (2010)].

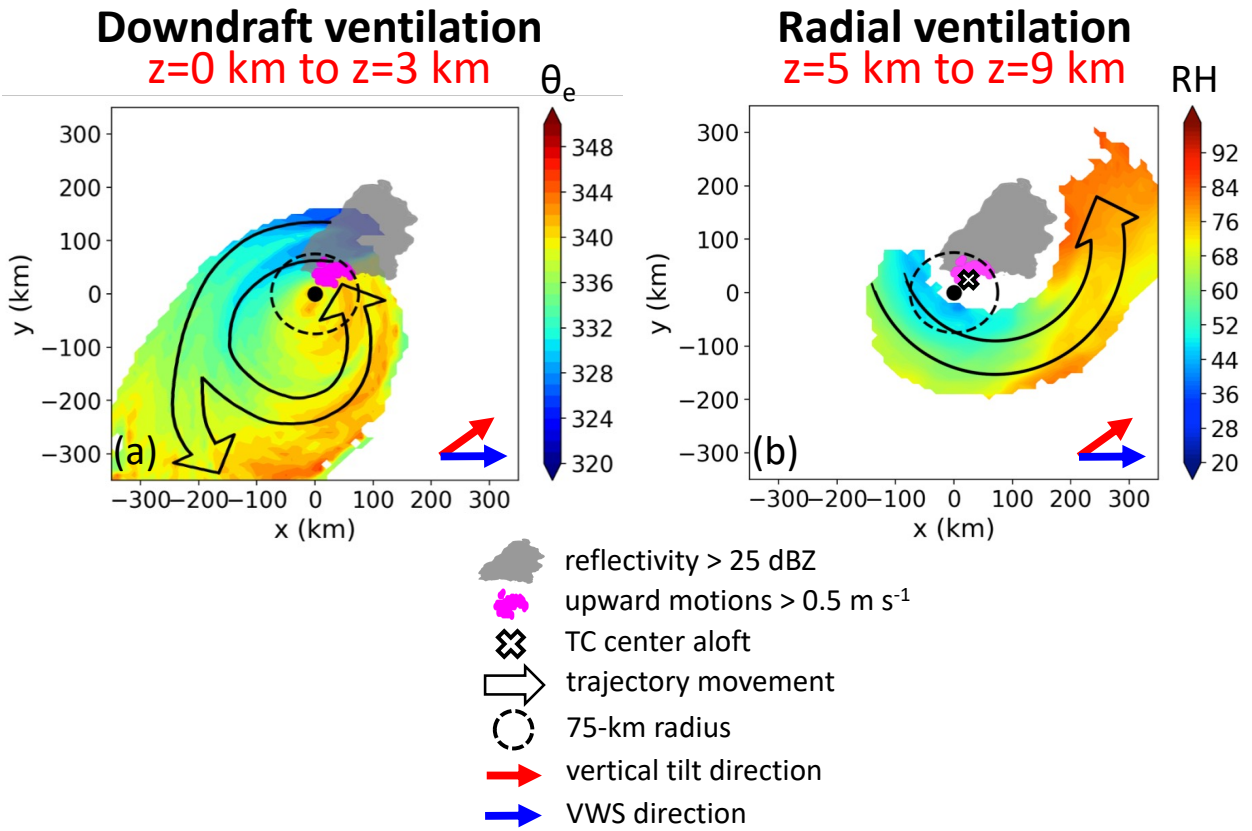
287 ventilation) act to suppress convection in a tilted vortex (Jones 1995; DeMaria 1996; Zawislak
288 et al. 2016). Entrainment of this relatively low- θ_e air into eyewall updrafts downshear can result
289 in shallower convection, less latent heating, a hydrostatic pressure rise in the eye, and reduced TC
290 intensity (Riemer et al. 2013; Riemer and Laliberté 2015; Zhang and Rogers 2019).

291 In contrast to a lack of recovery, several studies provide evidence of enhanced surface fluxes
292 counteracting the debilitating effects of downdraft ventilation, allowing for a complete recovery of
293 low- θ_e air upon entry into eyewall updrafts (Tang and Emanuel 2012a; Tao and Zhang 2014; Juračić
294 and Raymond 2016; Gao et al. 2017; Nguyen et al. 2019; Chen, X. et al. 2021; Alland and Davis
295 2022). The likelihood of recovery increases for warmer SST environments (Chen, X. et al. 2021),
296 air that is closer to the sea surface (Wadler et al. 2021a), and more intense TCs (Finocchio and
297 Rios-Berrios 2021). For early-stage storms that have not yet formed an eyewall, downdraft-cooled
298 parcels that recover can ascend in the left-of-shear quadrants, develop into deep convection at
299 the leading edge (i.e., cyclonically downwind) of a tilt-related convective precipitation shield, and
300 contribute to eyewall formation (Chen, X. et al. 2021).

301 2) RADIAL VENTILATION

315 Simpson and Riehl (1958) were the first, to the authors' knowledge, to document radial ventilation.
316 Radial ventilation refers to the horizontal transport of low- θ_e air from the surrounding environment
317 into the TC inner core by storm-relative radial inflow, horizontal eddy fluxes, or both (discussed
318 further in the following two paragraphs). This can result in the reduced areal extent of convection
319 in the inner core and acts as a constraint on the TC heat engine (Bender 1997; Shelton and Molinari
320 2009; Munsell et al. 2013; Shu et al. 2014; Nguyen et al. 2017; Alland et al. 2021a; Alland and
321 Davis 2022).

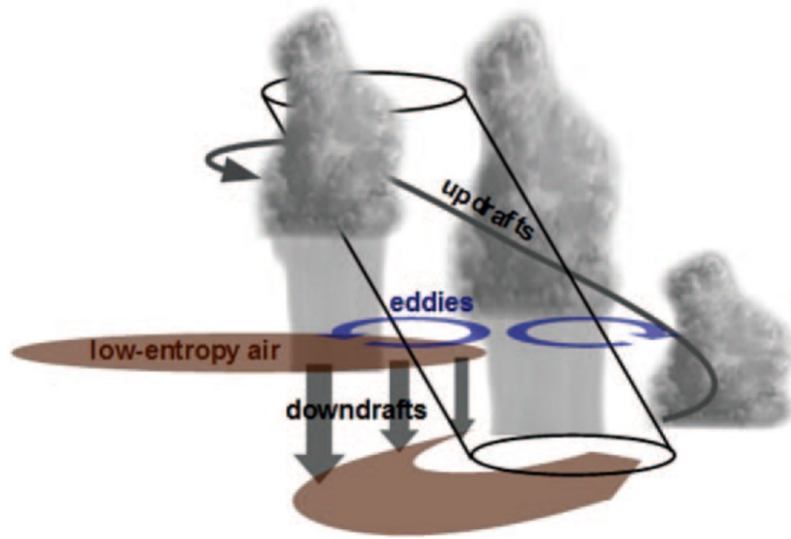
322 Radial ventilation can occur in the mid and upper troposphere via storm-relative inflow associated
323 with the superposition of a tilted TC circulation in a vertically-sheared background flow (Simpson
324 and Riehl 1958; Willoughby et al. 1984; Marks et al. 1992; Bender 1997; Cram et al. 2007; Shelton
325 and Molinari 2009; Davis and Ahijevych 2012; Nguyen et al. 2017; Alland et al. 2021b; Fischer
326 et al. 2023a, see Fig. 4b). Radial inflow maximizes upshear and right-of-shear (Corbosiero and
327 Molinari 2003; Reasor et al. 2013; DeHart et al. 2014), which can transport low- θ_e air into the TC
328 inner core. If the radial ventilation occurs in upper levels where the TC warm anomaly is generally



302 FIG. 4. Conceptual diagrams of ventilation pathways showing, in shading, the (a) average equivalent potential
 303 temperature (K) of trajectories initialized in downdraft ventilation regions between heights of 0 and 3 km, and
 304 (b) average RH (%) of trajectories initialized in radial ventilation regions between heights of 5 and 9 km. Other
 305 information includes reflectivity greater than 25 dBZ (gray shading), upward motions greater than 0.5 m s^{-1}
 306 (magenta dots), the TC center averaged between heights of 5 and 9 km (white x), parcel movement (black arrows),
 307 the inner 75 km (dashed circle), the vertical tilt direction from the surface to 6 km (red arrow), and the VWS
 308 direction (blue arrow). [Adapted from Fig. 17 of Alland et al. (2021a) and Fig. 13 of Alland et al. (2021b).]

329 most prominent, it has been hypothesized to result in a top-down weakening of the TC by inducing
 330 a hydrostatic increase in the surface pressure, a decrease in troposphere-mean diabatic heating, and
 331 a weakening of the mean secondary circulation (Gray 1968; Frank and Ritchie 2001; Kwon and
 332 Frank 2008; Fu et al. 2019).

333 Radial ventilation in midlevels can also be associated with shear-induced eddies that are excited in
 334 response to a TC's vertical tilt (e.g., Cram et al. 2007; Tang and Emanuel 2010, 2012a). This venti-
 335 lation pathway, which is shown conceptually in Fig. 5 along with the downdraft ventilation pathway



309 FIG. 5. A conceptual illustration of a TC undergoing two types of ventilation. Radial ventilation is depicted
 310 as horizontal eddies (blue arrows) that transport low-entropy air from the environment into eyewall convection
 311 of the tilted vortex. Downdraft ventilation is depicted by gray arrows labeled “downdrafts”, which are the result
 312 of precipitation falling from the asymmetric convection in the tilted TC into subsaturated air below. Regions of
 313 low-entropy air in the mid-levels and in the subcloud layer are denoted by brown shading. [Figure adapted from
 314 Fig. 1 in Tang and Emanuel (2012a).

336 described above, locally decreases θ_e within the upward branch of the secondary circulation. In
 337 axisymmetric models of TCs with parameterized radial ventilation, this type of radial ventilation is
 338 capable of weakening TCs in environments that, by all other measures, favor intensification (Tang
 339 and Emanuel 2010, 2012b).

340 The extent to which radial and downdraft ventilation in the mid levels disrupts a TC depends not
 341 only on the magnitude of VWS, but also on the environmental humidity. A TC is more likely to
 342 resist ventilation if the air being transported from the surrounding environment into the inner core
 343 has higher θ_e (Tang and Emanuel 2010; Alland et al. 2021a,b). Tang and Emanuel (2012b) created
 344 a ventilation index that combines environmental VWS, the entropy deficit of the surrounding mid-
 345 level environment, the air-sea vapor pressure deficit, and the potential intensity. This index is able
 346 to distinguish environments that are favorable for developing versus non-developing TCs. Larger
 347 and more intense TCs are also more resilient to radial ventilation because the stronger and more

348 expansive tangential wind field increases the inertial stability of the vortex and thereby prevents
349 radial intrusions of air parcels from the surrounding environment with relatively lower θ_e into the
350 inner-core (Riemer and Montgomery 2011; Finocchio and Rios-Berrios 2021).

351 Radial and downdraft ventilation can work together to affect TC structure and intensity. In the
352 middle and upper troposphere, dry air from radial ventilation (Fischer et al. 2023a), as well as
353 convergence of storm-relative inflow with the TC's upper-tropospheric outflow upshear (Dai et al.
354 2021), can result in troposphere-deep subsidence (i.e., downdraft ventilation). These combined
355 ventilation pathways dry and stabilize the upshear TC inner core. In the lower and middle
356 troposphere, descending radial inflow from rainband activity can flush lower- θ_e air into the subcloud
357 layer, reduce the areal extent of convection in the inner core, and limit TC development (Barnes
358 et al. 1983; Powell 1990; Hince and Houze 2008; Didlake and Houze 2009, 2013), (see Fig. 4a).

359 3) RELATIVE IMPORTANCE OF VENTILATION PATHWAYS

360 The relative importance of the downdraft and radial ventilation pathways in modulating a TC's
361 convective structure and intensity remains an open question with contrasting views in the literature,
362 and may be case-dependent. Alland et al. (2021a) showed in idealized simulations that downdraft
363 and radial ventilation can operate at the same time, while Alland and Davis (2022) showed in
364 simulations of Hurricane Michael (2018) that downdraft ventilation preceded radial ventilation
365 in limiting TC development. Riemer et al. (2010) and Riemer and Laliberté (2015) suggested
366 that downdraft ventilation at low levels may be more destructive to TC development than radial
367 ventilation above the boundary layer because downdraft ventilation directly impacts the energy
368 cycle of a TC in the subcloud layer where convection initiates. In addition, the inflowing air in
369 the mid and upper troposphere associated with radial ventilation may be deflected by the TC's
370 swirling winds, effectively limiting its destructive potential (Willoughby et al. 1984; Riemer and
371 Montgomery 2011). For weaker TCs, though, this deflection may be less prominent, resulting in
372 stronger interaction between the environment and the inner core (Alland et al. 2021b; Finocchio
373 and Rios-Berrios 2021). Tang and Emanuel (2012a) suggested that radial ventilation is less
374 effective at interfering with the development of a TC when it occurs primarily in the upper levels
375 because radial gradients of θ_e are smaller in the upper troposphere than in the lower and middle
376 troposphere. However, Fu et al. (2019) showed that radial ventilation aloft can be particularly

377 effective at weakening already intense TCs due to the combination of a well-developed warm core
378 and stronger storm-relative flows in the upper levels compared to in the mid and low levels.

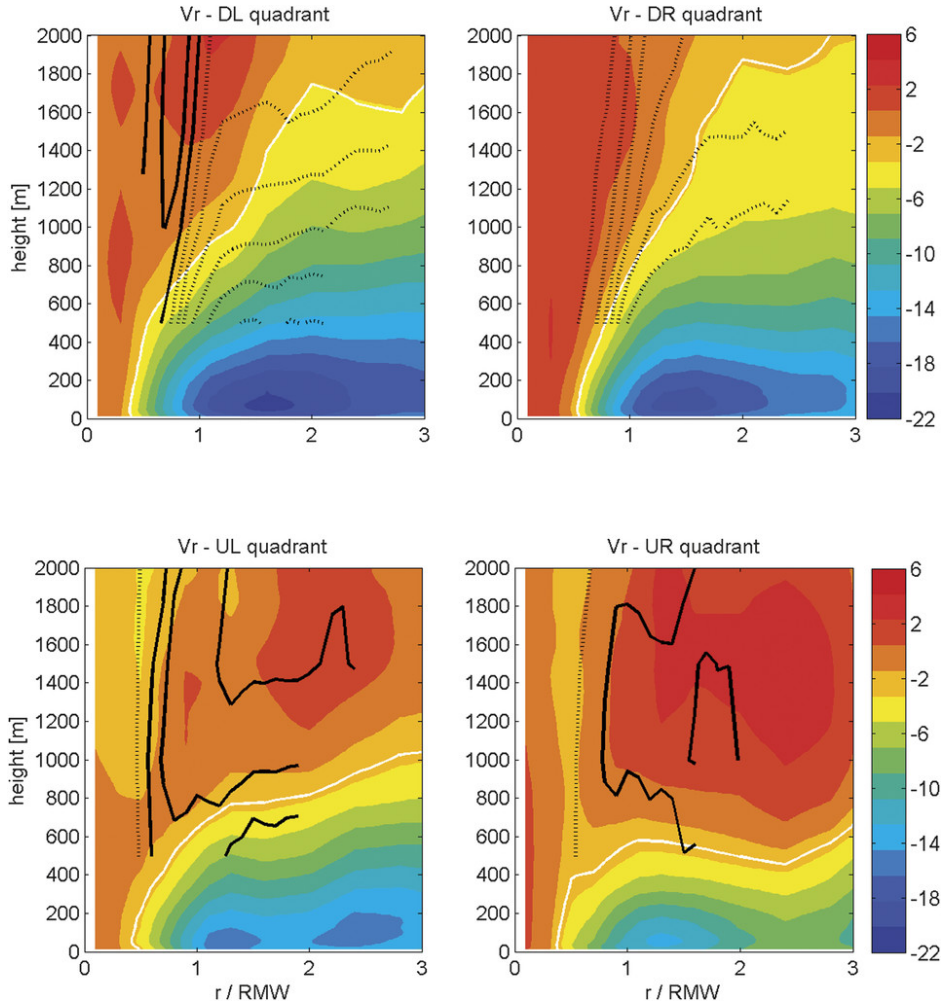
379 The importance and timing of ventilation pathway(s), or the ability of a TC's resiliency to venti-
380 lation, are likely dependent on the storm conditions (e.g., the size and intensity), and environmental
381 conditions (e.g., the vertical and radial locations of the dry air and VWS) (Finocchio and Rios-
382 Berrios 2021). Despite our improved understanding of ventilation, more research is still needed
383 to better understand why ventilation negatively affects some TCs and has only a limited effect on
384 others.

385 *d. Boundary layer asymmetries*

386 Deep-layer VWS also introduces distinct thermodynamic and kinematic asymmetries within the
387 TC boundary layer. As a consequence of the aforementioned effects of downdraft ventilation
388 and subsequent boundary layer recovery, θ_e is generally lowest in the left-of-shear quadrant and
389 highest in the downshear-right quadrant (e.g., Riemer et al. 2010; Zhang et al. 2013; Nguyen et al.
390 2017; Chen, X. et al. 2019; Alland et al. 2021a). The downdraft-modified boundary layer parcels
391 enhance surface enthalpy fluxes left of shear, enabling a subsequent boundary layer recovery of
392 these low- θ_e parcels. Thus, a wavenumber-one asymmetry in the azimuthal distribution of θ_e and
393 surface enthalpy fluxes has been observed in sheared TCs (Zhang et al. 2013; Nguyen et al. 2019).

394 The amplitude of the wavenumber-one asymmetry in boundary-layer θ_e is related to factors other
395 than just the magnitude of VWS (Riemer et al. 2010; Nguyen et al. 2019; Wadler et al. 2022). A
396 composite analysis of dropsondes collected in relatively weak TCs showed that TCs with higher
397 intensification rates have larger values of surface enthalpy fluxes in the upshear quadrants compared
398 to the downshear quadrants (Nguyen et al. 2019). TCs in environments with a southerly component
399 of VWS have also been found to have a larger wavenumber-one asymmetry in boundary-layer θ_e
400 outside of the radius of maximum winds than TCs in environments with a northerly component
401 of VWS (Wadler et al. 2022). This asymmetry likely results from the superposition of
402 large-scale advection of θ_e on the shear-induced θ_e asymmetries.

408 For the kinematic boundary layer structure, both observational and modeling studies (Zhang et al.
409 2013; Gu et al. 2016; Zhang et al. 2023) indicate that the boundary-layer height, either represented
410 by inflow layer depth or the height of maximum tangential wind, tends to increase with radius in



403 FIG. 6. Dropsonde composites of the relative radial wind velocity (shaded, every 2 m s^{-1}) as a function of
 404 altitude and the normalized radius to the storm center for the four quadrants relative to the shear direction. The
 405 white line in each panel represents the height of 10% peak inflow. Doppler radar composite results are shown in
 406 the black lines with solid lines representing outflow and dotted lines representing inflow with a contour interval
 407 of 0.5 m s^{-1} . Adapted from Fig. 4 of Zhang et al. (2013).

411 each shear-relative quadrant. The boundary-layer inflow is strongest and deepest in the downshear
 412 quadrants (Fig. 6), which is aligned with the location of the downshear convergence zone. However,
 413 the strongest tangential winds are located to the left of shear (Zhang et al. 2013; Rogers et al. 2015;
 414 Gu et al. 2016). Thermodynamically, the boundary-layer inflow is an ideal conduit to bring low- θ_e
 415 parcels into the inner-core convection (Section 2c and Ahern et al. (2021)). However, the inflow
 416 also can accelerate the tangential wind in the downshear-left quadrant through the inward advection

417 of absolute angular momentum and immediately downwind through azimuthal advection, while
418 the tangential winds in the right-of-shear quadrants steadily weaken. In fact, Gu et al. (2016) found
419 that during the initial weakening stage of modeled TCs in VWS, the left-of-shear tangential winds
420 can continue to intensify for a few hours while the tangential winds to the right of shear decay.

421 Given that the TC boundary layer is relatively under sampled with in-situ observations, more
422 research is needed to understand the shear-induced asymmetries within that layer. The limited
423 evidence discussed herein suggests that VWS induces both thermal and kinematic boundary-layer
424 asymmetries. Those asymmetries can have important implications by, for example, determining
425 the location of maximum near-surface winds. Their effects on turbulent aspects that affect mixing
426 and updraft development should also be investigated.

427 **3. Compound Effects of VWS and Other Factors on TC Structure and Intensity**

428 While many studies have isolated the effects of VWS *magnitude* on TC structure and intensity, that
429 metric alone cannot fully capture the myriad ways in which a TC responds to a given environment.
430 Additional external factors—including details of the environmental wind profile, the relative
431 direction of surface flow with respect to the shear direction, environmental moisture, and underlying
432 SSTs—also influence vortex and precipitation asymmetries that emerge under VWS. This section
433 discusses interactions between VWS magnitude and those factors with the goal of exposing the
434 complex nature of TC-VWS interactions.

435 *a. Details of the wind profile*

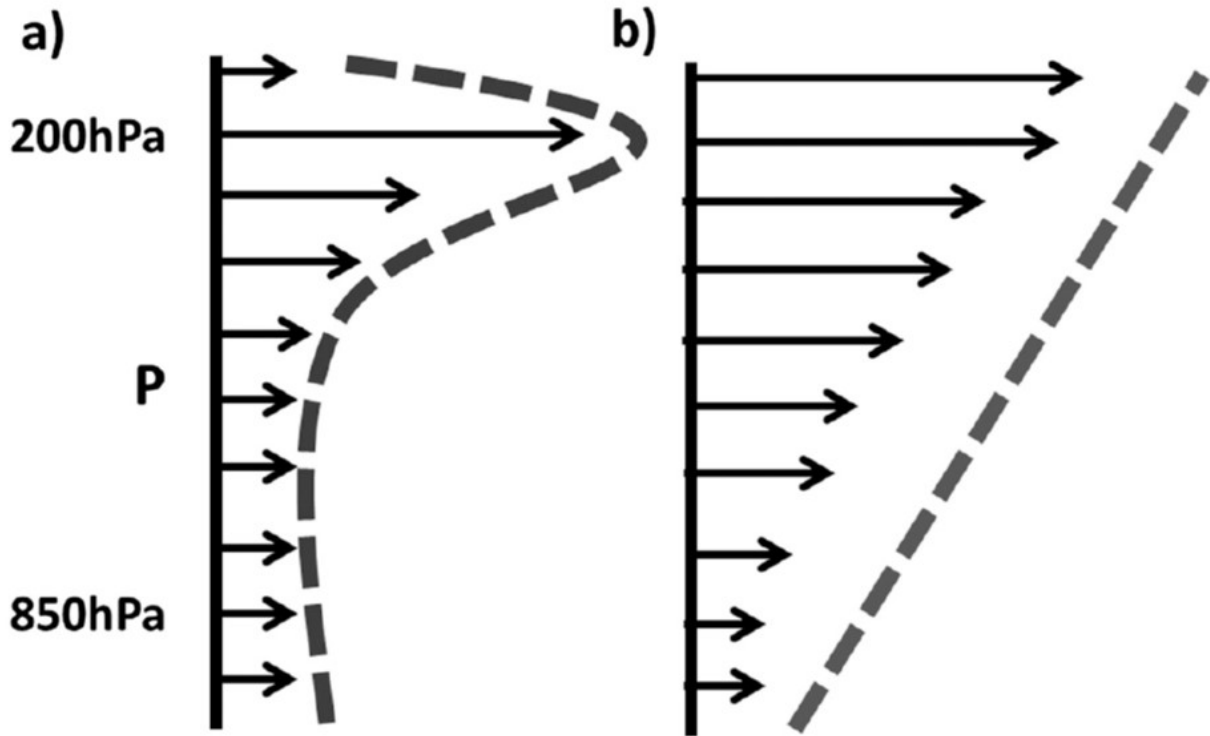
436 The magnitude of the deep-layer VWS is often the only metric used to characterize how favorable
437 an environmental wind profile is for TC intensification. Historically, this was due to a paucity of
438 real-time satellite-derived atmospheric motion vectors in the middle troposphere, which hindered
439 operational estimates of shear in layers other than 200-850 hPa (Velden and Sears 2014). However,
440 details of the environmental wind profile beyond the deep-layer shear magnitude can have a strong
441 influence on TC structure and intensity.

442 Studies primarily focused on TC genesis have explored whether the impacts of VWS on devel-
443 oping disturbances depend on the shear direction. Tuleya and Kurihara (1981) found that easterly
444 shear was more favorable for genesis than westerly shear of the same magnitude, which they ar-

445 gued was due to easterly shear allowing for greater coupling between the upper and lower parts
446 of westward-propagating disturbances within the deep tropics. The intrinsic northwesterly beta
447 shear of the TC vortex partially offsets easterly environmental shear, which could also explain why
448 easterly shear has been found to be less destructive to a TC than the same magnitude of westerly
449 shear (Ritchie and Frank 2007). Statistical studies based on large samples of cyclogenesis and
450 post-genesis TC cases are mostly consistent with the result that easterly shear is more favorable
451 for genesis and intensification than westerly shear (Zeng et al. 2010; Nolan and McGauley 2012).
452 However, in idealized simulations on the beta plane that isolate the impact of shear direction from
453 factors such as maximum potential intensity, Nolan and McGauley (2012) found westerly shear
454 was actually more favorable for genesis than easterly shear. This suggests that easterly shear only
455 appears to be more favorable for TC genesis because it tends to occur in regions where other en-
456 vironmental factors such as SST are also favorable. The shear direction sensitivity may also differ
457 for genesis cases compared to more developed TCs. Wei et al. (2018) found that, for post-genesis
458 TCs in the Western North Pacific, westerly shear was more strongly correlated with short-term
459 weakening than easterly shear after controlling for SST.

466 The vertical distribution of shear through the troposphere can also influence TC development.
467 Elsberry and Jeffries (1996) described two hypothetical wind profiles with the same deep-layer
468 shear: one with all of the shear concentrated in the upper troposphere (Fig. 7a), and the other with
469 shear linearly distributed through the depth of the troposphere (Fig. 7b). They hypothesized that
470 the upper-level shear profile is more favorable for TC development because the TC outflow can
471 counteract upper-level shear, while more deeply distributed shear is more likely to tilt and ventilate
472 the TC inner core. Ryglicki et al. (2018a) usefully pointed out that TC environments with deeply-
473 distributed shear (as in Fig. 7a) tend to be associated with upper-level troughs, while environments
474 with upper-level shear (as in Fig. 7b) tend to be associated with upper-level anticyclones.

475 A consensus has yet to emerge on whether upper or lower-level shear is more favorable for TC
476 intensification. Finocchio et al. (2016) conducted idealized simulations exposing weak, symmetric
477 vortices to environmental wind profiles with 10 m s^{-1} of westerly VWS maximized at different
478 heights and extending through different depths of the troposphere. They found that shear concen-
479 trated lower in the troposphere was more destructive to a developing TC than upper-level shear
480 because it tilted the vortices further downshear and caused stronger downward fluxes of low- θ_e air



460 FIG. 7. Schematics of two vertical wind profiles typical of environmental flow regimes that impinge on TCs,
 461 but which provide identical 200–850 hPa wind shear values as traditionally calculated. These two profiles arise
 462 from a (a) low-latitude systems with the strongest upper-tropospheric winds concentrated in a shallow layer and
 463 (b) linearly distributed wind profile over a deep layer as might exist poleward of the deep tropics and associated
 464 with transient midlatitude troughs. Adapted from Fig. 1 in Velden and Sears (2014), and reproduced from Fig.
 465 11 in Elsberry and Jeffries (1996).

481 into the TC boundary layer from convective downdrafts. These findings are consistent with earlier
 482 (Frank and Ritchie 1999) and subsequent (Ryglicki et al. 2018b) modeling studies that involved
 483 experiments exposing developing TCs to different vertical distributions of VWS.

484 In contrast to these studies, Xu and Wang (2013) and Fu et al. (2019) exposed mature hurricanes
 485 to different wind profiles with 10 m s^{-1} of easterly VWS and found that simulated TCs in upper-level
 486 shear weakened more and exhibited stronger inner-core asymmetries than the TCs in lower-level
 487 shear. Fu et al. (2019) attributed the greater weakening in upper-level shear to stronger upper-level
 488 ventilation of the warm core. They hypothesized that upper-level shear is less destructive to the
 489 weak TCs examined in previous modeling studies because the weaker storms are too shallow to

490 be exposed to the strongest storm-relative flows aloft (e.g., Nam and Bell 2021). However, more
491 research is needed to understand the different responses to upper- versus lower-level shear and how
492 they might relate to shear direction and aspects of the TC vortex.

493 Statistical analyses of real sheared TCs have generally found that low-level shear is more com-
494 monly associated with weakening than upper-level shear (Zeng et al. 2010; Wang et al. 2015).
495 However, Finocchio and Majumdar (2017b) did not find a clear relationship between TC intensity
496 change and their metrics describing the vertical distribution of VWS. These contradictory findings
497 could be due to differences in the metrics used to define the VWS height and/or the geographic
498 focus areas among the different statistical studies. The vertical distribution of VWS may also have
499 a larger and more consistent impact on the intensity of developing disturbances and weak TCs
500 compared to the more developed storms considered in these studies. More detailed statistical and
501 observational analysis of weak and developing storms is needed to better understand the apparent
502 disagreements regarding the impacts of different VWS profiles on TC intensity change.

503 Different multi-directional shear flows can also have distinct impacts on TC intensity and struc-
504 ture. In the mid-latitudes, environments with winds that rotate clockwise with altitude (positive
505 helicity) favor stronger and longer-lived convective updrafts (Davies-Jones et al. 1990). Positive
506 TC-relative environmental helicity is also more favorable for TC intensification. Nolan (2011) and
507 Onderlinde and Nolan (2014) used idealized simulations of TCs in horizontally uniform environ-
508 ments with a mean wind vector that rotates either clockwise (positive helicity) or counterclockwise
509 (negative helicity) with increasing altitude. Both studies found the clockwise-rotating wind profile
510 (positive helicity) resulted in more TC intensification, despite all experiments having the same
511 deep-layer VWS magnitude.

512 Onderlinde and Nolan (2016) reasoned that positive helicity is more favorable for TCs than neg-
513 ative helicity because, in their simulations, air parcels ingested into downshear convective updrafts
514 experienced more warming and moistening via surface enthalpy fluxes in positive helicity environ-
515 ments. However, Gu et al. (2018) demonstrated that balanced (dry) dynamics alone can explain
516 why positive helicity is more favorable for TC development: a clockwise-rotating environmental
517 wind profile advects the lower part of the vortex azimuthally downwind of the overall vortex tilt
518 vector, resulting in a superposition of positive local helicity and balanced ascent associated with
519 the tilted vortex. This configuration promotes the propagation of convection toward the upshear

520 quadrants. In identical experiments but with active moist physics, diabatic heating in convection
521 keeps the moist vortices more vertically coupled than in the corresponding dry simulations (Gu
522 et al. 2019). Moreover, the favorable configuration of vortex tilt and convection established early in
523 the experiments sets up a positive feedback with diabatic heating in convection that allows for the
524 faster upshear precession of vortices in positive-helicity environments. In other words, favorable
525 dry dynamics set the stage for subsequent convective feedbacks that hasten vortex alignment in
526 multi-directional shear environments with positive helicity. Collectively, these model-based results
527 suggest that, with all else being equal, TCs in negative helicity environments are more likely to
528 remain misaligned than TCs in unidirectional shear or positive helicity environments.

529 *b. Surface flow*

530 The surface flow in the TC environment modulates the TC intensity and structural response
531 to VWS by influencing the horizontal distribution of boundary layer convergence and surface
532 enthalpy fluxes. The distribution of low-level convergence around a TC partly determines where
533 the stationary rainband complex forms (Willoughby et al. 1984; Riemer 2016), while the surface
534 enthalpy fluxes determine the extent of thermodynamic recovery of downdraft air parcels in the
535 TC boundary layer (Powell 1990). Riemer and Montgomery (2011) also demonstrated how storm-
536 relative surface flow distorts the circulation in the lower levels of a TC, determining the extent to
537 which environmental air is able to reach the inner core.

538 Only recently have the combined effects of low-level flow and VWS on TC structure and intensity
539 been explored systematically. Rappin and Nolan (2012) showed that surface flow counter-aligned
540 with the shear vector is more favorable for TC genesis than surface flow aligned with the shear
541 vector. In the counter-aligned scenario, the superposition of the vortex circulation and the surface
542 wind results in a surface wind maximum to the left of the shear vector, which increases surface
543 enthalpy fluxes ahead of the asymmetric convective complex. This favors the upshear propagation
544 of asymmetric convection, leading to a more rapid reduction in vortex tilt.

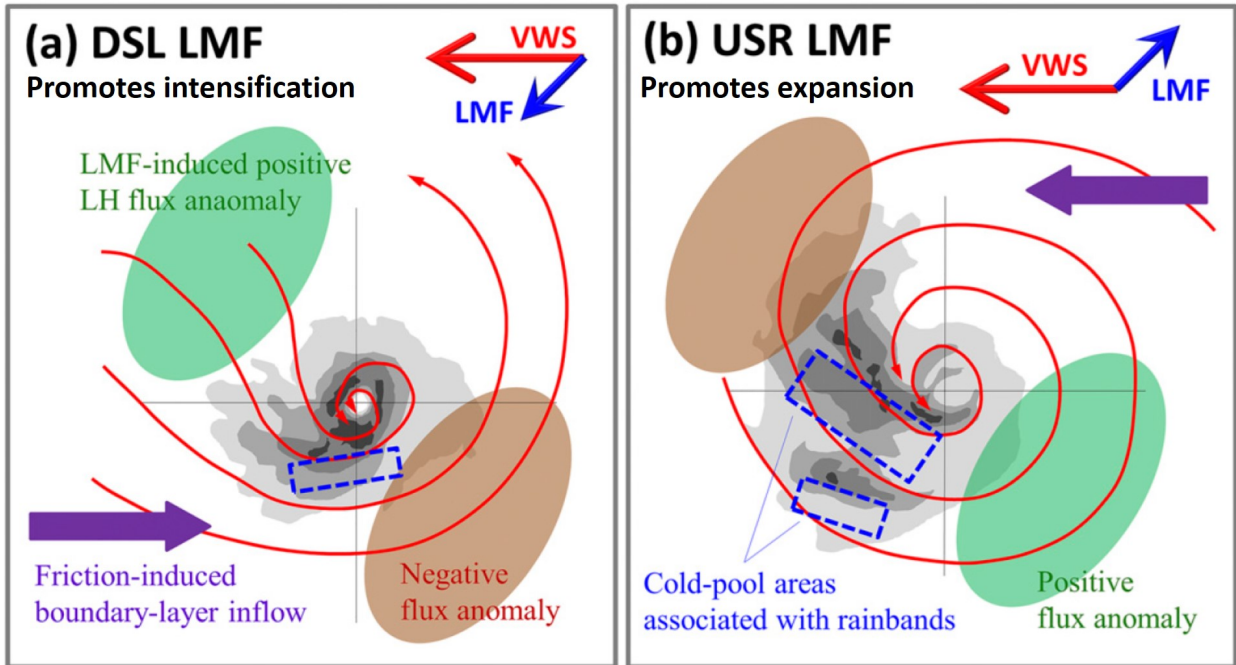
545 Chen, B.-F. et al. (2018) examined a wide array of low-level flow orientations relative to the
546 deep-layer shear vector using analysis and observational composites of post-genesis TC cases.
547 They found low-level flow directed toward the right of shear favors expansion of the 34-kt wind
548 radius, while low-level flow directed toward the left of shear favors intensification. They conducted

549 idealized simulations to explore the reasons for this result and found that low-level flow pointing
550 toward the upshear-right quadrant favors wind-field expansion because of enhanced rainband
551 activity (Chen, B.-F. et al. (2019), Fig. 8b). The opposite orientation of the low-level flow relative
552 to the shear vector increases the mean low-level inflow downshear and the humidity of air parcels
553 ingested into inner-core convection. This promotes intensification through the earlier development
554 of a symmetric eyewall (Fig. 8a). Similar to Rappin and Nolan (2012), upshear-oriented low-level
555 flow generally favored intensification more than downshear low-level flow in the Chen, B.-F. et al.
556 (2019) study, but only in their simulations over a warmer prescribed SST. However, comparisons
557 between these two studies is complicated by the fact that Rappin and Nolan (2012) conducted their
558 simulations in radiative-convective equilibrium environments, where warmer SST results in higher
559 saturation deficits that must be overcome in order for genesis to occur. In a follow-up analysis of
560 real TC cases, Chen, B.-F. et al. (2021) showed that TC intensification is favored in environments
561 with low-level flow directed toward the downshear-left quadrant regardless of the background SST,
562 deep-layer shear magnitude, or environmental humidity.

563 Lee et al. (2021) conducted similar simulations to Chen, B.-F. et al. (2019), except they imposed
564 the shear and the different low-level flows on more mature TCs. They found that for these more
565 intense storms, the low-level flow associated with the fastest intensification is directed upshear-
566 left (c.f. downshear-left in Chen, B.-F. et al. (2019)). This low-level flow orientation results in
567 surface fluxes maximized downshear, which invigorates upshear-left convection and promotes a
568 more symmetric diabatic heating structure.

573 *c. Environmental moisture*

574 The tropics generally have a minimum in θ_e near 700 hPa (Jordan 1958; Ooyama 1969; Dunion
575 2011). As such, moistening of the lower and middle troposphere is necessary for the development
576 and sustenance of deep convection within the TC vortex (Gray 1968; Emanuel 1989; Bister and
577 Emanuel 1997; Nolan 2007; Raymond et al. 1998; Rappin et al. 2010; Komaromi 2013; Zawislak
578 and Zipser 2014; Helms and Hart 2015; Rios-Berrios et al. 2016b). In idealized simulations
579 of weak TCs in environments with no VWS, Braun et al. (2012) showed that a layer of dry air
580 between 850 and 600 hPa could only limit TC intensification when it was initialized very close
581 to the storm center. Dry air can only weaken a TC if it is able to penetrate into the inner core



569 FIG. 8. Conceptual models showing the responses of a Northern Hemisphere TC to (a) downshear-left (DSL)
 570 low-level mean flow (LMF) and (b) upshear-right (USR) LMF. Gray shading indicates radar reflectivity. Red
 571 streamlines represent the boundary layer trajectories in a shear-relative coordinate system. Adapted from Fig. 1
 572 of Chen, B.-F. et al. (2021).

582 to reduce the upward vertical mass flux and convergence of angular momentum in the subcloud
 583 layer (Montgomery and Smith 2014; Tang and Zhang 2016; Alland et al. 2017). If dry air does not
 584 penetrate into the inner core, it can still reduce convection outside the moist region (Tao and Zhang
 585 2014), which can reduce the radial extent of the moist envelope and leave a TC more vulnerable to
 586 subsequent dry air intrusions (Kimball 2006; Hill and Lackmann 2009; Braun et al. 2012).

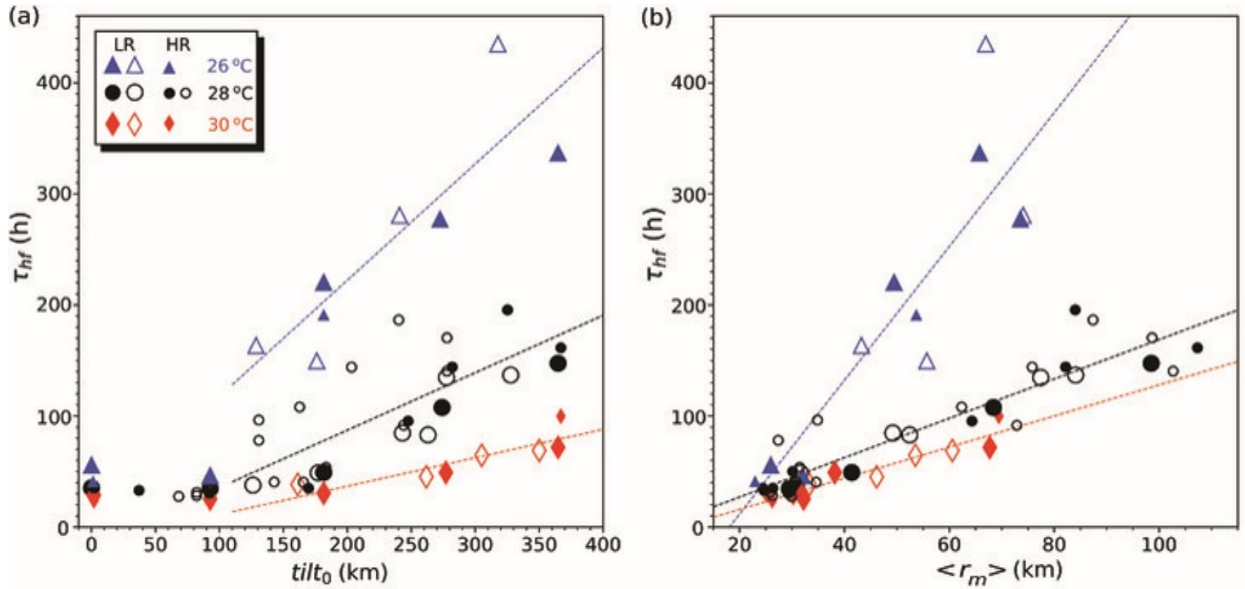
587 The combination of VWS and dry air around a vortex can be particularly effective at limiting
 588 TC intensification of weak TCs (Tang and Emanuel 2012a; Molinari et al. 2013; Tao and Zhang
 589 2014; Rios-Berrios et al. 2016a,b; Rios-Berrios and Torn 2017; Nguyen et al. 2017, 2019; Alland
 590 et al. 2021a). For example, Molinari et al. (2013) analyzed observations of a tropical storm under
 591 strong VWS ($11\text{--}15\text{ m s}^{-1}$) and exceptionally dry air (15% relative humidity). The tropical storm
 592 remained fairly asymmetric and weak, which Molinari et al. (2013) hypothesized was a result of
 593 radial and downdraft ventilation through the combination of strong VWS and dry environmental

594 air. Nguyen et al. (2017) also attributed the asymmetric convective structure of Tropical Storm
595 Cristobal to the combination of dry air and strong VWS. In general, as environmental relative
596 humidity decreases, the likelihood for radial and downdraft ventilation increases (Riemer et al.
597 2010, 2013; Alland et al. 2021a,b).

598 The location of dry air with respect to the VWS is also important. Ge et al. (2013) found in
599 idealized simulations that mid-tropospheric dry air initially located to the right of the shear vector
600 is advected by the TC's cyclonic flow toward the downshear quadrants, where it limits convection
601 and thwarts the realignment of a tilted TC vortex. Consistent with this result, Rios-Berrios et al.
602 (2016b) found in an ensemble simulation of a moderately sheared TC that members simulating a
603 stronger storm had higher humidity in the lower troposphere to the right-of-shear. In composites
604 of moderately sheared TCs, Rios-Berrios and Torn (2017) found that intensifying storms have
605 higher mid-tropospheric relative humidity upshear compared to steady-state or weakening storms.
606 Rios-Berrios and Torn (2017) suggest that the higher humidity upshear may reduce midlevel dry
607 air intrusions and allow for a more symmetric distribution of convection. Source regions of
608 dry air entering the TC inner core at a particular level are closely related to the environmental
609 storm-relative flow. For example, the flow topology of a TC in westerly storm-relative flow favors
610 environmental intrusions from the northwest quadrant (Riemer and Montgomery 2011). The inner
611 cores of stronger TCs are also more insulated from intrusions of environmental air than weak
612 TCs. However, more research is needed to better understand the dependence of TC structure
613 and intensity change on different configurations of VWS and dry air, including the altitude and
614 azimuthal location of dry air relative to the strongest storm-relative flows (i.e., ventilation).

615 *d. Sea-surface temperature*

616 The underlying ocean temperatures, commonly characterized by the sea-surface temperature
617 (SST), also affect the outcome of TC-VWS interactions. Studies have identified two contrasting
618 SST impacts on sheared TCs: a positive impact of higher SST on TC development through enhanced
619 surface fluxes (Tao and Zhang 2014; Chen, X. et al. 2018a, 2021; Alland and Davis 2022; Schecter
620 2022), and a perhaps less-intuitive negative impact of higher SST mainly found under radiative
621 convective equilibrium (RCE) conditions (Nolan and Rappin 2008; Rappin and Nolan 2012).



630 FIG. 9. (a) Length of the hurricane formation period (τ_{hf}) vs. the initial tilt magnitude ($tilt_0$). The color and
 631 shape of each symbol corresponds to the SST (legend). The dashed lines are linear regressions among all points
 632 in each SST group with $tilt_0 > 100$ km. (b) Relationship between τ_{hf} and the radius of maximum surface wind
 633 speed $\langle r_m \rangle$ time averaged during the hurricane formation period. Dashed lines are linear regressions as in (a),
 634 but over all data points within the pertinent SST group. Figure adapted from Fig. 1 in Schecter (2022).

622 With higher SST, the low- θ_e air flushed into the boundary layer via shear-induced downdrafts
 623 (Section 2c.1) is refueled by surface fluxes more rapidly before becoming entrained in inner-core
 624 convection. The enhanced surface fluxes thereby reduce the effect of downdraft ventilation and
 625 strengthen the connection between the midlevel and low-level vortices (Tao and Zhang 2014; Chen,
 626 X. et al. 2018a, 2021; Alland and Davis 2022). Meanwhile, higher SST excites more vigorous
 627 convective activity at larger radii, which broadens the vortex circulation and increases TC resistance
 628 to shear (Schecter 2022). The rate of tilt reduction is sensitive to SST such that the higher the SST,
 629 the faster reduction of tilt magnitude (Schecter 2022, and Fig. 9).

635 In contrast, Nolan and Rappin (2008) found in idealized simulations of sheared TCs in RCE
 636 environments that higher SST can actually make a TC less resilient to VWS. They found that the
 637 higher SST increases the height of the freezing level, which in turn increases the altitude of the
 638 developing mid-level vortex. For the wind profile used in their simulations, the higher altitude
 639 of the midlevel vortex meant it was exposed to stronger storm-relative flow and shear-induced

640 ventilation. In addition, Rappin et al. (2010) found that increasing SST in RCE simulations results
641 in a drier midlevel environment and, hence, stronger ventilation due to shear at the altitude of
642 the midlevel vortex. Although RCE may be a valid approximation for the large-scale tropical
643 environment on daily time scales and longer, the local environment around TCs can be far from
644 RCE. Therefore, more research is needed on the validity of the RCE assumption as it relates to
645 TC-VWS interactions.

646 **4. Pathways to TC Development and Intensification in Shear**

647 Despite the substantial body of research highlighting the predominantly negative impacts of VWS
648 on TC structure and intensity discussed so far, VWS is not always destructive to a TC. An emerging
649 line of research has sought to better understand the intensification of TCs in environments with
650 VWS magnitudes that are neither too weak nor too strong (e.g., Molinari et al. 2004, 2006; Molinari
651 and Vollaro 2010; Montgomery et al. 2010; Foerster et al. 2014; Stevenson et al. 2014; Rios-Berrios
652 et al. 2016a,b; Zawislak et al. 2016; Nguyen et al. 2017; Ryglicki et al. 2018a; Chen, X. et al. 2018a;
653 Rogers et al. 2020, and many others). This range of VWS magnitudes is commonly referred to
654 as “moderate shear.” Four pathways to TC intensification under moderate shear have emerged
655 from the literature: vortex tilt reduction, vortex reformation, axisymmetrization of precipitation,
656 and outflow blocking. This section reviews each pathway separately even though they may not be
657 mutually exclusive; for example, vortex tilt reduction may occur together with vortex reformation.
658 These pathways most likely explain the intensification of weak, disorganized TCs (e.g., tropical
659 depressions and tropical storms) into major hurricanes.

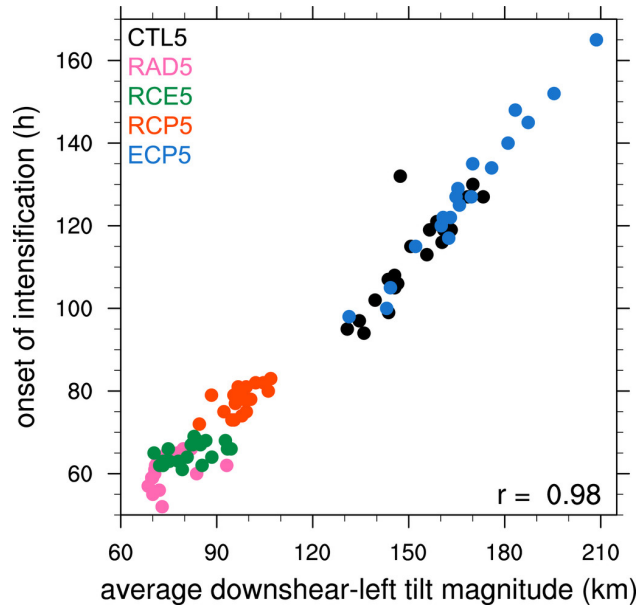
660 *a. Vortex tilt reduction*

661 Multiple studies have suggested that a nearly aligned vortex is often a precursor to TC intensi-
662 fication, including the onset of rapid intensification (Frank and Ritchie 2001; Reasor et al. 2004;
663 Reasor and Eastin 2012; Rappin and Nolan 2012; Zhang and Tao 2013; Tao and Zhang 2014;
664 Rogers et al. 2015; Nguyen and Molinari 2015; Rios-Berrios et al. 2016b, 2018; Chen, X. et al.
665 2019; Rogers et al. 2020; Rios-Berrios 2020; Alvey et al. 2020; Schecter and Menelaou 2020; Nam
666 et al. 2023). While the literature often uses the terminology “vortex re-alignment” to describe how
667 a TC vortex evolves from being tilted to being nearly aligned, recent work (discussed below) has

668 uncovered different pathways that explain such evolution. Therefore, we adopt the concept of “tilt
669 reduction” herein to acknowledge the multiple processes that explain the transition from a tilted to
670 a nearly aligned TC vortex.

671 Idealized TC simulations have been extensively used to study the relationship between VWS,
672 vortex tilt, and TC intensity (Jones 1995; DeMaria 1996; Frank and Ritchie 1999, 2001; Jones
673 2000a,b, 2004; Patra 2004; Wong and Chan 2004; Kwon and Frank 2005, 2008; Rappin and
674 Nolan 2012; Riemer et al. 2013; Zhang and Tao 2013; Tao and Zhang 2014; Miyamoto and Nolan
675 2018; Rios-Berrios et al. 2018; Tao and Zhang 2019; Rios-Berrios 2020; Schecter and Menelaou
676 2020; Schecter 2022; Nam et al. 2023). These simulations use models of varying complexities
677 ranging from dry, nonhydrostatic models (Jones 1995; DeMaria 1996; Jones 2000a,b; Patra 2004;
678 Wong and Chan 2004; Kwon and Frank 2005) to models that include moist processes (Flatau
679 et al. 1994; Wang and Holland 1996; Frank and Ritchie 1999; Wong and Chan 2004; Kwon and
680 Frank 2008; Rappin and Nolan 2012; Riemer et al. 2013; Zhang and Tao 2013; Tao and Zhang
681 2014; Miyamoto and Nolan 2018; Rios-Berrios et al. 2018; Tao and Zhang 2019; Rios-Berrios
682 2020; Ryglicki et al. 2018b; Schecter and Menelaou 2020; Schecter 2022; Nam et al. 2023). A
683 cloud-free, vertically aligned TC-like vortex is usually specified in the initial conditions along with
684 environmental flow and a thermodynamic sounding characteristic of the tropical atmosphere. The
685 vortex is initially tilted towards the downshear quadrant, followed by an azimuthal rotation of the
686 tilt vector towards the downshear-left and upshear-left quadrant. If the vortex is not completely
687 sheared apart, intensification typically follows after a substantial reduction in tilt magnitude that
688 typically coincides with a left-of-shear tilt configuration. For example, Fig. 10 shows that the onset
689 of rapid intensification in multiple idealized TC simulations is strongly correlated with the vortex
690 tilt magnitude. This figure implies that for larger vortex tilt, the onset of rapid intensification occurs
691 later or becomes less likely.

699 Limited observational evidence also supports that a small vortex tilt or tilt reduction precede
700 intensification under moderate and strong VWS. Reasor and Eastin (2012) used the concept of
701 “resiliency” to shear to describe TCs that maintain a small vortex tilt under moderate and strong
702 VWS. Their observational analysis of Hurricane Guillermo (1997) showed that the persistent small
703 vortex tilt explained (at least partly) how Guillermo was able to resist and intensify in strong
704 VWS. Additional observational studies of individual TCs have also found a relatively small vortex



692 FIG. 10. Comparison between the onset of intensification and 400–900-hPa tilt magnitude averaged only during
 693 the time period when the tilt vector pointed downshear left (defined as a mathematical angle between 0° and
 694 90°). Colors represent different 20-member ensembles with the same 5 m s^{-1} shear magnitude: (black) a control
 695 configuration without radiation (CTL5), (pink) a configuration with radiation (RAD5), (green) a configuration in
 696 radiative-convective equilibrium (RCE5), (orange) a configuration with reduced cold pools (RCP5), and (blue)
 697 a configuration with enhanced cold pools (ECP5). Pearson’s correlation coefficient appears at the lower-right
 698 corner. Adapted from Fig. 16 of Rios-Berrios (2020).

705 tilt coinciding with intensification under moderate and strong VWS (e.g., Molinari et al. 2006;
 706 Stevenson et al. 2014; Rogers et al. 2015, 2020; Alvey et al. 2022). More recently, an observational
 707 analysis of hundreds of airborne Doppler radar analyses demonstrated that early-stage TCs with
 708 small vortex tilt were associated with greater rates of intensification (Fischer et al. 2023b). Given
 709 that a tilted vortex is strongly coupled to convection (Section 2a), satellite imagery has also provided
 710 evidence that a small vortex tilt precedes TC intensification (Ryglicki et al. 2018a, 2021).

711 The importance of vortex tilt reduction for TC intensification has motivated many studies aimed
 712 at identifying the physical processes responsible for changes in vortex tilt. As discussed in Section
 713 2a, early investigations focused on the role of dry dynamics. These studies found a preferred tilt
 714 orientation along—and to the left of—the VWS vector (Jones 1995; Wang and Holland 1996; Frank
 715 and Ritchie 2001; Reasor et al. 2004). Simulations with sheared barotropic vortices demonstrated

716 that once the vortex tilts upshear, differential vorticity advection of the sheared flow acts to realign
717 the vortex (Jones 1995). A different paradigm describes vortex tilt reduction through inviscid
718 damping of vortex Rossby waves, which are excited by VWS (Reasor and Montgomery 2001;
719 Schechter et al. 2002; Schechter and Montgomery 2003; Reasor et al. 2004; Reasor and Montgomery
720 2015). In this paradigm, the tilt evolution is described by a vortex Rossby wave asymmetry, often
721 referred to as the “quasi-mode” on a background azimuthally-averaged flow. Moving outward
722 from the TC center, a critical radius exists where the rotation rate of the background flow is
723 equal to the precession frequency of the vortex tilt mode, where resonance between the two can
724 occur. Stirring of the flow at this critical radius requires a damping of the vortex tilt at a rate
725 proportional to the local vorticity gradient, provided the radial vorticity gradient is negative. While
726 this mechanism invokes dry dynamics, additional studies (Schechter and Montgomery 2007; Reasor
727 and Montgomery 2015) demonstrated that the location of the critical radius is dependent upon the
728 static stability, or “cloudiness”, of the TC core, with the critical radius shifting to smaller radii as
729 static stability decreases. Thus, diabatic processes have been hypothesized to indirectly affect the
730 vortex resilience by modifying the static stability and the TC’s radial vorticity profile (Reasor et al.
731 2004).

732 More recent studies have emphasized the direct role of moist diabatic processes in vortex tilt
733 reduction. Including moist processes in idealized simulations yield smaller vortex tilt magnitudes
734 for otherwise similar but dry configurations, which led to the hypothesis that diabatic heating is
735 important for vortex tilt reduction under VWS (Flatau et al. 1994; Wang and Holland 1996; Frank
736 and Ritchie 1999). This hypothesis was challenged by Jones (2004), who demonstrated that TCs
737 could experience a small vortex tilt in the absence of moist processes and that vortex tilt depends
738 on the Rossby penetration depth and vortex strength. Yet, more recent studies that have relied
739 on full-physics idealized TC simulations continue to emphasize the complex role of moisture and
740 diabatic processes during vortex tilt reduction, especially in TCs below hurricane intensity. The
741 main precipitating regions in these TCs is strongly coupled to the midtropospheric vortex, and
742 their co-evolution can reduce or amplify the vortex tilt induced by VWS (Rios-Berrios et al. 2018;
743 Ryglicki et al. 2018b; Chen, B.-F. et al. 2021). A substantial vortex tilt reduction happens through
744 a relatively rapid re-structuring of the TC vortex (Miyamoto and Nolan 2018; Rios-Berrios et al.
745 2018; Rogers et al. 2020; Schechter and Menelaou 2020; Schechter 2022; Alvey and Hazelton 2022;

746 Alvey et al. 2022), instead of through the gradual alignment of distinct lower and midlevel vorticity
747 anomalies. This process may take several iterations (Ryglicki et al. 2018b) especially in marginal
748 environments of moderate VWS and dry air (Nam et al. 2023).

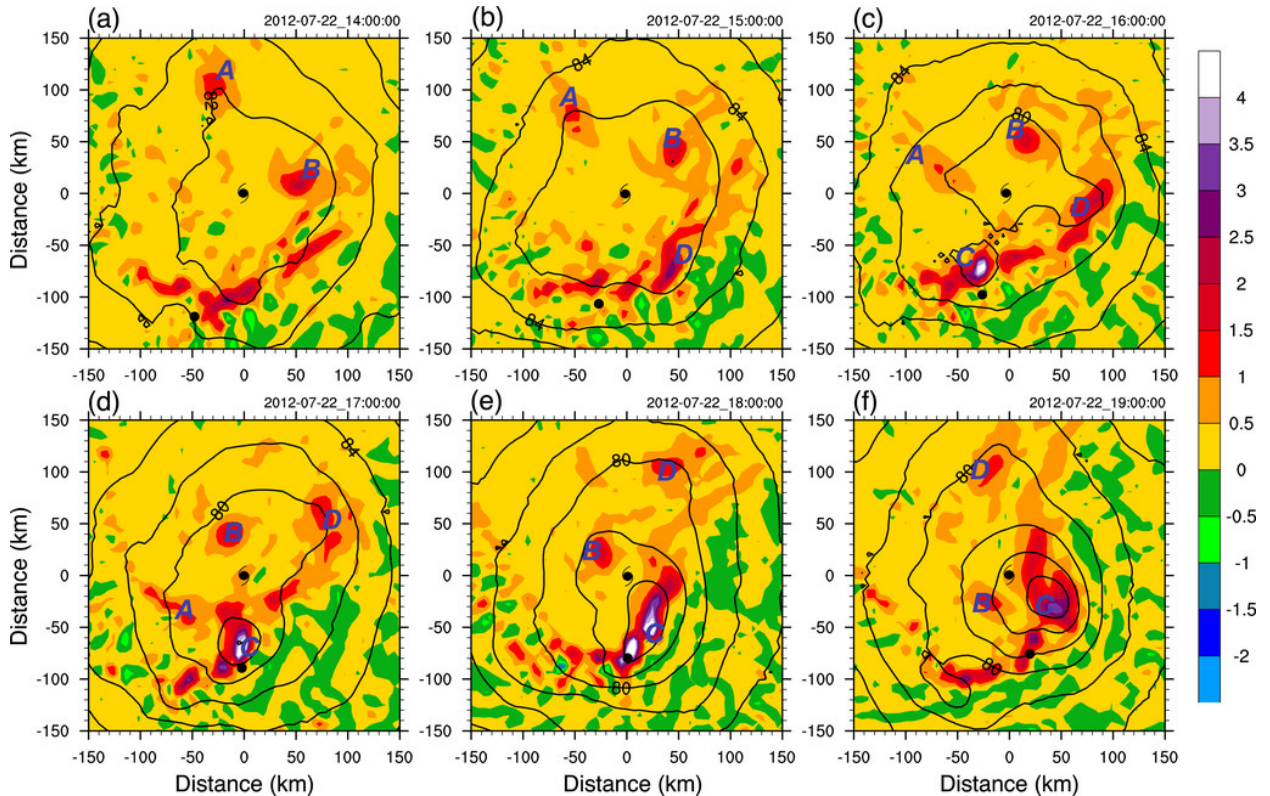
749 During the re-structuring process, convectively coupled vorticity anomalies aid the establishment
750 of a nearly aligned and deep TC vortex (Miyamoto and Nolan 2018; Rios-Berrios et al. 2018). At
751 the same time, precipitation transitions from being highly asymmetric to being more symmetric
752 with an established eyewall. The established eyewall aids TC intensification through increased
753 axisymmetric diabatic heating (Tao and Zhang 2014) while the nearly aligned vortex is more likely
754 to intensify via surface heat fluxes (Molinari et al. 2004) and boundary-layer vortex stretching
755 (Rios-Berrios et al. 2018). Divergent outflow from the shear-induced convection also counteracts
756 the sheared environmental flow (Ryglicki et al. 2018b, 2019, 2021). Observations and model
757 simulations of real-world TCs also support this re-structuring process (Molinari et al. 2004; Rogers
758 et al. 2020; Ryglicki et al. 2021; Alvey and Hazelton 2022; Stone et al. 2023), although the precise
759 pathway to vortex tilt reduction can include vortex precession and vortex reformation in some cases
760 (Alvey and Hazelton 2022). Vortex reformation is described in greater detail in the next subsection.

761 While vortex tilt reduction increases the likelihood that a TC will intensify, there is no unanimous
762 consensus about the relationship between vortex tilt and intensity changes. In an observational
763 composite analysis of TCs of hurricane intensity, Rogers et al. (2013) found no significant difference
764 in the magnitude of vortex tilt between the intensifying and steady-state hurricanes. Some studies
765 have also proposed that the onset of rapid intensification precedes a complete vortex alignment
766 (e.g., Chen and Gopalakrishnan 2015; Judt et al. 2016; Chen, X. et al. 2018a; Alvey et al. 2022).
767 However, Fischer et al. (2023b) found that a vortex tilt is more important for intensity changes of TCs
768 below hurricane intensity than for stronger TCs. These discrepancies could stem from differences
769 in datasets (i.e., model simulations vs. observations), challenges of defining and identifying vortex
770 tilt, the rapid evolution of convective processes, amongst other factors. Future work should seek to
771 elucidate how external influences affect the relationship between TC intensity change and vortex
772 tilt magnitude, and further explore cases that intensify prior to substantial tilt reduction.

773 *b. Reformation*

774 Observational and modeling studies have indicated that early-stage TCs (including tropical
775 depressions, tropical storms, and category-1 hurricanes) are able to resist moderate-to-strong VWS
776 by generating a new vorticity core or low-level circulation beneath or near the mid-level circulation
777 in the downshear quadrant. This pathway has been termed downshear reformation (Molinari et al.
778 2004, 2006), and occurs most frequently for tropical storms (e.g., Davis et al. 2008; Molinari
779 and Vollaro 2010; Nguyen and Molinari 2012; Chen, X. et al. 2018a; Rogers et al. 2020; Alvey
780 and Hazelton 2022). In this pathway, a broad and relatively weak parent TC circulation and the
781 resulting weak axisymmetrization allow the development of a reformed vorticity core in a region
782 of sustained diabatic heating (Schechter 2020). Downshear reformation notably alters the vortex
783 structure and the thermodynamic state within the core, as a more compact and vertically-aligned
784 TC inner core forms in a more humid downshear environment. This sets up a more favorable
785 configuration for TC intensification and, sometimes, rapid intensification. How fast a TC will
786 intensify has been found to depend on the vortex tilt and the saturation fraction within the core
787 after reformation (Chen, X. et al. 2019). As reformation and the related structural changes occur
788 within a few hours, they remain extremely difficult to observe and predict. The reformation can
789 also change the steering flow the TC feels due to the center relocation, which has a long-term
790 impact on the track forecasts. Thus, it is not surprising to see large forecast errors for both track
791 and intensity when downshear reformation occurs (e.g., Chen, X. et al. 2018a; Alvey et al. 2022).

792 The development of the reformed vorticity core relies crucially on the stretching, tilting, and
793 upward advection of vorticity through convective processes (Nguyen and Molinari 2015; Chen, X.
794 et al. 2018a; Rogers et al. 2020). The timing of reformation is thereby intrinsically dependent on
795 the factors affecting the downshear convective activity, including TC intensity, VWS magnitude,
796 and thermodynamic instability. The preference for reformation to occur at tropical-storm intensity
797 suggests that the new vortex can become the dominant vortex when the pre-existing circulation is
798 relatively weak. The presence of moderate-to-strong VWS also implies that sufficiently strong
799 balanced lifting (cf. Jones 1995) and Ekman-like pumping (Schechter 2022) in the downshear
800 region are important prerequisites, especially in the scenario where the surface enthalpy flux is
801 nearly zero (Davis et al. 2008).



802 FIG. 11. Hourly evolution of 900-hPa relative vorticity (shading; 10^{-3} s^{-1}) and geopotential height (contoured
 803 every $2 \times 10^2 \text{ m}^{-2} \text{ s}^{-2}$) from (a) 1400 to (f) 1900 UTC 22 Jul. The black hurricane symbol (dot) in each panel
 804 denotes the surface (500 hPa) TC center. Labels A–D denote different mesovortices, and mesovortex C becomes
 805 the reformed inner vortex of simulated Typhoon Vicente (2012). The 200–850 hPa VWS is heading southwest.
 806 From Fig. 7 in Chen et al. (2018b).

807 Another favorable condition for reformation is the counter-aligned surface wind and deep-layer
 808 VWS, which positions the maximum surface wind left-of-shear such that the enhanced surface
 809 enthalpy fluxes can support stronger asymmetric convection (Chen, X. et al. 2018a). The timing of
 810 reformation is also related to a downshear environment characterized by weak instability (Raymond
 811 et al. 2011) and high column moisture. Such conditions favor bottom-heavy mass flux profiles
 812 and low-level vorticity stretching (Rios-Berrios et al. 2018; Rogers et al. 2020), which can be an
 813 outcome of several previous episodes of deep convection. These episodes of deep convection can
 814 induce the formation of multiple mesovortices that propagate downstream (Chen, X. et al. 2018a);
 815 however, only the mesovortex that successfully grows in size and strength with time becomes the

816 reformed inner vortex (e.g., mesovortex C in Fig. 11) whereas the other mesovortices weaken after
817 leaving the downshear convergence zone (Wang et al. 2022). In some cases, convective processes
818 leading to reformation can benefit from diurnal, radiative influences (Alvey and Hazelton 2022),
819 or interactions with island topography (Alvey et al. 2022). Despite these insightful findings, more
820 research utilizing different observational platforms and high-resolution numerical simulations is
821 needed to quantify the frequency and predictability of vortex reformation.

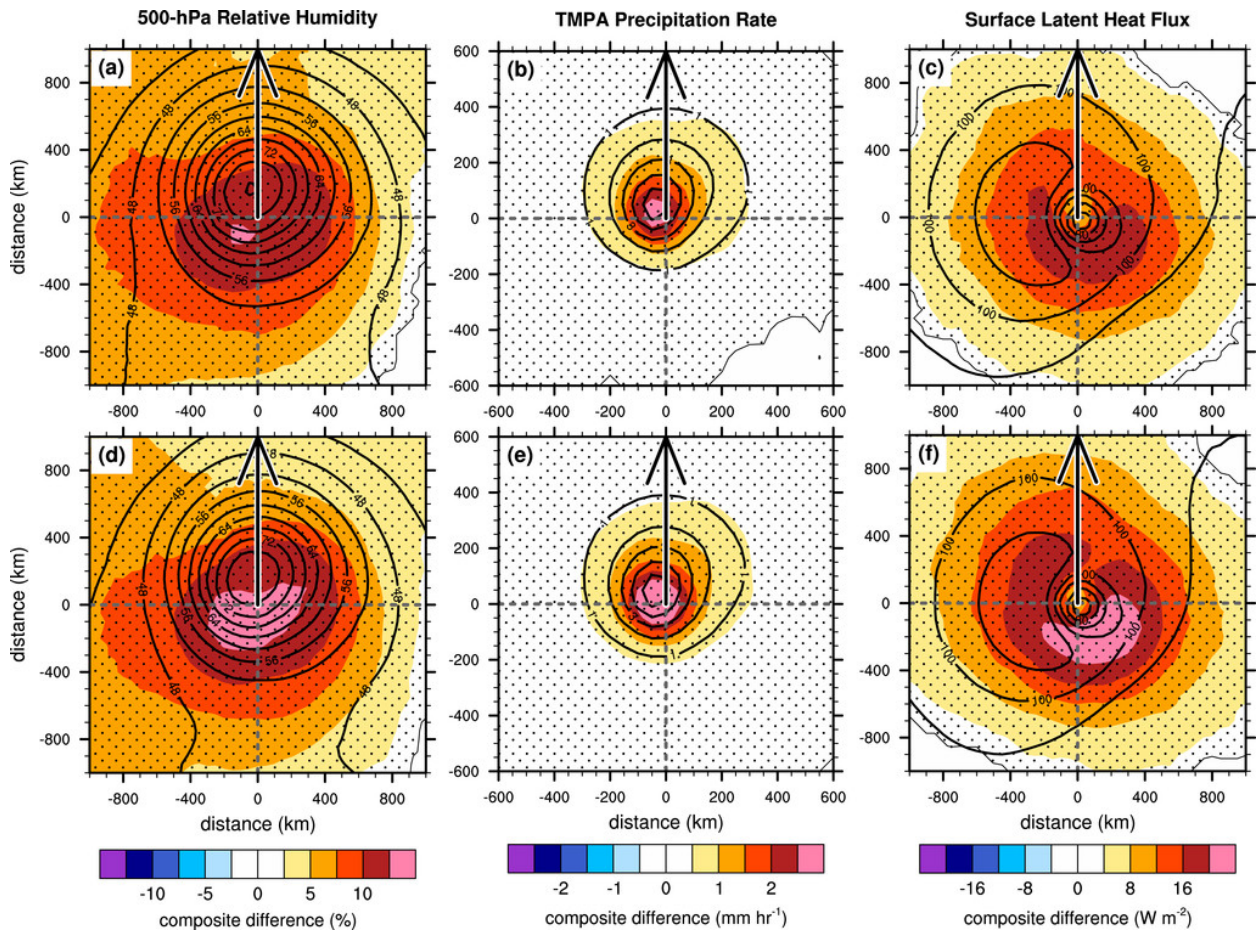
822 *c. Precipitation Axisymmetrization*

823 From a kinematic perspective, TC intensification requires the inward advection of angular mo-
824 mentum surfaces across the location of the radius of maximum wind within the boundary layer
825 (e.g., Smith et al. 2009; Montgomery and Smith 2014; Smith and Montgomery 2015). This pro-
826 cess is typically achieved due to sufficient diabatic heating within the TC inner core; however, as
827 previously discussed, the pattern of diabatic heating in sheared TCs is asymmetric. Some stud-
828 ies have hypothesized TC intensification can be achieved through asymmetric processes, such as
829 the injection of high-entropy air from the low-level TC eye into the eyewall region (Persing and
830 Montgomery 2003; Cram et al. 2007; Reasor et al. 2009, e.g.), the mixing of momentum between
831 the TC eye and eyewall (Schubert et al. 1999; Kossin and Schubert 2001; Rozoff et al. 2009),
832 or sufficiently intense asymmetric convection with robust warming via compensating subsidence
833 (e.g., Heymsfield et al. 2001; Guimond et al. 2010; Nguyen and Molinari 2012; Guimond et al.
834 2016; Rogers et al. 2016; Hazelton et al. 2017; Wadler et al. 2018). Intense asymmetric regions of
835 convection can also spin up the TC primary circulation via the axisymmetrization of local potential
836 vorticity anomalies (e.g., Möller and Montgomery 2000; Hendricks et al. 2004; Montgomery and
837 Smith 2014).

838 Nevertheless, through the use of dry, idealized simulations of hurricane-like vortices, Nolan
839 et al. (2007) demonstrated TC intensification is significantly more responsive to the axisymmetric
840 projection of heating than localized, asymmetric heating. Consistent with this idea, an increasing
841 number of studies have begun to identify a relationship between the TC intensification rate and the
842 degree of precipitation axisymmetry. For instance, multiple observational case studies of TCs in
843 shear have linked TC intensification to increases in upshear precipitation and more axisymmetric
844 convective structures (e.g., Stevenson et al. 2014; Rogers et al. 2015; Susca-Lopata et al. 2015;

845 Zawislak et al. 2016; Rogers et al. 2016; Munsell et al. 2021). Additional studies of multiple
846 TC cases have corroborated these results, showing that TCs with more axisymmetric precipitation
847 structures tend to intensify more rapidly (e.g., Harnos and Nesbitt 2011; Jiang and Ramirez 2013;
848 Zagrodnik and Jiang 2014; Alvey III et al. 2015; Tao and Jiang 2015; Harnos and Nesbitt 2016;
849 Tao et al. 2017; Fischer et al. 2018; Ryglicki et al. 2018a). Using a satellite-based precipitation
850 partitioning scheme, Tao et al. (2017) indicated an increase in stratiform precipitation—especially
851 in the upshear quadrants—was particularly important for the initiation of rapid intensification. Tao
852 et al. (2017) hypothesized the increase in stratiform precipitation may be linked to a moistening
853 of the inner core, promoting a local thermodynamic environment that favors more axisymmetric
854 heating during rapid intensification. This hypothesis is consistent with a comparison of steady-state
855 and intensifying TCs in the presence of moderate VWS by Rios-Berrios and Torn (2017), who
856 found intensifying TCs have a more humid mid-troposphere and a greater coverage of upshear pre-
857 cipitation (Fig. 12). Composite analyses from other observational platforms, such as geostationary
858 satellite imagery (Fischer et al. 2018; Shi and Chen 2021), airborne Doppler radar analyses (Rogers
859 et al. 2013; Wadler et al. 2018), and global lightning detection networks (Stevenson et al. 2018),
860 have also emphasized the importance of greater convective axisymmetry for increased rates of TC
861 intensification.

868 Full-physics numerical simulations similarly point toward the significance of greater precipitation
869 axisymmetry for increased rates of TC intensification in environments with VWS (e.g., Miyamoto
870 and Takemi 2012; Rios-Berrios et al. 2016b; Onderlinde and Nolan 2016; Chen, X. et al. 2018a;
871 Leighton et al. 2018; Miyamoto and Nolan 2018; Tao and Zhang 2019; Alvey et al. 2020; Hazelton
872 et al. 2020; Alland et al. 2021b). Analyses of such simulations have inspired hypotheses to
873 explain the increased precipitation axisymmetry of sheared TCs. Some studies have suggested the
874 significance of vortex alignment in facilitating more axisymmetric precipitation structures (e.g.,
875 Tao and Zhang 2014; Chen, X. et al. 2018b; Rios-Berrios et al. 2018; Ryglicki et al. 2018b; Tao and
876 Zhang 2019; Alvey et al. 2020; Hazelton et al. 2020; Rios-Berrios 2020; Alland et al. 2021b; Chen,
877 X. et al. 2021). As discussed in the previous subsection, vortex tilt and asymmetric convection are
878 strongly coupled to each other and, consequently, a nearly aligned vortex is also associated with a
879 more axisymmetric distribution of precipitation. Other studies have emphasized the important role
880 of the boundary layer in facilitating precipitation axisymmetry. In a comparison of two simulations



882 FIG. 12. Storm-centered, shear-relative analyses of (a),(d) 500-hPa RH (%); (b),(e) precipitation rate (mm
 883 h⁻¹); and (c),(f) surface LHF (W m⁻²) at (top) 0 h and (bottom) averaged between 0 and 24 h. Black contours
 884 represent the mean of all intensifying and steady-state events, shading represents the composite difference between
 885 intensifying and steady-state events, and the stippling pattern represents statistically significant differences at the
 886 99.9% confidence level. All fields were rotated with respect to the 200–850-hPa shear vector such that the shear
 887 vector (black and white arrow) points along the positive ordinate. From Fig. 11 in Rios-Berrios and Torn (2017).

881 of the same TC vortex over different SSTs, Chen, X. et al. (2021) demonstrated how enhanced
 882 surface enthalpy fluxes—in this case from warmer sea surface temperatures—promoted more
 883 vigorous inner-core convection that propagated farther upshear, leading to greater precipitation
 884 axisymmetry and increased TC intensification rates. Likewise, dropsonde observations (Nguyen
 885 et al. 2019), reanalysis output (Rios-Berrios and Torn 2017; Richardson et al. 2022), and other

886 numerical simulations (Rappin and Nolan 2012) generally agree that larger upshear surface enthalpy
887 fluxes favor increased precipitation axisymmetry and subsequent TC intensification.

888 *d. Outflow blocking*

889 The divergent upper-level outflow of a TC can in some cases counteract storm-relative flows due
890 to VWS, enabling TCs to intensify in shear. Black and Anthes (1971) recognized the ability of the
891 TC outflow to deflect the upper-tropospheric flow in which the TC is embedded, but more recent
892 work has revealed the implications of this flow deflection for the intensification of sheared TCs.
893 Ryglicki et al. (2018a) identified a class of storms that undergo rapid intensification in moderate
894 to strong deep-layer VWS. A common feature of these storms is that they all exhibit bursts of
895 convection that increase the component of outflow directed upshear, which tends to occur once the
896 vortex tilts to the left of shear (Ryglicki et al. 2020).

897 Outflow blocking promotes the intensification of sheared TCs by re-routing the environmental
898 flow away from the TC center (Ryglicki et al. 2019, 2021). This reduces the radial thermodynamic
899 ventilation of the warm core in the upper troposphere (Finocchio and Rios-Berrios 2021) and locally
900 reduces the effective wind shear over the TC inner core (Dai et al. 2021). In a climatological study
901 of several TCs in the Northern Hemisphere, Shi and Chen (2021) found that, consistent with
902 Ryglicki et al. (2020), rapid intensification in moderate to strong shear is preceded by an increase in
903 the component of outflow directed upshear and a coincident reduction of the total shear near the TC
904 inner core. Idealized simulations have identified an asymmetric divergent flow within the outflow
905 layer of sheared TCs that is responsible for locally reducing the vertical wind shear over the inner
906 core (Xu and Wang 2013; Ryglicki et al. 2019; Dai et al. 2021). Because the TC outflow is confined
907 to the upper troposphere, the asymmetric divergent flow is more effective at counteracting VWS
908 that is also concentrated in the upper troposphere (Elsberry and Jeffries 1996; Ryglicki et al. 2018b;
909 Shi and Chen 2021). As discussed in Section 3a, upper-level anticyclones are usually responsible
910 for these types of upper-level shear environments (Ryglicki et al. 2018a). Shi and Chen (2021)
911 found that 76% of TCs that rapidly intensify in moderate to strong shear are sheared by an upper-
912 level anticyclone, indicating a possible relationship between the large-scale shearing mechanism
913 and the likelihood for the outflow to counteract VWS. From an operational forecasting perspective,
914 such relationships between the large-scale flow and the likelihood for TC intensification in shear

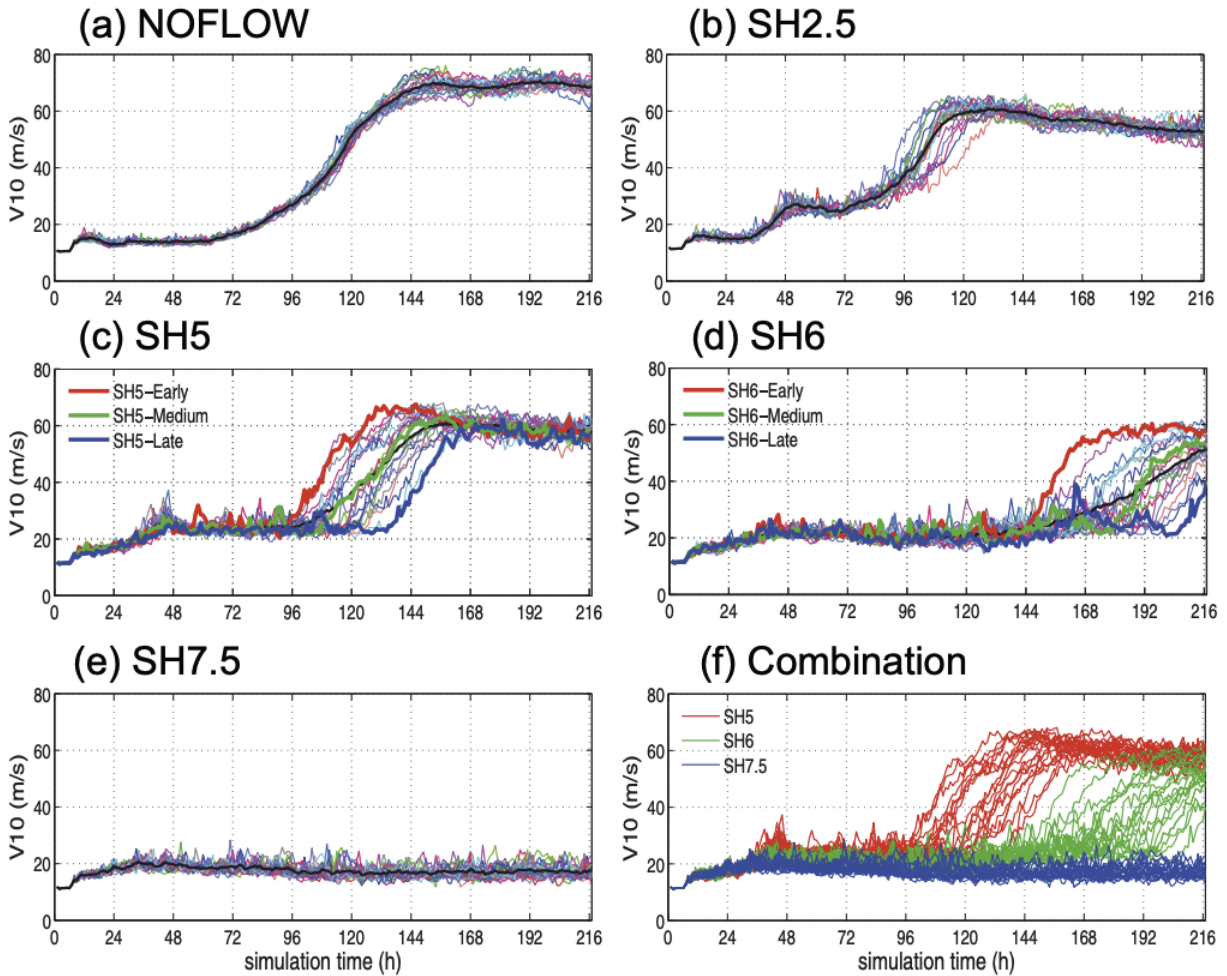
915 are particularly valuable in the moderate VWS environments that are frequently associated with
916 lower TC predictability.

917 **5. Effects of Shear on TC Predictability**

918 The presence of VWS increases the complexity of interactions between the TC and its surrounding
919 environment that can strongly limit skillful predictions of TC structure and intensity change.
920 Bhatia and Nolan (2013) found that the short-range intensity forecast errors from both the National
921 Hurricane Center and operational statistical and dynamical models at the time were largest for
922 hurricane-strength storms in moderate magnitudes ($5\text{--}10\text{ m s}^{-1}$) of deep-layer VWS. This range of
923 VWS magnitudes is near the threshold values that are traditionally used in operational settings to
924 broadly distinguish favorable from unfavorable flow environments. Although operational intensity
925 forecast skill has improved since Bhatia and Nolan (2013), TCs in moderate VWS environments
926 are still widely considered to be less predictable than TCs in weak or strong shear.

927 Numerous studies over the last several decades have examined how VWS, and in particular
928 moderate VWS, affects both the intrinsic and practical predictability of a TC. Intrinsic predictability
929 refers to “the extent to which prediction is possible if an optimum procedure is used” (Lorenz
930 2006). Zhang and Tao (2013) studied the intrinsic predictability of weak TCs in shear using
931 idealized ensemble simulations in which they added small, random moisture perturbations in the
932 TC boundary layer of each ensemble member. They found that as the deep-layer VWS magnitude
933 increased, the uncertainty in the timing of TC intensification increased until the shear became
934 strong enough to prevent intensification in any of the ensemble members (Fig. 13). Tao and
935 Zhang (2015) further explored this result and found that the large ensemble spread in RI onset
936 times of the moderately sheared TCs was attributed to moist convection. The chaotic nature of
937 moist convection introduces small-scale differences among the ensemble members which grow up
938 to the vortex-scale as the TCs precess through the downshear-left quadrant, ultimately resulting in
939 differences in vortex precession rates and the timing of RI onset.

944 VWS also reduces a TC’s practical predictability, which is “the extent to which we ourselves are
945 able to predict by the best-known procedures, either currently or in the foreseeable future” (Lorenz
946 2006). The presence of VWS heightens the sensitivity of the storm to environmental characteristics
947 that are often poorly observed, such as mid-level humidity. Munsell et al. (2013) studied an ensem-



940 FIG. 13. Time evolution of tropical cyclone intensity in terms of the 10-m maximum wind speed for ensembles
 941 with (a) no shear (“NOFLOW”), (b) SH2.5, (c) SH5, (d) SH6, (e) SH7.5, and (f) combination of SH5, SH6,
 942 and SH7.5. The numbers after “SH” indicate the magnitude of westerly deep-layer VWS in each ensemble. All
 943 simulations have SST=27°C. Adapted from Fig. 2 in Tao and Zhang (2015).

948 ble of a sheared Tropical Storm Erika (2009) and showed how large variability in midlevel dry-air
 949 intrusions played a key role in increasing the ensemble forecast intensity spread. Rios-Berrios
 950 et al. (2016a,b) analyzed ensemble simulations of TC Katia (2011) and Hurricane Ophelia (2011)
 951 respectively, and found that the key differences between developing and non-developing members
 952 were the lower-tropospheric moisture in the right-of-shear quadrant for Katia and midtropospheric
 953 moisture in the downshear and left-of-shear quadrants for Ophelia. Uncertainty in the environ-
 954 mental VWS itself also introduces uncertainties into TC intensity forecasts (Emanuel et al. 2004).

955 Both idealized and real TC modeling studies have demonstrated how small variations in the wind
956 profile can lead to bifurcating TC intensity responses that are related to differences in vortex tilt
957 and convective bursts near the radius of maximum winds (Finocchio et al. 2016; Finocchio and
958 Majumdar 2017a; Munsell et al. 2017).

959 Other factors related to numerical weather prediction techniques, such as radiation schemes,
960 also influence how VWS affects the practical predictability of a TC. Rios-Berrios (2020) found
961 that using a comprehensive radiation scheme in idealized simulations increases predictability of
962 sheared TCs by stabilizing the lower troposphere, thereby reducing the variability of the non-
963 linear feedbacks among lower-tropospheric ventilation, cold pools, convection, and vortex tilt.
964 More research is needed on how cloud microphysical parameterizations influence the practical
965 predictability of sheared TCs.

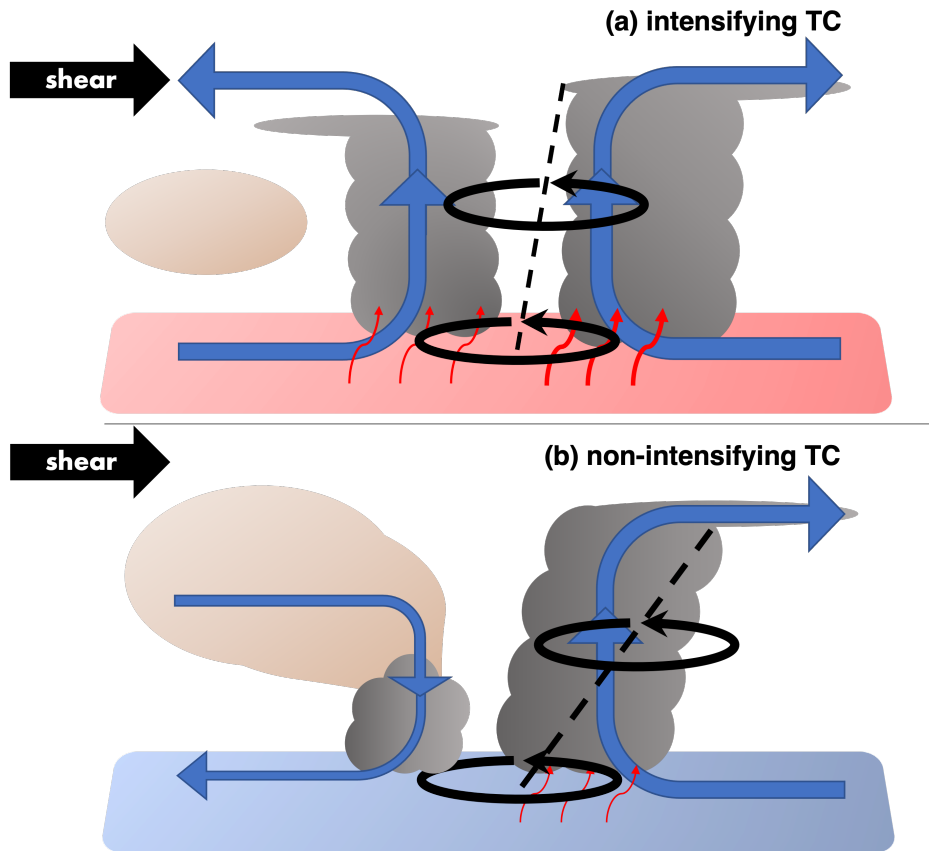
966 The presence of VWS also affects the structural predictability of a TC through its influence on the
967 evolution of wind, cloud, and precipitation asymmetries. Judt et al. (2016) examined TC structural
968 predictability by azimuthally decomposing the tangential wind field of Hurricane Earl (2010). The
969 mean vortex and wavenumber-one asymmetry had the longest intrinsic predictability of at least
970 seven days. Notably, they found that the predictability of the mean vortex and wavenumber-one
971 asymmetry was strongly influenced by the predictability of the environmental deep-layer VWS,
972 which itself remains predictable for longer than a week (Komaromi and Majumdar 2014, 2015).
973 At the scales of individual convective cells (azimuthal wave numbers >20), however, errors grow
974 more rapidly in both magnitude and scale, resulting in a much shorter predictability horizon of
975 only 6–12 h (Judt et al. 2016). Similar to the tangential winds, the low-wavenumber asymmetries
976 of the precipitation structure of a sheared TC remain predictable longer than the convective-
977 scale asymmetries (Finocchio and Majumdar 2017a). Moderate shear environments are generally
978 associated with lower intrinsic predictability of TC structure due to heightened sensitivity to the
979 environmental wind profile (Finocchio and Majumdar 2017a), and a higher uncertainty in the vortex
980 tilt evolution (Tao and Zhang 2015; Yu et al. 2023) and the occurrence of eyewall replacement
981 cycles (Zhang et al. 2017).

982 **6. Conclusions and Recommendations**

983 Deep-layer VWS, broadly defined as the 200–850 hPa shear of the horizontal wind, has profound
984 effects on TC structure and intensity. This review article summarizes the growing body of research
985 into those effects in terms of their influence on the likelihood and timing of TC intensification. VWS
986 tilts the TC vortex, organizes precipitation into a wavenumber-one asymmetric pattern, and causes
987 thermal and kinematic asymmetries. While VWS is a useful metric for TC intensity forecasting,
988 recent research demonstrates how shear alone often cannot fully capture the myriad ways in which a
989 TC responds to a given environmental flow. A particularly challenging forecasting situation, which
990 is the focus of several studies reviewed herein, involves an intermediate range of shear magnitudes
991 commonly referred to as moderate shear. Within this range of shear magnitudes, the sensitivity of
992 a TC to subtle aspects of both the storm and its environment are amplified, such that the response
993 of the TC becomes exceedingly difficult to predict.

994 Several recent studies have identified underlying processes that limit the predictability of moder-
995 ately sheared TCs. A focus of many of these studies has been on the surprising ability of some TCs
996 to intensify in moderate-to-strong VWS. Figure 14 shows a summary of the key structural features
997 that distinguish intensifying from non-intensifying TCs under moderate-to-strong VWS, based on
998 the *existing* knowledge reviewed herein. This review article summarized four different pathways
999 by which a TC can become resilient to such shear environments. Those pathways include the
1000 reduction of shear-induced vortex tilt, the formation of a new TC vortex within the shear-organized
1001 convection, the transition from a highly asymmetric to nearly symmetric precipitation structure,
1002 and the reduction of shear-induced ventilation by outflow blocking (Fig. 14). Several of these
1003 pathways operate simultaneously; for example, shear-organized asymmetric convection can lead
1004 to the formation of a new, nearly aligned vortex and the associated outflow can counteract the
1005 storm-relative inflow due to shear.

1015 Despite the remarkable progress in understanding TC-VWS interactions, many open questions
1016 and opportunities for future research remain. There is no widely-accepted definition of VWS that
1017 can be generally applied in operational and research applications. Some methods estimate VWS
1018 by simply taking an area average of the 200 and 850 hPa winds over a large enough radii (e.g., 500
1019 km or 200–800 km) to sample the environment, whereas other methods remove the contributions
1020 from the TC vortex before taking such area averages. The specific radii are largely based on



1006 FIG. 14. Summary schematics of key structural properties of (a) intensifying and (b) non-intensifying TCs
 1007 under moderate VWS. The intensifying TC is associated with nearly symmetric convection (represented by
 1008 the clouds), a relatively small vortex tilt (represented by the circulations), and relatively strong surface fluxes
 1009 (represented by the small red arrows) in all quadrants. Dry air (represented by the brown circle), if present, is not
 1010 able to disrupt the TC secondary circulation. The non-intensifying TC is associated with asymmetric convection
 1011 in the downshear half, a relatively large vortex tilt, and relatively strong surface fluxes in the downshear half.
 1012 Dry air is able to disrupt the TC through either radial ventilation, downward ventilation, or a combination of
 1013 both. The intensifying TC is over relatively warmer ocean temperatures than the non-intensifying TC. Inspired
 1014 by schematics from Nguyen et al. (2017), Richardson et al. (2022), and others.

1021 legacy from previous studies without physically based justifications. The precise VWS magnitude
 1022 can vary substantially from one method to another as noted, for example, by Velden and Sears
 1023 (2014), Ryglicki et al. (2019), and Ryglicki et al. (2021). More broadly, it is unclear how much
 1024 the calculated shear and other environmental parameters truly affect a TC. For example, does the
 1025 inner-core vortex of a TC experience the environmental shear that is calculated from a 200–800

1026 km radial averaging around it? Although the answer to this question will depend on many factors
1027 (e.g., TC size, vortex depth, etc.), a broadly agreed upon and physically based definition is much
1028 needed.

1029 Another area of much opportunity is better understanding the response of early-stage TCs
1030 (i.e., below major hurricane intensity) to VWS. Much of the theoretical work on TC intensity
1031 and structure is based on the assumption of an axisymmetric vortex; however, early-stage TCs
1032 challenge that assumption due to their disorganized and asymmetric nature. For example, how
1033 strongly coupled are the displaced circulations of a weak TC in comparison to a vertically tilted
1034 vortex of a mature hurricane? Which processes govern the azimuthal distribution and intensity of
1035 precipitation of weak TCs? The emerging work on TC intensification under moderate VWS has
1036 largely focused on early-stage TCs, but that work has heavily relied on model simulations. Recent
1037 advancements in observing platforms (e.g., GOES-R, small satellites, uncrewed aircraft) and
1038 increased research flights into early-stage TCs are potential avenues for expanding our knowledge
1039 and aiding theoretical developments applicable to weak and mature TCs alike.

1040 Future studies should continue to interconnect the four pathways discussed here to explain
1041 TC intensification under moderate VWS. It is evident that the coupling between circulation and
1042 convection is important; however, there are some findings that need clarification. While a recent
1043 series of studies emphasizes the role of divergent outflow from shear-induced convection enabling
1044 vortex tilt reduction (Ryglicki et al. 2018a,b, 2019, 2020, 2021), other studies focus on boundary-
1045 layer processes that promote and sustain convection leading to vortex tilt reduction (Rios-Berrios
1046 et al. 2018; Rios-Berrios 2020; Chen, X. et al. 2021). These processes are not necessarily
1047 independent of each other. Hence, more studies are needed to unify these processes.

1048 Many of the studies discussed herein used idealized TC simulations of different complexities,
1049 but their numerical configuration could be improved to advance our process-based understanding
1050 of TC-VWS interactions. These simulations usually apply spatially and temporally homogeneous
1051 VWS, but Rios-Berrios and Torn (2017) showed that such assumption is valid for less than 36
1052 h in real-world TCs. New methods to account for the spatial and temporal variability of VWS
1053 (e.g., Onderlinde and Nolan 2017) should be used more often to mimic more closely the evolution
1054 of observed TCs. Moreover, details of the experimental configuration vary substantially amongst
1055 studies including: the specified profile of environmental winds, the choice to introduce shear

1056 in the initial conditions or abruptly at some point in the simulation, the inclusion of warm rain
1057 processes alone vs. also including ice processes, the inclusion of radiative processes, etc. This
1058 could potentially be alleviated by developing and adopting a generalized configuration. However,
1059 details of the simulations will inevitably depend on the underlying model and choices of model
1060 parameterizations. To date, all simulations have used convection-permitting or coarser resolution,
1061 but large-eddy simulations (LES) remain an area of future research. LES experiments could
1062 shed new light on the role of convective processes during TC-VWS interactions; for example, is
1063 ventilation a mesoscale process, turbulent process affecting cloudy updrafts, or both?

1064 Lastly, there is a critical need for bridging the gap between operational and research efforts.
1065 Real-time observational strategies should be informed by the findings of process-based research by
1066 developing observational technologies and techniques that sample relevant regions and quantities
1067 (such as upshear moisture or boundary-layer wind asymmetries). Co-located observations of
1068 moisture and winds near ventilation regions could help characterize ventilation in real time. At the
1069 same time, future research and forecast product development should be informed by the needs of
1070 forecasters given the limited predictability of sheared TCs.

1071 To sum up, we offer the following recommendations for future research on sheared TCs:

- 1072 • Develop physically-based and general methods to diagnose VWS in both operational and
1073 research applications.
- 1074 • Adapt observational strategies and exploit existing observations to better quantify TC-VWS
1075 interactions.
- 1076 • Conduct more research to understand when VWS is detrimental versus beneficial for TC
1077 intensity, to further explore the dependency of VWS impacts on TC structure and intensity,
1078 and to better interconnect the pathways to intensification under moderate VWS.

1079 Research and operational efforts on the topics above would be highly beneficial for advancing our
1080 understanding and improving the prediction of TC formation and intensification.

1081 *Acknowledgments.* We thank Michael Riemer, Yuqing Wang, David Nolan, and two anonymous
1082 reviewers for their thoughtful feedback during the peer review process. We also thank Robert F.
1083 Rogers, Paul D. Reasor, Josh Cossuth, and two anonymous reviewers from the National Hurricane
1084 Center for providing valuable feedback on an earlier version of this manuscript. This material
1085 is based upon work supported by the National Center for Atmospheric Research, which is a
1086 major facility sponsored by the National Science Foundation under Cooperative Agreement No.
1087 1852977. RRB, PF, and MSF also acknowledge funding from the Office of Naval Research under
1088 grant numbers PE 0601153N, N00014-20-1-2071, and ONR-005722, respectively, as part of the
1089 Tropical Cyclone Rapid Intensification Departmental Research Initiative.

1090 *Data availability statement.* No datasets were generated or analyzed during the current study.

1091 **References**

- 1092 Ahern, K., R. E. Hart, and M. A. Bourassa, 2021: Asymmetric hurricane boundary layer structure
1093 during storm decay. Part I: Formation of descending inflow. *Mon. Wea. Rev.*, **149** (11), 3851–
1094 3874, <https://doi.org/10.1175/mwr-d-21-0030.1>, URL <https://doi.org/10.1175/mwr-d-21-0030.1>.
1095 1.
- 1096 Alland, J. J., and C. A. Davis, 2022: Effects of surface fluxes on ventilation pathways and the
1097 intensification of Hurricane Michael (2018). *J. Atmos. Sci.*, **79** (4), 1211–1229, <https://doi.org/10.1175/jas-d-21-0166.1>, URL <https://doi.org/10.1175/jas-d-21-0166.1>.
1098 10.1175/jas-d-21-0166.1, URL <https://doi.org/10.1175/jas-d-21-0166.1>.
- 1099 Alland, J. J., B. H. Tang, and K. L. Corbosiero, 2017: Effects of midlevel dry air on develop-
1100 ment of the axisymmetric tropical cyclone secondary circulation. *J. Atmos. Sci.*, **74** (5), 1455–
1101 1470, <https://doi.org/10.1175/JAS-D-16-0271.1>, URL [http://journals.ametsoc.org/doi/10.1175/](http://journals.ametsoc.org/doi/10.1175/JAS-D-16-0271.1)
1102 [JAS-D-16-0271.1](http://journals.ametsoc.org/doi/10.1175/JAS-D-16-0271.1).
- 1103 Alland, J. J., B. H. Tang, K. L. Corbosiero, and G. H. Bryan, 2021a: Combined effects of
1104 midlevel dry air and vertical wind shear on tropical cyclone development. Part I: Downdraft
1105 ventilation. *J. Atmos. Sci.*, **78** (3), 763–782, <https://doi.org/10.1175/jas-d-20-0054.1>, URL <https://doi.org/10.1175/jas-d-20-0054.1>.
1106 [//doi.org/10.1175/jas-d-20-0054.1](https://doi.org/10.1175/jas-d-20-0054.1).
- 1107 Alland, J. J., B. H. Tang, K. L. Corbosiero, and G. H. Bryan, 2021b: Combined effects of midlevel
1108 dry air and vertical wind shear on tropical cyclone development. part II: Radial ventilation. *J.*

1109 *Atmos. Sci.*, **78** (3), 783–796, <https://doi.org/10.1175/jas-d-20-0055.1>, URL <https://doi.org/10.1175/jas-d-20-0055.1>.

1111 Alvey, G. R., M. Fischer, P. Reasor, J. Zawislak, and R. Rogers, 2022: Observed processes
1112 underlying the favorable vortex repositioning early in the development of Hurricane Dorian
1113 (2019). *Mon. Wea. Rev.*, **150** (1), 193–213, <https://doi.org/10.1175/mwr-d-21-0069.1>, URL
1114 <https://doi.org/10.1175/mwr-d-21-0069.1>.

1115 Alvey, G. R., and A. Hazelton, 2022: How do weak, misaligned tropical cyclones evolve to-
1116 ward alignment? A multi-case study using the hurricane analysis and forecast system. *J.*
1117 *Geophys. Res. Atmos.*, **127** (20), <https://doi.org/10.1029/2022jd037268>, URL [https://doi.org/](https://doi.org/10.1029/2022jd037268)
1118 [10.1029/2022jd037268](https://doi.org/10.1029/2022jd037268).

1119 Alvey, G. R., E. Zipser, and J. Zawislak, 2020: How does Hurricane Edouard (2014) evolve
1120 toward symmetry before rapid intensification? A high-resolution ensemble study. *J. Atmos.*
1121 *Sci.*, **77** (4), 1329–1351, <https://doi.org/10.1175/jas-d-18-0355.1>, URL [https://doi.org/10.1175/](https://doi.org/10.1175/1175/jas-d-18-0355.1)
1122 [jas-d-18-0355.1](https://doi.org/10.1175/jas-d-18-0355.1).

1123 Alvey III, G. R., J. Zawislak, and E. Zipser, 2015: Precipitation properties observed during
1124 tropical cyclone intensity change. *Mon. Wea. Rev.*, **143** (11), 4476–4492, <https://doi.org/10.1175/MWR-D-15-0065.1>, URL <http://journals.ametsoc.org/doi/10.1175/MWR-D-15-0065.1>.

1126 Barnes, G. M., E. J. Zipser, D. Jorgenson, and F. J. Marks, 1983: Mesoscale and convective
1127 structure of a hurricane rainband. *J. Atmos. Sci.*, **40** (9), 2125–2137, [https://doi.org/10.1175/](https://doi.org/10.1175/1520-0469(1983)040<2125:MACSOA>2.0.CO;2)
1128 [1520-0469\(1983\)040<2125:MACSOA>2.0.CO;2](https://doi.org/10.1175/1520-0469(1983)040<2125:MACSOA>2.0.CO;2).

1129 Bender, M. A., 1997: The effect of relative flow on the asymmetric structure in the interior of
1130 hurricanes. *J. Atmos. Sci.*, **54** (6), 703–724, [https://doi.org/10.1175/1520-0469\(1997\)054<0703:](https://doi.org/10.1175/1520-0469(1997)054<0703:teorfo>2.0.co;2)
1131 [teorfo>2.0.co;2](https://doi.org/10.1175/1520-0469(1997)054<0703:teorfo>2.0.co;2), URL [https://doi.org/10.1175/1520-0469\(1997\)054<0703:teorfo>2.0.co;2](https://doi.org/10.1175/1520-0469(1997)054<0703:teorfo>2.0.co;2).

1132 Bhatia, K. T., and D. S. Nolan, 2013: Relating the skill of tropical cyclone intensity
1133 forecasts to the synoptic environment. *Wea. Forecasting*, **28** (4), 961–980, [https://doi.org/](https://doi.org/10.1175/WAF-D-12-00110.1)
1134 [10.1175/WAF-D-12-00110.1](https://doi.org/10.1175/WAF-D-12-00110.1).

- 1135 Bister, M., and K. A. Emanuel, 1997: The genesis of Hurricane Guillermo: TEXMEX analyses and
1136 a modeling study. *Mon. Wea. Rev.*, **125**, 2662–2682, [https://doi.org/10.1175/1520-0493\(1997\)](https://doi.org/10.1175/1520-0493(1997)125<2662:TGOHGT>2.0.CO;2)
1137 125<2662:TGOHGT>2.0.CO;2.
- 1138 Black, M. L., J. F. Gamache, F. D. Marks, C. E. Samsury, and H. E. Willoughby, 2002: East-
1139 ern Pacific Hurricanes Jimena of 1991 and Olivia of 1994: The effect of vertical shear
1140 on structure and intensity. *Mon. Wea. Rev.*, **130** (9), 2291–2312, [https://doi.org/10.1175/](https://doi.org/10.1175/1520-0493(2002)130<2291:EPHJOA>2.0.CO;2)
1141 1520-0493(2002)130<2291:EPHJOA>2.0.CO;2, URL [http://journals.ametsoc.org/doi/full/10.](http://journals.ametsoc.org/doi/full/10.1175/1520-0493(2002)130%3C2291%3AEPHJOA%3E2.0.CO%3B2)
1142 1175/1520-0493(2002)130%3C2291%3AEPHJOA%3E2.0.CO%3B2.
- 1143 Black, P. G., and R. A. Anthes, 1971: On the asymmetric structure of the tropical cyclone
1144 outflow layer. *J. Atmos. Sci.*, **28** (8), 1348 – 1366, [https://doi.org/https://doi.org/10.1175/](https://doi.org/https://doi.org/10.1175/1520-0469(1971)028<1348:OTASOT>2.0.CO;2)
1145 1520-0469(1971)028<1348:OTASOT>2.0.CO;2.
- 1146 Boehm, A. M., and M. M. Bell, 2021: Retrieved thermodynamic structure of Hurricane Rita
1147 (2005) from airborne multi-doppler radar data. *J. Atmos. Sci.*, **78** (5), 1583–1605, [https://doi.org/](https://doi.org/10.1175/jas-d-20-0195.1)
1148 10.1175/jas-d-20-0195.1, URL <https://doi.org/10.1175/jas-d-20-0195.1>.
- 1149 Braun, S. A., M. T. Montgomery, and Z. Pu, 2006: High-resolution simulation of Hurricane
1150 Bonnie (1998). Part I: The organization of eyewall vertical motion. *J. Atmos. Sci.*, **63** (1), 19–42,
1151 <https://doi.org/10.1175/jas3598.1>, URL <https://doi.org/10.1175/jas3598.1>.
- 1152 Braun, S. A., J. A. Sippel, and D. S. Nolan, 2012: The impact of dry midlevel air on hurricane
1153 intensity in idealized simulations with no mean flow. *J. Atmos. Sci.*, **69**, 236–257, [https://doi.org/](https://doi.org/10.1175/JAS-D-10-05007.1)
1154 10.1175/JAS-D-10-05007.1.
- 1155 Bukunt, B. P., and G. M. Barnes, 2015: The subtropical jet stream delivers the coup de grÃ¢ce
1156 to Hurricane Felicia (2009). *Wea. Forecasting*, **30** (4), 1039–1049, [https://doi.org/10.1175/](https://doi.org/10.1175/WAF-D-15-0004.1)
1157 WAF-D-15-0004.1, URL <http://journals.ametsoc.org/doi/abs/10.1175/WAF-D-15-0004.1>.
- 1158 Cecil, D. J., 2007: Satellite-derived rain rates in vertically sheared tropical cyclones. *Geophys.*
1159 *Res. Lett.*, **34** (2), <https://doi.org/10.1029/2006GL027942>, URL [http://doi.wiley.com/10.1029/](http://doi.wiley.com/10.1029/2006GL027942)
1160 2006GL027942.
- 1161 Chen, H., and S. G. Gopalakrishnan, 2015: A study on the asymmetric rapid intensification of
1162 Hurricane Earl (2010) using the HWRF system. *J. Atmos. Sci.*, **72** (2), 531–550, <https://doi.org/>

- 1163 10.1175/JAS-D-14-0097.1, URL [http://journals.ametsoc.org/doi/abs/10.1175/JAS-D-14-0097.](http://journals.ametsoc.org/doi/abs/10.1175/JAS-D-14-0097.1)
1164 1.
- 1165 Chen, S. S., J. A. Knaff, and F. D. Marks, 2006: Effects of vertical wind shear and storm motion
1166 on tropical cyclone rainfall asymmetries deduced from TRMM. *Mon. Wea. Rev.*, **134** (11),
1167 3190–3208, <https://doi.org/10.1175/MWR3245.1>.
- 1168 Chen, B.-F., C. A. Davis, and Y.-H. Kuo, 2018: Effects of low-level flow orientation and vertical
1169 shear on the structure and intensity of tropical cyclones. *Mon. Wea. Rev.*, **146** (8), 2447–2467,
1170 <https://doi.org/10.1175/mwr-d-17-0379.1>, URL <https://doi.org/10.1175/mwr-d-17-0379.1>.
- 1171 Chen, B.-F., C. A. Davis, and Y.-H. Kuo, 2019: An idealized numerical study of shear-relative
1172 low-level mean flow on tropical cyclone intensity and size. *J. Atmos. Sci.*, **76** (8), 2309–2334,
1173 <https://doi.org/10.1175/jas-d-18-0315.1>, URL <https://doi.org/10.1175/jas-d-18-0315.1>.
- 1174 Chen, B.-F., C. A. Davis, and Y.-H. Kuo, 2021: Examination of the combined effect of deep-
1175 layer vertical shear direction and lower-tropospheric mean flow on tropical cyclone intensity
1176 and size based on the ERA5 reanalysis. *Mon. Wea. Rev.*, **149** (12), 4057–4076, [https://doi.org/](https://doi.org/10.1175/mwr-d-21-0120.1)
1177 [10.1175/mwr-d-21-0120.1](https://doi.org/10.1175/mwr-d-21-0120.1), URL <https://doi.org/10.1175/mwr-d-21-0120.1>.
- 1178 Chen, X., J.-F. Gu, J. A. Zhang, F. D. Marks, R. F. Rogers, and J. J. Cione, 2021: Boundary layer
1179 recovery and precipitation symmetrization preceding rapid intensification of tropical cyclones
1180 under shear. *J. Atmos. Sci.*, **78** (5), 1523–1544, <https://doi.org/10.1175/jas-d-20-0252.1>, URL
1181 <https://doi.org/10.1175/jas-d-20-0252.1>.
- 1182 Chen, X., Y. Wang, J. Fang, and M. Xue, 2018a: A numerical study on rapid intensification of
1183 Typhoon Vicente (2012) in the South China Sea. Part II: Roles of inner-core processes. *J. Atmos.*
1184 *Sci.*, **75** (1), 235–255, <https://doi.org/10.1175/JAS-D-17-0129.1>, URL [http://journals.ametsoc.](http://journals.ametsoc.org/doi/10.1175/JAS-D-17-0129.1)
1185 [org/doi/10.1175/JAS-D-17-0129.1](http://journals.ametsoc.org/doi/10.1175/JAS-D-17-0129.1).
- 1186 Chen, X., M. Xue, and J. Fang, 2018b: Rapid intensification of Typhoon Mujigae (2015) under
1187 different sea surface temperatures: Structural changes leading to rapid intensification. *J. Atmos.*
1188 *Sci.*, **75**, 4313–4335, <https://doi.org/10.1175/JAS-D-18-0017.1>.

- 1189 Chen, X., J. A. Zhang, and F. D. Marks, 2019: A thermodynamic pathway leading to rapid inten-
1190 sification of tropical cyclones in shear. *Geophys. Res. Lett.*, **46** (15), 9241–9251, [https://doi.org/](https://doi.org/10.1029/2019gl083667)
1191 10.1029/2019gl083667, URL <https://doi.org/10.1029/2019gl083667>.
- 1192 Corbosiero, K. L., and J. Molinari, 2002: The effects of vertical wind shear on the distribution of
1193 convection in tropical cyclones. *Mon. Wea. Rev.*, **130** (8), 2110–2123, [https://doi.org/10.1175/](https://doi.org/10.1175/1520-0493(2002)130<2110:TEOVWS>2.0.CO;2)
1194 1520-0493(2002)130<2110:TEOVWS>2.0.CO;2.
- 1195 Corbosiero, K. L., and J. Molinari, 2003: The relationship between storm motion, vertical
1196 wind shear, and convective asymmetries in tropical cyclones. *J. Atmos. Sci.*, **60** (2), 366–
1197 376, [https://doi.org/10.1175/1520-0469\(2003\)060<0366:trbsmv>2.0.co;2](https://doi.org/10.1175/1520-0469(2003)060<0366:trbsmv>2.0.co;2), URL [https://doi.org/](https://doi.org/10.1175/1520-0469(2003)060<0366:trbsmv>2.0.co;2)
1198 10.1175/1520-0469(2003)060<0366:trbsmv>2.0.co;2.
- 1199 Cram, T. A., J. Persing, M. T. Montgomery, and S. A. Braun, 2007: A Lagrangian trajectory
1200 view on transport and mixing processes between the eye, eyewall, and environment using
1201 a high-resolution simulation of Hurricane Bonnie (1998). *J. Atmos. Sci.*, **64** (6), 1835–1856,
1202 <https://doi.org/10.1175/JAS3921.1>, URL [http://journals.ametsoc.org/doi/abs/10.1175/JAS3921.](http://journals.ametsoc.org/doi/abs/10.1175/JAS3921.1)
1203 1.
- 1204 Dai, Y., S. J. Majumdar, and D. S. Nolan, 2021: Tropical cyclone resistance to strong environmental
1205 shear. *J. Atmos. Sci.*, **78** (4), 1275–1293, <https://doi.org/10.1175/jas-d-20-0231.1>, URL <https://doi.org/10.1175/jas-d-20-0231.1>.
1206 <https://doi.org/10.1175/jas-d-20-0231.1>.
- 1207 Davis, C. A., and D. A. Ahijevych, 2012: Mesoscale structural evolution of three tropical weather
1208 systems observed during PREDICT. *J. Atmos. Sci.*, **69** (4), 1284–1305, [https://doi.org/10.1175/](https://doi.org/10.1175/JAS-D-11-0225.1)
1209 JAS-D-11-0225.1.
- 1210 Davis, C. A., S. C. Jones, and M. Riemer, 2008: Hurricane vortex dynamics during Atlantic
1211 extratropical transition. *J. Atmos. Sci.*, **65** (3), 714–736, <https://doi.org/10.1175/2007JAS2488.1>,
1212 URL <http://journals.ametsoc.org/doi/abs/10.1175/2007JAS2488.1>.
- 1213 DeHart, J. C., R. A. Houze, and R. F. Rogers, 2014: Quadrant distribution of tropical cyclone
1214 inner-core kinematics in relation to environmental shear. *J. Atmos. Sci.*, **71** (7), 2713–2732,
1215 <https://doi.org/10.1175/JAS-D-13-0298.1>.

- 1216 DeMaria, M., 1996: The effect of vertical shear on tropical cyclone intensity change. *J. Atmos. Sci.*,
1217 **53 (14)**, 2076–2088, [https://doi.org/10.1175/1520-0469\(1996\)053<2076:TEOVSO>2.0.CO;2](https://doi.org/10.1175/1520-0469(1996)053<2076:TEOVSO>2.0.CO;2).
- 1218 DeMaria, M., and J. Kaplan, 1994: A Statistical Hurricane Intensity Prediction Scheme (SHIPS) for
1219 the Atlantic basin. *Wea. Forecasting*, **9 (2)**, 209–220, [https://doi.org/10.1175/1520-0434\(1994\)](https://doi.org/10.1175/1520-0434(1994)009<0209:ASHIPS>2.0.CO;2)
1220 [009<0209:ASHIPS>2.0.CO;2](https://doi.org/10.1175/1520-0434(1994)009<0209:ASHIPS>2.0.CO;2), URL [http://journals.ametsoc.org/doi/abs/10.1175/1520-0434%](http://journals.ametsoc.org/doi/abs/10.1175/1520-0434%281994%29009%3C0209%3AASHIPS%3E2.0.CO%3B2)
1221 [281994%29009%3C0209%3AASHIPS%3E2.0.CO%3B2](http://journals.ametsoc.org/doi/abs/10.1175/1520-0434%281994%29009%3C0209%3AASHIPS%3E2.0.CO%3B2).
- 1222 DeMaria, M., and J. Kaplan, 1999: An updated Statistical Hurricane Intensity Predic-
1223 tion Scheme (SHIPS) for the Atlantic and Eastern North Pacific basins. *Wea. Forecast-*
1224 *ing*, **14 (3)**, 326–337, [https://doi.org/10.1175/1520-0434\(1999\)014<0326:AUSHIP>2.0.CO;](https://doi.org/10.1175/1520-0434(1999)014<0326:AUSHIP>2.0.CO;2)
1225 [2](https://doi.org/10.1175/1520-0434(1999)014<0326:AUSHIP>2.0.CO;2), URL [http://journals.ametsoc.org/doi/abs/10.1175/1520-0434%](http://journals.ametsoc.org/doi/abs/10.1175/1520-0434%281999%29014%3C0326%3AAUSHIP%3E2.0.CO%3B2)
1226 [281999%29014%3C0326%](http://journals.ametsoc.org/doi/abs/10.1175/1520-0434%281999%29014%3C0326%3AAUSHIP%3E2.0.CO%3B2)
[3AAUSHIP%3E2.0.CO%3B2](http://journals.ametsoc.org/doi/abs/10.1175/1520-0434%281999%29014%3C0326%3AAUSHIP%3E2.0.CO%3B2).
- 1227 DeMaria, M., M. Mainelli, L. K. Shay, J. A. Knaff, and J. Kaplan, 2005: Further improve-
1228 ments to the Statistical Hurricane Intensity Prediction Scheme (SHIPS). *Wea. Forecasting*,
1229 **20 (4)**, 531–543, <https://doi.org/10.1175/WAF862.1>, URL [http://journals.ametsoc.org/doi/abs/](http://journals.ametsoc.org/doi/abs/10.1175/WAF862.1)
1230 [10.1175/WAF862.1](http://journals.ametsoc.org/doi/abs/10.1175/WAF862.1).
- 1231 Didlake, A. C., and R. A. Houze, 2009: Convective-scale downdrafts in the principal rainband
1232 of Hurricane Katrina (2005). *Mon. Wea. Rev.*, **137 (10)**, 3269–3293, [https://doi.org/10.1175/](https://doi.org/10.1175/2009MWR2827.1)
1233 [2009MWR2827.1](https://doi.org/10.1175/2009MWR2827.1).
- 1234 Didlake, A. C., and R. A. Houze, 2013: Convective-scale variations in the inner-core rainbands of
1235 tropical cyclones. *J. Atmos. Sci.*, **70 (2)**, 504–523, <https://doi.org/10.1175/JAS-D-12-0134.1>.
- 1236 Didlake, A. C., and M. R. Kumjian, 2018: Examining storm asymmetries in Hurricane Irma
1237 (2017) using polarimetric radar observations. *Geophys. Res. Lett.*, **45 (24)**, [https://doi.org/10.](https://doi.org/10.1029/2018gl080739)
1238 [1029/2018gl080739](https://doi.org/10.1029/2018gl080739), URL <https://doi.org/10.1029/2018gl080739>.
- 1239 Didlake, A. C., P. D. R. Reasor, R. F. Rogers, and W.-C. Lee, 2018: Dynamics of the transition
1240 from spiral rainbands to a secondary eyewall in Hurricane Earl (2010). *J. Atmos. Sci.*, **75 (9)**,
1241 [2909–2929](https://doi.org/10.1175/JAS-D-17-0348.1), <https://doi.org/10.1175/JAS-D-17-0348.1>.
- 1242 Dunion, J. P., 2011: Rewriting the climatology of the tropical North Atlantic and Caribbean Sea
1243 atmosphere. *J. Climate*, **24**, 893–908, <https://doi.org/10.1175/2010jcli3496.1>.

- 1244 Elsberry, R. L., and R. A. Jeffries, 1996: Vertical Wind Shear Influences on Tropical Cyclone For-
1245 mation and Intensification during TCM-92 and TCM-93. *Mon. Wea. Rev.*, **124** (7), 1374–1387,
1246 [https://doi.org/10.1175/1520-0493\(1996\)124<1374:VWSIOT>2.0.CO;2](https://doi.org/10.1175/1520-0493(1996)124<1374:VWSIOT>2.0.CO;2), URL [http://journals.ametsoc.org/doi/abs/10.1175/1520-0493\(1996\)124%3C1374%3AVWSIOT%3E2.0.CO%3B2](http://journals.ametsoc.org/doi/abs/10.1175/1520-0493(1996)124%3C1374%3AVWSIOT%3E2.0.CO%3B2).
- 1248 Emanuel, K., 2003: Tropical cyclones. *Annu. Rev. Fluid Mech.*, **31** (1), 75–104, <https://doi.org/10.1146/annurev.earth.31.100901.141259>, URL <https://doi.org/10.1146/annurev.earth.31.100901.141259>.
- 1251 Emanuel, K., 2018: 100 years of progress in tropical cyclone research. *Meteor. Monogr.*,
1252 **59**, 15.1–15.68, <https://doi.org/10.1175/amsmonographs-d-18-0016.1>, URL <https://doi.org/10.1175/amsmonographs-d-18-0016.1>.
- 1254 Emanuel, K., C. DesAutels, C. Holloway, and R. Korty, 2004: Environmental Control of Tropical
1255 Cyclone Intensity. *J. Atmos. Sci.*, **61** (7), 843–858, [https://doi.org/10.1175/1520-0469\(2004\)061<0843:ECOTCI>2.0.CO;2](https://doi.org/10.1175/1520-0469(2004)061<0843:ECOTCI>2.0.CO;2).
- 1257 Emanuel, K. A., 1989: The finite-amplitude nature of tropical cyclogenesis. *J. Atmos. Sci.*, **46**,
1258 3431–3456, [https://doi.org/10.1175/1520-0469\(1989\)046<3431:tfanot>2.0.co;2](https://doi.org/10.1175/1520-0469(1989)046<3431:tfanot>2.0.co;2).
- 1259 Feng, Y.-C., and M. M. Bell, 2019: Microphysical characteristics of an asymmetric eyewall in
1260 major Hurricane Harvey (2017). *Geophys. Res. Lett.*, **46** (1), 461–471, <https://doi.org/10.1029/2018gl080770>, URL <https://doi.org/10.1029/2018gl080770>.
- 1262 Finocchio, P. M., and S. J. Majumdar, 2017a: The Predictability of Idealized Tropical Cy-
1263 clones in Environments with Time-Varying Vertical Wind Shear. *J. Adv. Model. Earth Syst.*,
1264 <https://doi.org/10.1002/2017MS001168>, URL <http://doi.wiley.com/10.1002/2017MS001168>.
- 1265 Finocchio, P. M., and S. J. Majumdar, 2017b: A Statistical Perspective on Wind Profiles and
1266 Vertical Wind Shear in Tropical Cyclone Environments of the Northern Hemisphere. *Mon. Wea. Rev.*, **145** (1), 361–378, <https://doi.org/10.1175/MWR-D-16-0221.1>, URL <http://journals.ametsoc.org/doi/10.1175/MWR-D-16-0221.1>.
- 1269 Finocchio, P. M., S. J. Majumdar, D. S. Nolan, and M. Iskandarani, 2016: Idealized Tropical
1270 Cyclone Responses to the Height and Depth of Environmental Vertical Wind Shear. *Mon. Wea.*

1271 *Rev.*, **144** (6), 2155–2175, <https://doi.org/10.1175/MWR-D-15-0320.1>, URL [http://journals.](http://journals.ametsoc.org/doi/full/10.1175/MWR-D-15-0320.1)
1272 [ametsoc.org/doi/full/10.1175/MWR-D-15-0320.1](http://journals.ametsoc.org/doi/full/10.1175/MWR-D-15-0320.1).

1273 Finocchio, P. M., and R. Rios-Berrios, 2021: The intensity- and size-dependent response of tropical
1274 cyclones to increasing vertical wind shear. *J. Atmos. Sci.*, [https://doi.org/10.1175/jas-d-21-0126.](https://doi.org/10.1175/jas-d-21-0126.1)
1275 [1](https://doi.org/10.1175/jas-d-21-0126.1), URL <https://doi.org/10.1175/jas-d-21-0126.1>.

1276 Fischer, M. S., P. D. Reasor, R. F. Rogers, and J. F. Gamache, 2022: An analysis of tropical cyclone
1277 vortex and convective characteristics in relation to storm intensity using a novel airborne doppler
1278 radar database. *Mon. Wea. Rev.*, **150** (9), 2255–2278, <https://doi.org/10.1175/mwr-d-21-0223.1>,
1279 URL <https://doi.org/10.1175/mwr-d-21-0223.1>.

1280 Fischer, M. S., P. D. Reasor, B. H. Tang, K. L. Corbosiero, R. D. Torn, and X. Chen, 2023a:
1281 A tale of two vortex evolutions: Using a high-resolution ensemble to assess the impacts of
1282 ventilation on a tropical cyclone rapid intensification event. *Mon. Wea. Rev.*, **151** (1), 297–320,
1283 <https://doi.org/10.1175/mwr-d-22-0037.1>, URL <https://doi.org/10.1175/mwr-d-22-0037.1>.

1284 Fischer, M. S., R. Rogers, P. Reasor, and J. Dunion, 2023b: The relationship between tropical
1285 cyclone vortex tilt, precipitation structure, and intensity change. *Mon. Wea. Rev.*

1286 Fischer, M. S., B. H. Tang, K. L. Corbosiero, and C. M. Rozoff, 2018: Normalized convective
1287 characteristics of tropical cyclone rapid intensification events in the North Atlantic and Eastern
1288 North Pacific. *Mon. Wea. Rev.*, **146** (4), 1133–1155, <https://doi.org/10.1175/mwr-d-17-0239.1>,
1289 URL <https://doi.org/10.1175/mwr-d-17-0239.1>.

1290 Flatau, M., W. H. Schubert, and D. E. Stevens, 1994: The role of baroclinic processes
1291 in tropical cyclone motion: The influence of vertical tilt. *J. Atmos. Sci.*, **51** (18), 2589–
1292 2601, [https://doi.org/10.1175/1520-0469\(1994\)051<2589:trobpi>2.0.co;2](https://doi.org/10.1175/1520-0469(1994)051<2589:trobpi>2.0.co;2), URL [https://doi.org/](https://doi.org/10.1175/1520-0469(1994)051<2589:trobpi>2.0.co;2)
1293 [10.1175/1520-0469\(1994\)051<2589:trobpi>2.0.co;2](https://doi.org/10.1175/1520-0469(1994)051<2589:trobpi>2.0.co;2).

1294 Foerster, A. M., M. M. Bell, P. A. Harr, and S. C. Jones, 2014: Observations of the eyewall
1295 structure of Typhoon Sinlaku (2008) during the transformation stage of extratropical transition.
1296 *Mon. Wea. Rev.*, **142** (9), 3372–3392, <https://doi.org/10.1175/MWR-D-13-00313.1>.

1297 Frank, W. M., and E. A. Ritchie, 1999: Effects of Environmental Flow upon Tropical Cyclone Struc-
1298 ture. *Mon. Wea. Rev.*, **127** (9), 2044–2061, [https://doi.org/10.1175/1520-0493\(1999\)127<2044:](https://doi.org/10.1175/1520-0493(1999)127<2044:)

- 1299 EOEUFUT>2.0.CO;2, URL <http://journals.ametsoc.org/doi/abs/10.1175/1520-0493%281999%29127%3C2044%3AEOEFUT%3E2.0.CO%3B2>.
- 1301 Frank, W. M., and E. A. Ritchie, 2001: Effects of Vertical Wind Shear on the Intensity and Structure
1302 of Numerically Simulated Hurricanes. *Mon. Wea. Rev.*, **129** (9), 2249–2269, [https://doi.org/10.1175/1520-0493\(2001\)129<2249:EOVWSO>2.0.CO;2](https://doi.org/10.1175/1520-0493(2001)129<2249:EOVWSO>2.0.CO;2), URL <http://journals.ametsoc.org/doi/abs/10.1175/1520-0493%282001%29129%3C2249%3AEOVWSO%3E2.0.CO%3B2>.
- 1305 Fu, H., Y. Wang, M. Riemer, and Q. Li, 2019: Effect of unidirectional vertical wind shear on
1306 tropical cyclone intensity change—lower-layer shear versus upper-layer shear. *J. Geophys. Res. Atmos.*, **124** (12), 6265–6282, <https://doi.org/10.1029/2019jd030586>, URL <https://doi.org/10.1029/2019jd030586>.
- 1309 Galarneau, T. J., and C. A. Davis, 2013: Diagnosing Forecast Errors in Tropical Cyclone Motion.
1310 *Mon. Wea. Rev.*, **141** (2), 405–430, <https://doi.org/10.1175/MWR-D-12-00071.1>.
- 1311 Gao, S., S. Zhai, B. Chen, and T. Li, 2017: Water budget and intensity change of tropical
1312 cyclones over the Western North Pacific. *Mon. Wea. Rev.*, **145** (8), 3009–3023, <https://doi.org/10.1175/mwr-d-17-0033.1>, URL <https://doi.org/10.1175/mwr-d-17-0033.1>.
- 1314 Ge, X., T. Li, and M. Peng, 2013: Effects of vertical shears and midlevel dry air on tropical cyclone
1315 developments. *J. Atmos. Sci.*, **70** (12), 3859–3875, <https://doi.org/10.1175/JAS-D-13-066.1>.
- 1316 Gray, W. M., 1968: Global View of the Origin of Tropical Disturbances and Storms. *Mon. Wea. Rev.*, **96** (10), 669–700.
- 1318 Gu, J.-F., Z.-M. Tan, and X. Qiu, 2016: Quadrant-dependent evolution of low-level tangential
1319 wind of a tropical cyclone in the shear flow. *J. Atmos. Sci.*, **73** (3), 1159–1177, <https://doi.org/10.1175/jas-d-15-0165.1>, URL <https://doi.org/10.1175/jas-d-15-0165.1>.
- 1321 Gu, J.-F., Z.-M. Tan, and X. Qiu, 2018: The evolution of vortex tilt and vertical motion of
1322 tropical cyclones in directional shear flows. *J. Atmos. Sci.*, **75** (10), 3565–3578, <https://doi.org/10.1175/jas-d-18-0024.1>, URL <https://doi.org/10.1175/jas-d-18-0024.1>.
- 1324 Gu, J.-F., Z.-M. Tan, and X. Qiu, 2019: Intensification variability of tropical cyclones in directional
1325 shear flows: Vortex tilt–convection coupling. *J. Atmos. Sci.*, **76** (6), 1827–1844, <https://doi.org/10.1175/jas-d-18-0282.1>, URL <https://doi.org/10.1175/jas-d-18-0282.1>.

- 1327 Guimond, S. R., G. M. Heymsfield, P. D. Reasor, and A. C. Didlake, 2016: The rapid intensification
1328 of Hurricane Karl (2010): New remote sensing observations of convective bursts from the global
1329 hawk platform. *J. Atmos. Sci.*, **73** (9), 3617–3639, <https://doi.org/10.1175/jas-d-16-0026.1>, URL
1330 <https://doi.org/10.1175/jas-d-16-0026.1>.
- 1331 Guimond, S. R., G. M. Heymsfield, and F. J. Turk, 2010: Multiscale observations of Hurricane
1332 Dennis (2005): The effects of hot towers on rapid intensification. *J. Atmos. Sci.*, **67** (3), 633–654,
1333 <https://doi.org/10.1175/2009jas3119.1>, URL <https://doi.org/10.1175/2009jas3119.1>.
- 1334 Harnos, D. S., and S. W. Nesbitt, 2011: Convective structure in rapidly intensifying tropical
1335 cyclones as depicted by passive microwave measurements. *Geophys. Res. Lett.*, **38** (7), n/a–n/a,
1336 <https://doi.org/10.1029/2011gl047010>, URL <https://doi.org/10.1029/2011gl047010>.
- 1337 Harnos, D. S., and S. W. Nesbitt, 2016: Passive microwave quantification of tropical cyclone inner-
1338 core cloud populations relative to subsequent intensity change. *Mon. Wea. Rev.*, **144** (11), 4461–
1339 4482, <https://doi.org/10.1175/mwr-d-15-0090.1>, URL [https://doi.org/10.1175/mwr-d-15-0090.](https://doi.org/10.1175/mwr-d-15-0090.1)
1340 1.
- 1341 Hazelton, A. T., R. E. Hart, and R. F. Rogers, 2017: Analyzing simulated convective bursts in two
1342 Atlantic hurricanes. Part II: Intensity change due to bursts. *Mon. Wea. Rev.*, **145** (8), 3095–3117,
1343 <https://doi.org/10.1175/mwr-d-16-0268.1>, URL <https://doi.org/10.1175/mwr-d-16-0268.1>.
- 1344 Hazelton, A. T., X. Zhang, S. Gopalakrishnan, W. Ramstrom, F. Marks, and J. A. Zhang, 2020:
1345 High-resolution ensemble HFV3 forecasts of Hurricane Michael (2018): Rapid intensification
1346 in shear. *Mon. Wea. Rev.*, **148** (5), 2009–2032, <https://doi.org/10.1175/mwr-d-19-0275.1>, URL
1347 <https://doi.org/10.1175/mwr-d-19-0275.1>.
- 1348 Helms, C. N., and R. E. Hart, 2015: The evolution of dropsonde-derived kinematic and thermo-
1349 dynamic structures in developing and nondeveloping Atlantic tropical convective systems. *Mon.*
1350 *Wea. Rev.*, **143**, 3109–3135, <https://doi.org/10.1175/MWR-D-14-00242.1>.
- 1351 Hence, D. A., and R. A. Houze, 2008: Kinematic structure of convective-scale elements in the
1352 rainbands of Hurricanes Katrina and Rita (2005). *J. Geophys. Res.*, **113**, D15 108, [https://doi.org/](https://doi.org/10.1029/2007JD009429)
1353 [10.1029/2007JD009429](https://doi.org/10.1029/2007JD009429).

- 1354 Hence, D. A., and R. A. Houze, 2011: Vertical structure of hurricane eyewalls as seen by the TRMM
1355 Precipitation Radar. *J. Atmos. Sci.*, **68** (8), 1637–1652, <https://doi.org/10.1175/2011JAS3578.1>,
1356 URL <http://journals.ametsoc.org/doi/abs/10.1175/2011JAS3578.1>.
- 1357 Hendricks, E. A., M. T. Montgomery, and C. A. Davis, 2004: The Role of Vortical Hot Towers in the
1358 Formation of Tropical Cyclone Diana (1984). *J. Atmos. Sci.*, **61** (11), 1209–1232, [https://doi.org/10.1175/1520-0469\(2004\)061<1209:TROVHT>2.0.CO;2](https://doi.org/10.1175/1520-0469(2004)061<1209:TROVHT>2.0.CO;2), URL <http://journals.ametsoc.org/doi/abs/10.1175/1520-0469%282004%29061%3C1209%3ATROVHT%3E2.0.CO%3B2>.
- 1361 Heymsfield, G. M., J. B. Halverson, J. Simpson, L. Tian, and T. P. Bui, 2001: ER-2 Doppler
1362 Radar Investigations of the Eyewall of Hurricane Bonnie during the Convection and Moisture
1363 Experiment-3. *J. Appl. Meteor.*, **40** (8), 1310–1330, [https://doi.org/10.1175/1520-0450\(2001\)
1364 040<1310:EDRIOT>2.0.CO;2](https://doi.org/10.1175/1520-0450(2001)040<1310:EDRIOT>2.0.CO;2), URL [http://journals.ametsoc.org/doi/abs/10.1175/1520-0450%
1365 282001%29040%3C1310%3AEDRIOT%3E2.0.CO%3B2](http://journals.ametsoc.org/doi/abs/10.1175/1520-0450%282001%29040%3C1310%3AEDRIOT%3E2.0.CO%3B2).
- 1366 Hill, K. A., and G. M. Lackmann, 2009: Influence of environmental humidity on tropical cyclone
1367 size. *Mon. Wea. Rev.*, **137**, 3294–3315, <https://doi.org/10.1175/2009mwr2679.1>.
- 1368 Hogsett, W. A., and S. R. Stewart, 2013: Dynamics of tropical cyclone intensification: Deep
1369 convective cyclonic “left movers”. *J. Atmos. Sci.*, **71** (1), 226–242, [https://doi.org/10.1175/
1370 jas-d-12-0284.1](https://doi.org/10.1175/jas-d-12-0284.1), URL <https://doi.org/10.1175/jas-d-12-0284.1>.
- 1371 Jiang, H., and E. M. Ramirez, 2013: Necessary Conditions for Tropical Cyclone Rapid In-
1372 tensification as Derived from 11 Years of TRMM Data. *J. Climate*, **26** (17), 6459–6470,
1373 <https://doi.org/10.1175/JCLI-D-12-00432.1>, URL [http://journals.ametsoc.org/doi/abs/10.1175/
1374 JCLI-D-12-00432.1](http://journals.ametsoc.org/doi/abs/10.1175/JCLI-D-12-00432.1).
- 1375 Jones, S. C., 1995: The Evolution of Vortices in Vertical Shear. I: Initially Barotropic Vortices.
1376 *Quart. J. Roy. Meteor.*, **121** (524), 821–851, <https://doi.org/10.1002/qj.49712152406>.
- 1377 Jones, S. C., 2000a: The Evolution of Vortices in Vertical Shear. II: Large-Scale Asymmetries.
1378 *Q. J. Roy. Meteor. Soc.*, **126** (570), 3137–3159, <https://doi.org/10.1002/qj.49712657008>, URL
1379 <http://doi.wiley.com/10.1002/qj.49712657008>.

- 1380 Jones, S. C., 2000b: The evolution of vortices in vertical shear. III: Baroclinic vortices. *Q.*
1381 *J. Roy. Meteor. Soc.*, **126 (570)**, 3161–3185, <https://doi.org/10.1002/qj.49712657009>, URL
1382 <http://doi.wiley.com/10.1002/qj.49712657009>.
- 1383 Jones, S. C., 2004: On the Ability of Dry Tropical-Cyclone-like Vortices to Withstand Vertical
1384 Shear. *J. Atmos. Sci.*, **61 (1)**, 114–119, [https://doi.org/10.1175/1520-0469\(2004\)061<0114:
1385 OTAODT>2.0.CO;2](https://doi.org/10.1175/1520-0469(2004)061<0114:OTAODT>2.0.CO;2), URL [http://journals.ametsoc.org/doi/abs/10.1175/1520-0469%
282004%29061%3C0114%3AOTAODT%3E2.0.CO%3B2](http://journals.ametsoc.org/doi/abs/10.1175/1520-0469%282004%
1386 29061%3C0114%3AOTAODT%3E2.0.CO%3B2).
- 1387 Jordan, C. L., 1958: Mean soundings for the West Indies area. *J. Meteor.*, **15**, 91–97, [https://doi.org/
1388 10.1175/1520-0469\(1958\)015<0091:msftwi>2.0.co;2](https://doi.org/10.1175/1520-0469(1958)015<0091:msftwi>2.0.co;2).
- 1389 Judt, F., S. S. Chen, and J. Berner, 2016: Predictability of tropical cyclone intensity: Scale-
1390 dependent forecast error growth in high-resolution stochastic kinetic-energy backscatter en-
1391 sembles. *Q. J. Roy. Meteor. Soc.*, **142 (694)**, 43–57, <https://doi.org/10.1002/qj.2626>, URL
1392 <http://doi.wiley.com/10.1002/qj.2626>.
- 1393 Juračić, A., and D. J. Raymond, 2016: The effects of moist entropy and moisture budgets on
1394 tropical cyclone development. *J. Geophys. Res. Atmos.*, **121 (16)**, 9458–9473, [https://doi.org/
1395 10.1002/2016jd025065](https://doi.org/10.1002/2016jd025065), URL <https://doi.org/10.1002/2016jd025065>.
- 1396 Kimball, S. K., 2006: A modeling study of hurricane landfall in a dry environment. *Mon. Wea.*
1397 *Rev.*, **134**, 1901–1918, <https://doi.org/10.1175/mwr3155.1>.
- 1398 Komaromi, W. A., 2013: An investigation of composite dropsonde profiles for developing and
1399 nondeveloping tropical waves during the 2010 PREDICT field campaign. *J. Atmos. Sci.*, **70**,
1400 542–558, <https://doi.org/10.1175/jas-d-12-052.1>.
- 1401 Komaromi, W. A., and S. J. Majumdar, 2014: Ensemble-based error and predictability metrics asso-
1402 ciated with tropical cyclogenesis. Part I: Basinwide perspective. *Mon. Wea. Rev.*, **142 (8)**, 2879–
1403 2898, <https://doi.org/10.1175/MWR-D-13-00370.1>, URL [http://journals.ametsoc.org/doi/abs/
10.1175/MWR-D-13-00370.1](http://journals.ametsoc.org/doi/abs/
1404 10.1175/MWR-D-13-00370.1).
- 1405 Komaromi, W. A., and S. J. Majumdar, 2015: Ensemble-based error and predictability met-
1406 rics associated with tropical cyclogenesis. Part II: Wave-relative framework. *Mon. Wea.*

1407 *Rev.*, **143** (5), 1665–1686, <https://doi.org/10.1175/MWR-D-14-00286.1>, URL [http://journals.](http://journals.ametsoc.org/doi/abs/10.1175/MWR-D-14-00286.1)
1408 [ametsoc.org/doi/abs/10.1175/MWR-D-14-00286.1](http://journals.ametsoc.org/doi/abs/10.1175/MWR-D-14-00286.1).

1409 Kossin, J. P., and W. H. Schubert, 2001: Mesovortices, polygonal flow patterns, and rapid pressure
1410 falls in hurricane-like vortices. *J. Atmos. Sci.*, **58** (15), 2196–2209, [https://doi.org/10.1175/](https://doi.org/10.1175/1520-0469(2001)058<2196:mpfpar>2.0.co;2)
1411 [1520-0469\(2001\)058<2196:mpfpar>2.0.co;2](https://doi.org/10.1175/1520-0469(2001)058<2196:mpfpar>2.0.co;2), URL [https://doi.org/10.1175/1520-0469\(2001\)](https://doi.org/10.1175/1520-0469(2001)058<2196:mpfpar>2.0.co;2)
1412 [058<2196:mpfpar>2.0.co;2](https://doi.org/10.1175/1520-0469(2001)058<2196:mpfpar>2.0.co;2).

1413 Kurihara, Y., M. A. Bender, and R. J. Ross, 1993: An Initialization Scheme of Hurricane Mod-
1414 els by Vortex Specification. *Mon. Wea. Rev.*, **121** (7), 2030–2045, [https://doi.org/10.1175/](https://doi.org/10.1175/1520-0493(1993)121<2030:AISOHM>2.0.CO;2)
1415 [1520-0493\(1993\)121<2030:AISOHM>2.0.CO;2](https://doi.org/10.1175/1520-0493(1993)121<2030:AISOHM>2.0.CO;2), URL [http://journals.ametsoc.org/doi/abs/10.](http://journals.ametsoc.org/doi/abs/10.1175/1520-0493(1993)121%3C2030%3AAISOHM%3E2.0.CO%3B2)
1416 [1175/1520-0493\(1993\)121%3C2030%3AAISOHM%3E2.0.CO%3B2](http://journals.ametsoc.org/doi/abs/10.1175/1520-0493(1993)121%3C2030%3AAISOHM%3E2.0.CO%3B2).

1417 Kwon, Y. C., and W. M. Frank, 2005: Dynamic instabilities of simulated hurricane-like vortices
1418 and their impacts on the core structure of hurricanes. Part I: Dry experiments. *J. Atmos. Sci.*,
1419 **62** (11), 3955–3973, <https://doi.org/10.1175/jas3575.1>, URL <https://doi.org/10.1175/jas3575.1>.

1420 Kwon, Y. C., and W. M. Frank, 2008: Dynamic instabilities of simulated hurricane-like vortices
1421 and their impacts on the core structure of hurricanes. Part II: Moist experiments. *J. Atmos. Sci.*,
1422 **65** (1), 106–122, <https://doi.org/10.1175/2007JAS2132.1>, URL [http://journals.ametsoc.org/doi/](http://journals.ametsoc.org/doi/abs/10.1175/2007JAS2132.1)
1423 [abs/10.1175/2007JAS2132.1](http://journals.ametsoc.org/doi/abs/10.1175/2007JAS2132.1).

1424 Laurencin, C. N., A. C. Didlake, S. D. Loeffler, M. R. Kumjian, and G. M. Heymsfield, 2020:
1425 Hydrometeor size sorting in the asymmetric eyewall of Hurricane Matthew (2016). *J. Geo-*
1426 *phys. Res. Atmos.*, **125** (17), <https://doi.org/10.1029/2020jd032671>, URL [https://doi.org/10.](https://doi.org/10.1029/2020jd032671)
1427 [1029/2020jd032671](https://doi.org/10.1029/2020jd032671).

1428 Lee, T.-Y., C.-C. Wu, and R. Rios-Berrios, 2021: The role of low-level flow direction on tropical
1429 cyclone intensity changes in a moderate-sheared environment. *J. Atmos. Sci.*, [https://doi.org/](https://doi.org/10.1175/jas-d-20-0360.1)
1430 [10.1175/jas-d-20-0360.1](https://doi.org/10.1175/jas-d-20-0360.1), URL <https://doi.org/10.1175/jas-d-20-0360.1>.

1431 Leighton, H., S. Gopalakrishnan, J. A. Zhang, R. F. Rogers, Z. Zhang, and V. Tallapragada, 2018:
1432 Azimuthal Distribution of Deep Convection, Environmental Factors, and Tropical Cyclone
1433 Rapid Intensification: A Perspective from HWRP Ensemble Forecasts of Hurricane Edouard

- 1434 (2014). *J. Atmos. Sci.*, **75** (1), 275–295, <https://doi.org/10.1175/JAS-D-17-0171.1>, URL <http://journals.ametsoc.org/doi/10.1175/JAS-D-17-0171.1>.
- 1435
- 1436 Lonfat, M., F. D. Marks, and S. S. Chen, 2004: Precipitation Distribution in Tropical Cyclones
1437 Using the Tropical Rainfall Measuring Mission (TRMM) Microwave Imager: A Global Perspec-
1438 tive. *Mon. Wea. Rev.*, **132** (7), 1645–1660, [https://doi.org/10.1175/1520-0493\(2004\)132<1645:
1439 PDITCU>2.0.CO;2](https://doi.org/10.1175/1520-0493(2004)132<1645:PDITCU>2.0.CO;2), URL [http://journals.ametsoc.org/doi/abs/10.1175/1520-0493%
1440 29132%3C1645%3APDITCU%3E2.0.CO%3B2](http://journals.ametsoc.org/doi/abs/10.1175/1520-0493%282004%29132%3C1645%3APDITCU%3E2.0.CO%3B2).
- 1441 Lonfat, M., R. Rogers, T. Marchok, and F. D. Marks, 2007: A Parametric Model for Predicting
1442 Hurricane Rainfall. *Mon. Wea. Rev.*, **135** (9), 3086–3097, <https://doi.org/10.1175/MWR3433.1>,
1443 URL <http://journals.ametsoc.org/doi/abs/10.1175/MWR3433.1>.
- 1444 López, R. E., 1968: Investigation of the Important of Cumulus Convection and Ventilation in Early
1445 Tropical Storm Development. Atmospheric Sciences Paper No. 124, Dept. of Atmospheric
1446 Sciences, Colorado State University, Fort Collins, CO.
- 1447 Lorenz, E. N., 2006: Predictability – a problem partly solved. *Predictability of Weather and*
1448 *Climate*, Cambridge University Press, 40–58, <https://doi.org/10.1017/cbo9780511617652.004>,
1449 URL <https://doi.org/10.1017/cbo9780511617652.004>.
- 1450 Lu, P., N. Lin, K. Emanuel, D. Chavas, and J. Smith, 2018: Assessing Hurricane Rainfall Mecha-
1451 nisms Using a Physics-Based Model: Hurricanes Isabel (2003) and Irene (2011). *J. Atmos. Sci.*,
1452 **75** (7), 2337–2358, <https://doi.org/10.1175/JAS-D-17-0264.1>, URL [http://journals.ametsoc.org/
1453 doi/10.1175/JAS-D-17-0264.1](http://journals.ametsoc.org/doi/10.1175/JAS-D-17-0264.1).
- 1454 Marks, F. D., R. A. H. Jr., and J. F. Gamache, 1992: Dual-aircraft investigation of the inner core
1455 of Hurricane Norbert. Part I: Kinematic structure. *J. Atmos. Sci.*, **49**, 919–942, [https://doi.org/
1456 10.1175/1520-0469\(1992\)049<0919:DAIOTI>2.0.CO;2](https://doi.org/10.1175/1520-0469(1992)049<0919:DAIOTI>2.0.CO;2).
- 1457 McBride, J. L., and R. Zehr, 1981: Observational Analysis of Tropical Cyclone Formation. Part II:
1458 Comparison of Non-Developing versus Developing Systems. *J. Atmos. Sci.*, **38** (6), 1132–1151,
1459 [https://doi.org/10.1175/1520-0469\(1981\)038<1132:OAOTCF>2.0.CO;2](https://doi.org/10.1175/1520-0469(1981)038<1132:OAOTCF>2.0.CO;2), URL [http://journals.
1460 ametsoc.org/doi/abs/10.1175/1520-0469\(1981\)038%3C1132%3AOAOTCF%3E2.0.CO%3B2](http://journals.ametsoc.org/doi/abs/10.1175/1520-0469(1981)038%3C1132%3AOAOTCF%3E2.0.CO%3B2).

- 1461 Merrill, R. T., 1988: Environmental Influences on Hurricane Intensification. *J. Atmos. Sci.*, **45** (11),
1462 1678–1687, [https://doi.org/10.1175/1520-0469\(1988\)045<1678:EIOHI>2.0.CO;2](https://doi.org/10.1175/1520-0469(1988)045<1678:EIOHI>2.0.CO;2).
- 1463 Miyamoto, Y., and D. S. Nolan, 2018: Structural Changes Preceding Rapid Intensification in
1464 Tropical Cyclones as Shown in a Large Ensemble of Idealized Simulations. *J. Atmos. Sci.*,
1465 **75** (2), 555–569, <https://doi.org/10.1175/JAS-D-17-0177.1>, URL <http://journals.ametsoc.org/doi/10.1175/JAS-D-17-0177.1>.
- 1467 Miyamoto, Y., and T. Takemi, 2012: A Transition Mechanism for the Spontaneous Axisymmetric
1468 Intensification of Tropical Cyclones. *J. Atmos. Sci.*, **70** (1), 112–129, <https://doi.org/10.1175/JAS-D-11-0285.1>, URL <http://journals.ametsoc.org/doi/abs/10.1175/JAS-D-11-0285.1>.
- 1470 Molinari, J., P. Dodge, D. Vollaro, K. L. Corbosiero, and F. Marks, 2006: Mesoscale Aspects of the
1471 Downshear Reformation of a Tropical Cyclone. *J. Atmos. Sci.*, **63** (1), 341–354, <https://doi.org/10.1175/JAS3591.1>.
- 1473 Molinari, J., J. Frank, and D. Vollaro, 2013: Convective Bursts, Downdraft Cooling, and
1474 Boundary Layer Recovery in a Sheared Tropical Storm. *Mon. Wea. Rev.*, **141** (3), 1048–
1475 1060, <https://doi.org/10.1175/MWR-D-12-00135.1>, URL <http://journals.ametsoc.org/doi/abs/10.1175/MWR-D-12-00135.1>.
- 1477 Molinari, J., and D. Vollaro, 2010: Rapid Intensification of a Sheared Tropical Storm. *Mon. Wea.*
1478 *Rev.*, **138** (10), 3869–3885, <https://doi.org/10.1175/2010MWR3378.1>.
- 1479 Molinari, J., D. Vollaro, and K. L. Corbosiero, 2004: Tropical Cyclone Formation in a
1480 Sheared Environment: A Case Study. *J. Atmos. Sci.*, **61** (21), 2493–2509, <https://doi.org/10.1175/JAS3291.1>.
- 1482 Möller, J. D., and M. T. Montgomery, 2000: Tropical cyclone evolution via potential vortic-
1483 ity anomalies in a three-dimensional balance model. *J. Atmos. Sci.*, **57** (20), 3366–3387,
1484 [https://doi.org/10.1175/1520-0469\(2000\)057<3366:tcevpv>2.0.co;2](https://doi.org/10.1175/1520-0469(2000)057<3366:tcevpv>2.0.co;2), URL [https://doi.org/10.1175/1520-0469\(2000\)057<3366:tcevpv>2.0.co;2](https://doi.org/10.1175/1520-0469(2000)057<3366:tcevpv>2.0.co;2).
- 1486 Montgomery, M. T., L. L. Lussier III, R. W. Moore, and Z. Wang, 2010: The genesis of Typhoon
1487 Nuri as observed during the Tropical Cyclone Structure 2008 (TCS-08) field experiment. Part

- 1488 1: The role of the easterly wave critical layer. *Atmos. Chem. Phys.*, **10** (20), 9879–9900,
1489 <https://doi.org/10.5194/acp-10-9879-2010>.
- 1490 Montgomery, M. T., and R. K. Smith, 2014: Paradigms for tropical cyclone intensification.
1491 *Australian Meteor. Oceanog. J.*, **64**, 37–66.
- 1492 Montgomery, M. T., and R. K. Smith, 2017: Recent developments in the fluid dynam-
1493 ics of tropical cyclones. *Annu. Rev. Fluid Mech.*, **49** (1), 541–574, [https://doi.org/10.1146/](https://doi.org/10.1146/annurev-fluid-010816-060022)
1494 [annurev-fluid-010816-060022](https://doi.org/10.1146/annurev-fluid-010816-060022), URL <https://doi.org/10.1146/annurev-fluid-010816-060022>.
- 1495 Munsell, E. B., S. A. Braun, and F. Zhang, 2021: GOES-16 observations of rapidly-intensifying
1496 tropical cyclones: Hurricanes Harvey (2017), Maria (2017), and Michael (2018). *Mon. Wea. Rev.*,
1497 <https://doi.org/10.1175/mwr-d-19-0298.1>, URL <https://doi.org/10.1175/mwr-d-19-0298.1>.
- 1498 Munsell, E. B., F. Zhang, J. A. Sippel, S. A. Braun, and Y. Weng, 2017: Dynamics and pre-
1499 dictability of the intensification of Hurricane Edouard (2014). *J. Atmos. Sci.*, **74** (2), 573–
1500 595, <https://doi.org/10.1175/JAS-D-16-0018.1>, URL [http://journals.ametsoc.org/doi/10.1175/](http://journals.ametsoc.org/doi/10.1175/JAS-D-16-0018.1)
1501 [JAS-D-16-0018.1](http://journals.ametsoc.org/doi/10.1175/JAS-D-16-0018.1).
- 1502 Munsell, E. B., F. Zhang, and D. P. Stern, 2013: Predictability and dynamics of a nonintensify-
1503 ing Tropical Storm: Erika (2009). *J. Atmos. Sci.*, **70** (8), 2505–2524, [https://doi.org/10.1175/](https://doi.org/10.1175/JAS-D-12-0243.1)
1504 [JAS-D-12-0243.1](http://journals.ametsoc.org/doi/abs/10.1175/JAS-D-12-0243.1), URL <http://journals.ametsoc.org/doi/abs/10.1175/JAS-D-12-0243.1>.
- 1505 Nam, C. C., and M. M. Bell, 2021: Multiscale shear impacts during the genesis of Hagupit
1506 (2008). *Mon. Wea. Rev.*, **149** (2), 551–569, <https://doi.org/10.1175/mwr-d-20-0133.1>, URL
1507 <https://doi.org/10.1175/mwr-d-20-0133.1>.
- 1508 Nam, C. C., M. M. Bell, and D. Tao, 2023: Bifurcation points for tropical cyclone genesis
1509 and intensification in sheared and dry environments. *J. Atmos. Sci.*, [https://doi.org/10.1175/](https://doi.org/10.1175/jas-d-22-0100.1)
1510 [jas-d-22-0100.1](https://doi.org/10.1175/jas-d-22-0100.1), URL <https://doi.org/10.1175/jas-d-22-0100.1>.
- 1511 Nguyen, L. T., and J. Molinari, 2012: Rapid Intensification of a Sheared, Fast-Moving Hur-
1512 ricane over the Gulf Stream. *Mon. Wea. Rev.*, **140** (10), 3361–3378, [https://doi.org/10.1175/](https://doi.org/10.1175/MWR-D-11-00293.1)
1513 [MWR-D-11-00293.1](http://journals.ametsoc.org/doi/abs/10.1175/MWR-D-11-00293.1), URL <http://journals.ametsoc.org/doi/abs/10.1175/MWR-D-11-00293.1>.

- 1514 Nguyen, L. T., and J. Molinari, 2015: Simulation of the Downshear Reformation of a Tropical
1515 Cyclone. *J. Atmos. Sci.*, 150820131246003, <https://doi.org/10.1175/JAS-D-15-0036.1>, URL
1516 <http://journals.ametsoc.org/doi/abs/10.1175/JAS-D-15-0036.1>.
- 1517 Nguyen, L. T., R. Rogers, J. Zawislak, and J. A. Zhang, 2019: Assessing the influence of convective
1518 downdrafts and surface enthalpy fluxes on tropical cyclone intensity change in moderate vertical
1519 wind shear. *Mon. Wea. Rev.*, **147** (10), 3519–3534, <https://doi.org/10.1175/mwr-d-18-0461.1>,
1520 URL <https://doi.org/10.1175/mwr-d-18-0461.1>.
- 1521 Nguyen, L. T., R. F. Rogers, and P. D. Reasor, 2017: Thermodynamic and Kinematic Influences on
1522 Precipitation Symmetry in Sheared Tropical Cyclones: Bertha and Cristobal (2014). *Mon. Wea.*
1523 *Rev.*, **145** (11), 4423–4446, <https://doi.org/10.1175/MWR-D-17-0073.1>, URL <http://journals.ametsoc.org/doi/10.1175/MWR-D-17-0073.1>.
- 1525 Nolan, D. S., 2007: What is the trigger for tropical cyclogenesis? *Aust. Meteor. Mag.*, **56**, 241–266.
- 1526 Nolan, D. S., 2011: Evaluating Environmental Favorableness for Tropical Cyclone De-
1527 velopment with the Method of Point-Downscaling. *J. Adv. Model. Earth Syst.*, **3** (3),
1528 M08 001, <https://doi.org/10.1029/2011MS000063>, URL [http://onlinelibrary.wiley.com/doi/10.](http://onlinelibrary.wiley.com/doi/10.1029/2011MS000063/abstract)
1529 [1029/2011MS000063/abstract](http://onlinelibrary.wiley.com/doi/10.1029/2011MS000063/abstract).
- 1530 Nolan, D. S., and M. G. McGauley, 2012: Tropical cyclogenesis in wind shear: Climatological
1531 relationships and physical processes. *Cyclones: Formation, Triggers and Control*, K. Oouchi,
1532 and H. Fudeyasu, Eds., Nova Science Publishers, Hapauge, New York.
- 1533 Nolan, D. S., Y. Moon, and D. P. Stern, 2007: Tropical Cyclone Intensification from Asymmetric
1534 Convection: Energetics and Efficiency. *J. Atmos. Sci.*, **64** (10), 3377–3405, [https://doi.org/](https://doi.org/10.1175/JAS3988.1)
1535 [10.1175/JAS3988.1](https://doi.org/10.1175/JAS3988.1), URL <http://journals.ametsoc.org/doi/abs/10.1175/JAS3988.1>.
- 1536 Nolan, D. S., and E. D. Rappin, 2008: Increased sensitivity of tropical cyclogenesis to wind shear in
1537 higher SST environments. *Geophys. Res. Lett.*, **35** (14), <https://doi.org/10.1029/2008GL034147>,
1538 URL <http://doi.wiley.com/10.1029/2008GL034147>.
- 1539 Nugent, A. D., and R. Rios-Berrios, 2018: Factors Leading to Extreme Precipitation on Dominica
1540 from Tropical Storm Erika (2015). *Mon. Wea. Rev.*, **146** (2), 525–541, [https://doi.org/10.1175/](https://doi.org/10.1175/MWR-D-17-0242.1)
1541 [MWR-D-17-0242.1](https://doi.org/10.1175/MWR-D-17-0242.1), URL <http://journals.ametsoc.org/doi/10.1175/MWR-D-17-0242.1>.

- 1542 Onderlinde, M. J., and D. S. Nolan, 2014: Environmental Helicity and Its Effects on Development
1543 and Intensification of Tropical Cyclones. *J. Atmos. Sci.*, **71** (11), 4308–4320, [https://doi.org/10.](https://doi.org/10.1175/JAS-D-14-0085.1)
1544 [1175/JAS-D-14-0085.1](https://doi.org/10.1175/JAS-D-14-0085.1), URL <http://journals.ametsoc.org/doi/abs/10.1175/JAS-D-14-0085.1>.
- 1545 Onderlinde, M. J., and D. S. Nolan, 2016: Tropical Cyclone-Relative Environmental Helicity and
1546 the Pathways to Intensification in Shear. *J. Atmos. Sci.*, **73** (2), 869–890, [https://doi.org/10.1175/](https://doi.org/10.1175/JAS-D-15-0261.1)
1547 [JAS-D-15-0261.1](https://doi.org/10.1175/JAS-D-15-0261.1), URL <http://journals.ametsoc.org/doi/full/10.1175/JAS-D-15-0261.1>.
- 1548 Onderlinde, M. J., and D. S. Nolan, 2017: The tropical cyclone response to changing wind shear us-
1549 ing the method of time-varying point-downscaling. *J. Adv. Model. Earth Syst.*, **9**, [https://doi.org/](https://doi.org/10.1002/2016MS000796)
1550 [10.1002/2016MS000796](https://doi.org/10.1002/2016MS000796), URL <http://doi.wiley.com/10.1002/2016MS000796>.
- 1551 Ooyama, K., 1969: Numerical simulation of the life cycle of tropical cyclones. *J. Atmos. Sci.*, **26**,
1552 3–40, [https://doi.org/10.1175/1520-0469\(1969\)026<0003:nsotlc>2.0.co;2](https://doi.org/10.1175/1520-0469(1969)026<0003:nsotlc>2.0.co;2).
- 1553 Patra, R., 2004: Idealised modeling of tropical cyclones in vertical wind shear: The role of saturated
1554 ascent. *26th Conf. on Hurricanes and Tropical Meteorology*, Amer. Meteor. Soc., Miami, FL,
1555 4A.6.
- 1556 Pei, Y., and H. Jiang, 2018: Quantification of precipitation asymmetries of tropical cyclones using
1557 16-year TRMM observations. *J. Geophys. Res. Atmos.*, **123** (15), 8091–8114, [https://doi.org/](https://doi.org/10.1029/2018jd028545)
1558 [10.1029/2018jd028545](https://doi.org/10.1029/2018jd028545), URL <https://doi.org/10.1029/2018jd028545>.
- 1559 Persing, J., and M. T. Montgomery, 2003: Hurricane superintensity. *J. Atmos. Sci.*, **60** (19), 2349–
1560 2371, [https://doi.org/10.1175/1520-0469\(2003\)060<2349:hs>2.0.co;2](https://doi.org/10.1175/1520-0469(2003)060<2349:hs>2.0.co;2), URL [https://doi.org/10.](https://doi.org/10.1175/1520-0469(2003)060<2349:hs>2.0.co;2)
1561 [1175/1520-0469\(2003\)060<2349:hs>2.0.co;2](https://doi.org/10.1175/1520-0469(2003)060<2349:hs>2.0.co;2).
- 1562 Powell, M. D., 1990: Boundary layer structure and dynamics in outer hurricane rainbands. Part
1563 II: Downdraft modification and mixed layer recovery. *Mon. Wea. Rev.*, **118** (4), 918–938,
1564 [https://doi.org/10.1175/1520-0493\(1990\)118<0918:BLSADI>2.0.CO;2](https://doi.org/10.1175/1520-0493(1990)118<0918:BLSADI>2.0.CO;2).
- 1565 Ramage, C. S., 1959: Hurricane development. *J. Meteor.*, **16** (3), 227–237, [https://doi.org/10.](https://doi.org/10.1175/1520-0469(1959)016<0227:HD>2.0.CO;2)
1566 [1175/1520-0469\(1959\)016<0227:HD>2.0.CO;2](https://doi.org/10.1175/1520-0469(1959)016<0227:HD>2.0.CO;2), URL [http://journals.ametsoc.org/doi/abs/10.](http://journals.ametsoc.org/doi/abs/10.1175/1520-0469(1959)016%3C0227%3AHD%3E2.0.CO%3B2)
1567 [1175/1520-0469\(1959\)016%3C0227%3AHD%3E2.0.CO%3B2](http://journals.ametsoc.org/doi/abs/10.1175/1520-0469(1959)016%3C0227%3AHD%3E2.0.CO%3B2).

- 1568 Rappin, E. D., and D. S. Nolan, 2012: The Effect of Vertical Shear Orientation on Tropical
1569 Cyclogenesis. *Q. J. Roy. Meteor. Soc.*, **138 (665)**, 1035–1054, <https://doi.org/10.1002/qj.977>,
1570 URL <http://doi.wiley.com/10.1002/qj.977>.
- 1571 Rappin, E. D., D. S. Nolan, and K. A. Emanuel, 2010: Thermodynamic control of tropical
1572 cyclogenesis in environments of radiative-convective equilibrium with shear. *Quart. J. Roy.
1573 Meteor. Soc.*, **136**, 1954–1971, <https://doi.org/10.1002/qj.706>.
- 1574 Raymond, D. J., C. López-Carrillo, and L. L. Cavazos, 1998: Case-studies of developing east
1575 Pacific easterly waves. *Quart. J. Roy. Meteor. Soc.*, **124**, 2005–2034, [https://doi.org/10.1002/qj.
1576 49712455011](https://doi.org/10.1002/qj.49712455011).
- 1577 Raymond, D. J., S. L. Sessions, and C. López Carrillo, 2011: Thermodynamics of tropical
1578 cyclogenesis in the northwest Pacific. *J. Geophys. Res.*, **116 (D18)**, [https://doi.org/10.1029/
1579 2011JD015624](https://doi.org/10.1029/2011JD015624), URL <http://doi.wiley.com/10.1029/2011JD015624>.
- 1580 Reasor, P. D., and M. D. Eastin, 2012: Rapidly Intensifying Hurricane Guillermo (1997). Part II: Re-
1581 siliance in Shear. *Mon. Wea. Rev.*, **140 (2)**, 425–444, [https://doi.org/10.1175/MWR-D-11-00080.
1582 1](https://doi.org/10.1175/MWR-D-11-00080.1), URL <http://journals.ametsoc.org/doi/abs/10.1175/MWR-D-11-00080.1>.
- 1583 Reasor, P. D., M. D. Eastin, and J. F. Gamache, 2009: Rapidly Intensifying Hurricane Guillermo
1584 (1997). Part I: Low-Wavenumber Structure and Evolution. *Mon. Wea. Rev.*, **137 (2)**, 603–
1585 631, <https://doi.org/10.1175/2008MWR2487.1>, URL [http://journals.ametsoc.org/doi/full/10.
1586 1175/2008MWR2487.1](http://journals.ametsoc.org/doi/full/10.1175/2008MWR2487.1).
- 1587 Reasor, P. D., and M. T. Montgomery, 2001: Three-Dimensional Alignment and Coro-
1588 tation of Weak, TC-like Vortices via Linear Vortex Rossby Waves. *J. Atmos. Sci.*,
1589 **58 (16)**, 2306–2330, [https://doi.org/10.1175/1520-0469\(2001\)058<2306:TDAACO>2.0.CO;
1590 2](https://doi.org/10.1175/1520-0469(2001)058<2306:TDAACO>2.0.CO;2), URL [http://journals.ametsoc.org/doi/abs/10.1175/1520-0469%282001%29058%3C2306%
1591 3ATDAACO%3E2.0.CO%3B2](http://journals.ametsoc.org/doi/abs/10.1175/1520-0469%282001%29058%3C2306%3ATDAACO%3E2.0.CO%3B2).
- 1592 Reasor, P. D., and M. T. Montgomery, 2015: Evaluation of a Heuristic Model for Tropical Cyclone
1593 Resilience. *J. Atmos. Sci.*, **72 (5)**, 1765–1782, <https://doi.org/10.1175/JAS-D-14-0318.1>, URL
1594 <http://journals.ametsoc.org/doi/abs/10.1175/JAS-D-14-0318.1>.

- 1595 Reasor, P. D., M. T. Montgomery, and L. D. Grasso, 2004: A New Look at the Problem of
1596 Tropical Cyclones in Vertical Shear Flow: Vortex Resiliency. *J. Atmos. Sci.*, **61** (1), 3–22,
1597 [https://doi.org/10.1175/1520-0469\(2004\)061<0003:ANLATP>2.0.CO;2](https://doi.org/10.1175/1520-0469(2004)061<0003:ANLATP>2.0.CO;2).
- 1598 Reasor, P. D., R. Rogers, and S. Lorsolo, 2013: Environmental Flow Impacts on Tropical Cyclone
1599 Structure Diagnosed from Airborne Doppler Radar Composites. *Mon. Wea. Rev.*, **141** (9), 2949–
1600 2969, <https://doi.org/10.1175/MWR-D-12-00334.1>, URL [http://journals.ametsoc.org/doi/abs/](http://journals.ametsoc.org/doi/abs/10.1175/MWR-D-12-00334.1)
1601 [10.1175/MWR-D-12-00334.1](http://journals.ametsoc.org/doi/abs/10.1175/MWR-D-12-00334.1).
- 1602 Richardson, J. C., R. D. Torn, and B. H. Tang, 2022: An analog comparison between rapidly
1603 and slowly intensifying tropical cyclones. *Mon. Wea. Rev.*, **150** (8), 2139–2156, [https://doi.org/](https://doi.org/10.1175/mwr-d-21-0260.1)
1604 [10.1175/mwr-d-21-0260.1](https://doi.org/10.1175/mwr-d-21-0260.1), URL <https://doi.org/10.1175/mwr-d-21-0260.1>.
- 1605 Riehl, H., and R. J. Shafer, 1944: The recurvature of tropical storms. *J. Meteor.*, **1** (1), 42–54,
1606 [https://doi.org/10.1175/1520-0469\(1944\)001<0001:TROTS>2.0.CO;2](https://doi.org/10.1175/1520-0469(1944)001<0001:TROTS>2.0.CO;2), URL [http://journals.](http://journals.ametsoc.org/doi/abs/10.1175/1520-0469(1944)001%3C0001:TROTS%3E2.0.CO%3B2)
1607 [ametsoc.org/doi/abs/10.1175/1520-0469\(1944\)001%3C0001:TROTS%3E2.0.CO%3B2](http://journals.ametsoc.org/doi/abs/10.1175/1520-0469(1944)001%3C0001:TROTS%3E2.0.CO%3B2).
- 1608 Riemer, M., 2016: Meso- β -scale environment for the stationary band complex of vertically sheared
1609 tropical cyclones. *Q. J. Royal Meteor. Soc.*, **142** (699), 2442–2451, [https://doi.org/10.1002/qj.](https://doi.org/10.1002/qj.2837)
1610 [2837](https://doi.org/10.1002/qj.2837), URL <https://doi.org/10.1002/qj.2837>.
- 1611 Riemer, M., and F. Laliberté, 2015: Secondary Circulation of Tropical Cyclones in Vertical Wind
1612 Shear: Lagrangian Diagnostic and Pathways of Environmental Interaction. *J. Atmos. Sci.*, **72** (9),
1613 3517–3536, <https://doi.org/10.1175/JAS-D-14-0350.1>, URL [http://journals.ametsoc.org/doi/10.](http://journals.ametsoc.org/doi/10.1175/JAS-D-14-0350.1)
1614 [1175/JAS-D-14-0350.1](http://journals.ametsoc.org/doi/10.1175/JAS-D-14-0350.1).
- 1615 Riemer, M., and M. T. Montgomery, 2011: Simple Kinematic Models for the Environmental
1616 Interaction of Tropical Cyclones in Vertical Wind Shear. *Atmos. Chem. Phys.*, **11** (17), 9395–
1617 9414, <https://doi.org/10.5194/acp-11-9395-2011>, URL [http://www.atmos-chem-phys.net/11/](http://www.atmos-chem-phys.net/11/9395/2011/)
1618 [9395/2011/](http://www.atmos-chem-phys.net/11/9395/2011/).
- 1619 Riemer, M., M. T. Montgomery, and M. E. Nicholls, 2010: A New Paradigm for Intensity
1620 Modification of Tropical Cyclones: Thermodynamic Impact of Vertical Wind Shear on the Inflow
1621 Layer. *Atmos. Chem. Phys.*, **10** (7), 3163–3188, <https://doi.org/10.5194/acp-10-3163-2010>.

- 1622 Riemer, M., M. T. Montgomery, and M. E. Nicholls, 2013: Further Examination of the
1623 Thermodynamic Modification of the Inflow Layer of Tropical Cyclones by Vertical Wind
1624 Shear. *Atmos. Chem. Phys.*, **13** (1), 327–346, <https://doi.org/10.5194/acp-13-327-2013>, URL
1625 <http://www.atmos-chem-phys.net/13/327/2013/>.
- 1626 Rios-Berrios, R., 2020: Impacts of radiation and cold pools on the intensity and vortex tilt of
1627 weak tropical cyclones interacting with vertical wind shear. *J. Atmos. Sci.*, **77** (2), 669–689,
1628 <https://doi.org/10.1175/jas-d-19-0159.1>, URL <https://doi.org/10.1175/jas-d-19-0159.1>.
- 1629 Rios-Berrios, R., C. A. Davis, and R. D. Torn, 2018: A Hypothesis for the Intensification
1630 of Tropical Cyclones under Moderate Vertical Wind Shear. *J. Atmos. Sci.*, **75** (12), 4149–
1631 4173, <https://doi.org/10.1175/JAS-D-18-0070.1>, URL <http://journals.ametsoc.org/doi/10.1175/JAS-D-18-0070.1>.
- 1633 Rios-Berrios, R., and R. D. Torn, 2017: Climatological Analysis of Tropical Cyclone In-
1634 tensity Changes under Moderate Vertical Wind Shear. *Mon. Wea. Rev.*, **145** (5), 1717–
1635 1738, <https://doi.org/10.1175/MWR-D-16-0350.1>, URL <http://journals.ametsoc.org/doi/10.1175/MWR-D-16-0350.1>.
- 1637 Rios-Berrios, R., R. D. Torn, and C. A. Davis, 2016a: An Ensemble Approach to Investigate
1638 Tropical Cyclone Intensification in Sheared Environments. Part I: Katia (2011). *J. Atmos. Sci.*,
1639 **73** (1), 71–93, <https://doi.org/10.1175/JAS-D-15-0052.1>, URL <http://journals.ametsoc.org/doi/abs/10.1175/JAS-D-15-0052.1>.
- 1641 Rios-Berrios, R., R. D. Torn, and C. A. Davis, 2016b: An Ensemble Approach to Investigate
1642 Tropical Cyclone Intensification in Sheared Environments. Part II: Ophelia (2011). *J. Atmos. Sci.*,
1643 **73** (4), 1555–1575, <https://doi.org/10.1175/JAS-D-15-0245.1>, URL <http://journals.ametsoc.org/doi/abs/10.1175/JAS-D-15-0245.1>.
- 1645 Ritchie, E. A., and W. M. Frank, 2007: Interactions between simulated tropical cyclones and an
1646 environment with a variable coriolis parameter. *Mon. Wea. Rev.*, **135**, 1889–1905, <https://doi.org/10.1175/MWR3359.1>, URL <http://journals.ametsoc.org/doi/abs/10.1175/MWR3359.1>.

- 1648 Rogers, R., S. Chen, J. Tenerelli, and H. Willoughby, 2003: A numerical study of the impact of
1649 vertical shear on the distribution of rainfall in Hurricane Bonnie (1998). *Mon. Wea. Rev.*, **131** (8),
1650 1577–1599, <https://doi.org/10.1175//2546.1>, URL <https://doi.org/10.1175//2546.1>.
- 1651 Rogers, R., P. Reasor, and S. Lorsolo, 2013: Airborne Doppler Observations of the Inner-Core
1652 Structural Differences between Intensifying and Steady-State Tropical Cyclones. *Mon. Wea.*
1653 *Rev.*, **141** (9), 2970–2991, <https://doi.org/10.1175/MWR-D-12-00357.1>.
- 1654 Rogers, R. F., P. D. Reasor, J. A. Zawislak, and L. T. Nguyen, 2020: Precipitation processes
1655 and vortex alignment during the intensification of a weak tropical cyclone in moderate vertical
1656 shear. *Mon. Wea. Rev.*, **148** (5), 1899–1929, <https://doi.org/10.1175/mwr-d-19-0315.1>, URL
1657 <https://doi.org/10.1175/mwr-d-19-0315.1>.
- 1658 Rogers, R. F., P. D. Reasor, and J. A. Zhang, 2015: Multiscale Structure and Evolution
1659 of Hurricane Earl (2010) during Rapid Intensification. *Mon. Wea. Rev.*, **143** (2), 536–
1660 562, <https://doi.org/10.1175/MWR-D-14-00175.1>, URL [http://journals.ametsoc.org/doi/abs/10.](http://journals.ametsoc.org/doi/abs/10.1175/MWR-D-14-00175.1)
1661 [1175/MWR-D-14-00175.1](http://journals.ametsoc.org/doi/abs/10.1175/MWR-D-14-00175.1).
- 1662 Rogers, R. F., J. A. Zhang, J. Zawislak, H. Jiang, G. R. Alvey, E. J. Zipser, and S. N. Stevenson,
1663 2016: Observations of the Structure and Evolution of Hurricane Edouard (2014) during Intensity
1664 Change. Part II: Kinematic Structure and the Distribution of Deep Convection. *Mon. Wea. Rev.*,
1665 **144** (9), 3355–3376, <https://doi.org/10.1175/MWR-D-16-0017.1>, URL [http://journals.ametsoc.](http://journals.ametsoc.org/doi/10.1175/MWR-D-16-0017.1)
1666 [org/doi/10.1175/MWR-D-16-0017.1](http://journals.ametsoc.org/doi/10.1175/MWR-D-16-0017.1).
- 1667 Rozoff, C. M., J. P. Kossin, W. H. Schubert, and P. J. Mulero, 2009: Internal control of hurricane
1668 intensity variability: The dual nature of potential vorticity mixing. *J. Atmos. Sci.*, **66** (1), 133–
1669 147, <https://doi.org/10.1175/2008jas2717.1>, URL <https://doi.org/10.1175/2008jas2717.1>.
- 1670 Ryglicki, D. R., J. H. Cossuth, D. Hodyss, and J. D. Doyle, 2018a: The Unexpected Rapid
1671 Intensification of Tropical Cyclones in Moderate Vertical Wind Shear. Part I: Overview and
1672 Observations. *Mon. Wea. Rev.*, **146** (11), 3773–3800, [https://doi.org/10.1175/MWR-D-18-0020.](https://doi.org/10.1175/MWR-D-18-0020.1)
1673 [1](http://journals.ametsoc.org/doi/10.1175/MWR-D-18-0020.1), URL <http://journals.ametsoc.org/doi/10.1175/MWR-D-18-0020.1>.
- 1674 Ryglicki, D. R., J. D. Doyle, D. Hodyss, J. H. Cossuth, Y. Jin, K. C. Viner, and J. M. Schmidt,
1675 2019: The unexpected rapid intensification of tropical cyclones in moderate vertical wind shear.

1676 part III: Outflow–environment interaction. *Mon. Wea. Rev.*, **147** (8), 2919–2940, [https://doi.org/](https://doi.org/10.1175/mwr-d-18-0370.1)
1677 [10.1175/mwr-d-18-0370.1](https://doi.org/10.1175/mwr-d-18-0370.1), URL <https://doi.org/10.1175/mwr-d-18-0370.1>.

1678 Ryglicki, D. R., J. D. Doyle, Y. Jin, D. Hodyss, and J. H. Cossuth, 2018b: The Unexpected
1679 Rapid Intensification of Tropical Cyclones in Moderate Vertical Wind Shear. Part II: Vortex
1680 Tilt. *Mon. Wea. Rev.*, **146** (11), 3801–3825, <https://doi.org/10.1175/MWR-D-18-0021.1>, URL
1681 <http://journals.ametsoc.org/doi/10.1175/MWR-D-18-0021.1>.

1682 Ryglicki, D. R., D. Hodyss, and G. Rainwater, 2020: The tropical cyclone as a divergent source in
1683 a background flow. *J. Atmos. Sci.*, **77** (12), 4189–4210, <https://doi.org/10.1175/jas-d-20-0030.1>,
1684 URL <https://doi.org/10.1175/jas-d-20-0030.1>.

1685 Ryglicki, D. R., C. S. Velden, P. D. Reasor, D. Hodyss, and J. D. Doyle, 2021: Observations
1686 of atypical rapid intensification characteristics in Hurricane Dorian (2019). *Mon. Wea. Rev.*,
1687 <https://doi.org/10.1175/mwr-d-20-0413.1>, URL <https://doi.org/10.1175/mwr-d-20-0413.1>.

1688 Schecter, D. A., 2020: Distinct intensification pathways for a shallow-water vortex subjected
1689 to asymmetric “diabatic” forcing. *Dyn. Atmos. Oceans*, **91**, 101–156, [https://doi.org/10.1016/j.](https://doi.org/10.1016/j.dynatmoce.2020.101156)
1690 [dynatmoce.2020.101156](https://doi.org/10.1016/j.dynatmoce.2020.101156), URL <https://doi.org/10.1016/j.dynatmoce.2020.101156>.

1691 Schecter, D. A., 2022: Intensification of tilted tropical cyclones over relatively cool and warm
1692 oceans in idealized numerical simulations. *J. Atmos. Sci.*, **79** (2), 485–512, [https://doi.org/](https://doi.org/10.1175/jas-d-21-0051.1)
1693 [10.1175/jas-d-21-0051.1](https://doi.org/10.1175/jas-d-21-0051.1), URL <https://doi.org/10.1175/jas-d-21-0051.1>.

1694 Schecter, D. A., and K. Menelaou, 2020: Development of a misaligned tropical cyclone. *J.*
1695 *Atmos. Sci.*, **77** (1), 79–111, <https://doi.org/10.1175/jas-d-19-0074.1>, URL [https://doi.org/10.](https://doi.org/10.1175/jas-d-19-0074.1)
1696 [1175/jas-d-19-0074.1](https://doi.org/10.1175/jas-d-19-0074.1).

1697 Schecter, D. A., and M. T. Montgomery, 2003: On the symmetrization rate of an intense geophysical
1698 vortex. *Dyn. Atmos. Oceans*, **37** (1), 55–88, [https://doi.org/10.1016/S0377-0265\(03\)00015-0](https://doi.org/10.1016/S0377-0265(03)00015-0),
1699 URL <https://www.sciencedirect.com/science/article/pii/S0377026503000150>.

1700 Schecter, D. A., and M. T. Montgomery, 2007: Waves in a cloudy vortex. *J. Atmos. Sci.*, **64** (2),
1701 314–337, <https://doi.org/10.1175/jas3849.1>, URL <https://doi.org/10.1175/jas3849.1>.

1702 Schecter, D. A., M. T. Montgomery, and P. D. Reasor, 2002: A theory for the vertical align-
1703 ment of a quasigeostrophic vortex. *J. Atmos. Sci.*, **59** (2), 150–168, <https://doi.org/10.1175/>

1704 1520-0469(2002)059<0150:atftva>2.0.co;2, URL [https://doi.org/10.1175/1520-0469\(2002\)](https://doi.org/10.1175/1520-0469(2002)059<0150:atftva>2.0.co;2)
1705 [059<0150:atftva>2.0.co;2](https://doi.org/10.1175/1520-0469(2002)059<0150:atftva>2.0.co;2).

1706 Schubert, W. H., M. T. Montgomery, R. K. Taft, T. A. Guinn, S. R. Fulton, J. P. Kossin, and J. P.
1707 Edwards, 1999: Polygonal eyewalls, asymmetric eye contraction, and potential vorticity mix-
1708 ing in hurricanes. *J. Atmos. Sci.*, **56** (9), 1197–1223, [https://doi.org/10.1175/1520-0469\(1999\)](https://doi.org/10.1175/1520-0469(1999)056<1197:peaeca>2.0.co;2)
1709 [056<1197:peaeca>2.0.co;2](https://doi.org/10.1175/1520-0469(1999)056<1197:peaeca>2.0.co;2), URL [https://doi.org/10.1175/1520-0469\(1999\)056<1197:peaeca>](https://doi.org/10.1175/1520-0469(1999)056<1197:peaeca>2.0.co;2)
1710 [2.0.co;2](https://doi.org/10.1175/1520-0469(1999)056<1197:peaeca>2.0.co;2).

1711 Shelton, K. L., and J. Molinari, 2009: Life of a Six-Hour Hurricane. *Mon. Wea. Rev.*, **137** (1),
1712 51–67, <https://doi.org/10.1175/2008MWR2472.1>.

1713 Shi, D., and G. Chen, 2021: The implication of outflow structure for the rapid intensification of trop-
1714 ical cyclones under vertical wind shear. *Mon. Wea. Rev.*, **149** (12), 4107–4127, [https://doi.org/](https://doi.org/10.1175/mwr-d-21-0141.1)
1715 [10.1175/mwr-d-21-0141.1](https://doi.org/10.1175/mwr-d-21-0141.1), URL <https://doi.org/10.1175/mwr-d-21-0141.1>.

1716 Shu, S., F. Zhang, J. Ming, and Y. Wang, 2014: Environmental influences on the intensity
1717 changes of tropical cyclones over the western North Pacific. *Atmos. Chem. Phys.*, **14**, 6329–6342,
1718 <https://doi.org/10.5194/acp-14-6329-2014>, 2014.

1719 Simpson, R., and R. Riehl, 1958: Mid-tropospheric ventilation as a constraint on hurricane
1720 development and maintenance. *Tech. Conf. on Hurricanes*, Amer. Meteor. Soc., Miami Beach,
1721 FL, D4–1–D4–10.

1722 Smith, R. K., and M. T. Montgomery, 2015: Toward clarity on understanding tropical cyclone
1723 intensification. *J. Atmos. Sci.*, **72** (8), 3020–3031, <https://doi.org/10.1175/JAS-D-15-0017.1>,
1724 URL <http://journals.ametsoc.org/doi/10.1175/JAS-D-15-0017.1>.

1725 Smith, R. K., M. T. Montgomery, and N. V. Sang, 2009: Tropical cyclone spin-up revisited.
1726 *Q. J. Royal Meteor. Soc.*, **135** (642), 1321–1335, <https://doi.org/10.1002/qj.428>, URL <https://doi.org/10.1002/qj.428>.
1727 [//doi.org/10.1002/qj.428](https://doi.org/10.1002/qj.428).

1728 Smith, R. K., W. Ulrich, and G. Sneddon, 2000: On the dynamics of hurricane-like vortices in
1729 vertical-shear flows. *Q. J. Royal Meteor. Soc.*, **126** (569), 2653–2670, [https://doi.org/10.1002/](https://doi.org/10.1002/qj.49712656903)
1730 [qj.49712656903](https://doi.org/10.1002/qj.49712656903), URL <https://onlinelibrary.wiley.com/doi/abs/10.1002/qj.49712656903>.

- 1731 Stevenson, S. N., K. L. Corbosiero, and S. F. Abarca, 2016: Lightning in Eastern North Pacific
1732 tropical cyclones: A comparison to the North Atlantic. *Mon. Wea. Rev.*, **144** (1), 225–239,
1733 <https://doi.org/10.1175/mwr-d-15-0276.1>, URL <https://doi.org/10.1175/mwr-d-15-0276.1>.
- 1734 Stevenson, S. N., K. L. Corbosiero, M. DeMaria, and J. L. Vigh, 2018: A 10-year survey of
1735 tropical cyclone inner-core lightning bursts and their relationship to intensity change. *Wea.*
1736 *Forecasting*, **33** (1), 23–36, <https://doi.org/10.1175/waf-d-17-0096.1>, URL [https://doi.org/10.](https://doi.org/10.1175/waf-d-17-0096.1)
1737 [1175/waf-d-17-0096.1](https://doi.org/10.1175/waf-d-17-0096.1).
- 1738 Stevenson, S. N., K. L. Corbosiero, and J. Molinari, 2014: The Convective Evolution
1739 and Rapid Intensification of Hurricane Earl (2010). *Mon. Wea. Rev.*, **142** (11), 4364–
1740 4380, <https://doi.org/10.1175/MWR-D-14-00078.1>, URL [http://journals.ametsoc.org/doi/abs/](http://journals.ametsoc.org/doi/abs/10.1175/MWR-D-14-00078.1)
1741 [10.1175/MWR-D-14-00078.1](https://doi.org/10.1175/MWR-D-14-00078.1).
- 1742 Stone, Z., G. R. Alvey, J. P. Dunion, M. S. Fischer, D. J. Raymond, R. F. Rogers, S. Sentic, and
1743 J. Zawislak, 2023: Thermodynamic contribution to vortex alignment and rapid intensification
1744 of Hurricane Sally (2020). *Mon. Wea. Rev.*, <https://doi.org/10.1175/MWR-D-22-0201.1>, URL
1745 <https://doi.org/10.1175/MWR-D-22-0201.1>.
- 1746 Susca-Lopata, G., J. Zawislak, E. J. Zipser, and R. F. Rogers, 2015: The role of observed envi-
1747 ronmental conditions and precipitation evolution in the rapid intensification of hurricane earl
1748 (2010). *Mon. Wea. Rev.*, **143** (6), 2207–2223, <https://doi.org/10.1175/mwr-d-14-00283.1>, URL
1749 <https://doi.org/10.1175/mwr-d-14-00283.1>.
- 1750 Tang, B., and K. Emanuel, 2010: Midlevel Ventilation’s Constraint on Tropical Cyclone Intensity.
1751 *J. Atmos. Sci.*, **67** (6), 1817–1830, <https://doi.org/10.1175/2010JAS3318.1>.
- 1752 Tang, B., and K. Emanuel, 2012a: Sensitivity of Tropical Cyclone Intensity to Ventilation in an Ax-
1753 isymmetric Model. *J. Atmos. Sci.*, **69** (8), 2394–2413, <https://doi.org/10.1175/JAS-D-11-0232.1>.
- 1754 Tang, B., and K. Emanuel, 2012b: A ventilation index for tropical cyclones. *Bull. Amer. Meteor.*
1755 *Soc.*, **93** (12), 1901–1912, <https://doi.org/10.1175/bams-d-11-00165.1>, URL [https://doi.org/10.](https://doi.org/10.1175/bams-d-11-00165.1)
1756 [1175/bams-d-11-00165.1](https://doi.org/10.1175/bams-d-11-00165.1).

- 1757 Tang, X., and F. Zhang, 2016: Impacts of the Diurnal Radiation Cycle on the Formation, Intensity,
1758 and Structure of Hurricane Edouard (2014). *J. Atmos. Sci.*, **73** (7), 2871–2892, [https://doi.org/](https://doi.org/10.1175/JAS-D-15-0283.1)
1759 10.1175/JAS-D-15-0283.1, URL <http://journals.ametsoc.org/doi/10.1175/JAS-D-15-0283.1>.
- 1760 Tao, C., and H. Jiang, 2015: Distributions of Shallow to Very Deep Precipitation-Convection
1761 in Rapidly Intensifying Tropical Cyclones. *J. Climate*, **28** (22), 8791–8824, [https://doi.org/10.](https://doi.org/10.1175/JCLI-D-14-00448.1)
1762 1175/JCLI-D-14-00448.1, URL <http://journals.ametsoc.org/doi/10.1175/JCLI-D-14-00448.1>.
- 1763 Tao, C., H. Jiang, and J. Zawislak, 2017: The Relative Importance of Stratiform and
1764 Convective Rainfall in Rapidly Intensifying Tropical Cyclones. *Mon. Wea. Rev.*, **145** (3),
1765 795–809, <https://doi.org/10.1175/MWR-D-16-0316.1>, URL [http://journals.ametsoc.org/doi/10.](http://journals.ametsoc.org/doi/10.1175/MWR-D-16-0316.1)
1766 1175/MWR-D-16-0316.1.
- 1767 Tao, D., and F. Zhang, 2014: Effect of Environmental Shear, Sea-Surface Temperature, and Am-
1768 bient Moisture on the Formation and Predictability of Tropical Cyclones: An Ensemble-Mean
1769 Perspective. *J. Adv. Model. Earth Syst.*, **6** (2), 384–404, <https://doi.org/10.1002/2014MS000314>.
- 1770 Tao, D., and F. Zhang, 2015: Effects of vertical wind shear on the predictability of tropical cyclones:
1771 Practical versus intrinsic limit. *J. Adv. Model. Earth Syst.*, **7** (4), 1534–1553, [https://doi.org/](https://doi.org/10.1002/2015MS000474)
1772 10.1002/2015MS000474, URL <http://doi.wiley.com/10.1002/2015MS000474>.
- 1773 Tao, D., and F. Zhang, 2019: Evolution of dynamic and thermodynamic structures before and
1774 during rapid intensification of tropical cyclones: Sensitivity to vertical wind shear. *Mon. Wea.*
1775 *Rev.*, **147** (4), 1171–1191, <https://doi.org/10.1175/mwr-d-18-0173.1>, URL [https://doi.org/10.](https://doi.org/10.1175/mwr-d-18-0173.1)
1776 1175/mwr-d-18-0173.1.
- 1777 Tuleya, R., and Y. Kurihara, 1981: A numerical study on the effects of environmental flow on
1778 tropical storm genesis. *Mon. Wea. Rev.*, **109**, 2487–2506.
- 1779 Velden, C. S., and J. Sears, 2014: Computing Deep-Tropospheric Vertical Wind Shear Analyses
1780 for Tropical Cyclone Applications: Does the Methodology Matter? *Wea. Forecasting*, **29** (5),
1781 1169–1180, <https://doi.org/10.1175/WAF-D-13-00147.1>, URL [http://journals.ametsoc.org/doi/](http://journals.ametsoc.org/doi/abs/10.1175/WAF-D-13-00147.1)
1782 <abs/10.1175/WAF-D-13-00147.1>.
- 1783 Wadler, J. B., J. J. Cione, J. A. Zhang, E. A. Kalina, and J. Kaplan, 2022: The effects of
1784 environmental wind shear direction on tropical cyclone boundary layer thermodynamics and

- 1785 intensity change from multiple observational datasets. *Mon. Wea. Rev.*, **150** (1), 115–134,
1786 <https://doi.org/10.1175/mwr-d-21-0022.1>, URL <https://doi.org/10.1175/mwr-d-21-0022.1>.
- 1787 Wadler, J. B., D. S. Nolan, J. A. Zhang, and L. K. Shay, 2021a: Thermodynamic characteristics of
1788 downdrafts in tropical cyclones as seen in idealized simulations of different intensities. *J. Atmos.*
1789 *Sci.*, **78** (11), 3503–3524, <https://doi.org/10.1175/JAS-D-21-0006.1>.
- 1790 Wadler, J. B., R. F. Rogers, and P. D. Reasor, 2018: The Relationship between Spatial Vari-
1791 ations in the Structure of Convective Bursts and Tropical Cyclone Intensification as Deter-
1792 mined by Airborne Doppler Radar. *Mon. Wea. Rev.*, **146** (3), 761–780, <https://doi.org/10.1175/MWR-D-17-0213.1>, URL <http://journals.ametsoc.org/doi/10.1175/MWR-D-17-0213.1>.
- 1794 Wadler, J. B., J. A. Zhang, R. F. Rogers, B. Jaimes, and L. K. Shay, 2021b: The rapid intensification
1795 of Hurricane Michael (2018): Storm structure and the relationship to environmental and air–sea
1796 interactions. *Mon. Wea. Rev.*, **149** (1), 245–267, <https://doi.org/10.1175/mwr-d-20-0145.1>, URL
1797 <https://doi.org/10.1175/mwr-d-20-0145.1>.
- 1798 Wang, C., J. Fang, and Y. Ma, 2022: Structural changes preceding the rapid intensification of
1799 Typhoon Lekim (2019) under moderate vertical wind shear. *J. Geophys. Res. Atmos.*, **127** (20),
1800 <https://doi.org/10.1029/2022jd036544>, URL <https://doi.org/10.1029/2022jd036544>.
- 1801 Wang, Y., and G. J. Holland, 1996: Tropical Cyclone Motion and Evolution in Vertical
1802 Shear. *J. Atmos. Sci.*, **53** (22), 3313–3332, [https://doi.org/10.1175/1520-0469\(1996\)053<3313:](https://doi.org/10.1175/1520-0469(1996)053<3313:TCMAEI>2.0.CO;2)
1803 [TCMAEI>2.0.CO;2](http://journals.ametsoc.org/doi/abs/10.1175/1520-0469(1996)053%3C3313%3ATCMAEI%3E2.0.CO%3B2), URL [http://journals.ametsoc.org/doi/abs/10.1175/1520-0469\(1996\)053%](http://journals.ametsoc.org/doi/abs/10.1175/1520-0469(1996)053%3C3313%3ATCMAEI%3E2.0.CO%3B2)
1804 [3C3313%3ATCMAEI%3E2.0.CO%3B2](http://journals.ametsoc.org/doi/abs/10.1175/1520-0469(1996)053%3C3313%3ATCMAEI%3E2.0.CO%3B2).
- 1805 Wang, Y., Y. Rao, Z.-M. Tan, and D. Schönemann, 2015: A Statistical Analysis of the Effects
1806 of Vertical Wind Shear on Tropical Cyclone Intensity Change over the Western North Pacific.
1807 *Mon. Wea. Rev.*, **143** (9), 3434–3453, <https://doi.org/10.1175/MWR-D-15-0049.1>, URL [http://](http://journals.ametsoc.org/doi/abs/10.1175/MWR-D-15-0049.1)
1808 journals.ametsoc.org/doi/abs/10.1175/MWR-D-15-0049.1.
- 1809 Wang, Y., and C.-C. Wu, 2004: Current understanding of tropical cyclone structure and in-
1810 tensity changes —A review. *Meteor. Atmos. Phys.*, **87** (4), 257–278, [https://doi.org/10.1007/](https://doi.org/10.1007/s00703-003-0055-6)
1811 [s00703-003-0055-6](https://doi.org/10.1007/s00703-003-0055-6), URL <https://doi.org/10.1007/s00703-003-0055-6>.

- 1812 Wang, Y.-F., and Z.-M. Tan, 2022: Essential dynamics of the vertical wind shear affecting the sec-
1813 ondary eyewall formation in tropical cyclones. *J. Atmos. Sci.*, **79** (11), 2909–2929, [https://doi.org/](https://doi.org/10.1175/JAS-D-21-0340.1)
1814 [10.1175/JAS-D-21-0340.1](https://doi.org/10.1175/JAS-D-21-0340.1).
- 1815 Wei, N., X. Zhang, L. Chen, and H. Hu, 2018: Comparison of the effect of easterly and westerly
1816 vertical wind shear on tropical cyclone intensity change over the western North Pacific. *Env.*
1817 *Res. Lett.*, **13**, 034 020, <https://doi.org/10.1088/1748-9326/aaa496>.
- 1818 Weightman, R. H., 1919: The West India hurricane of September, 1919, in the light of sounding ob-
1819 servations. *Mon. Wea. Rev.*, **47** (10), 717–721, [https://doi.org/10.1175/1520-0493\(1919\)47<717:](https://doi.org/10.1175/1520-0493(1919)47<717:TWIHOS>2.0.CO;2)
1820 [TWIHOS>2.0.CO;2](https://doi.org/10.1175/1520-0493(1919)47%3C717%3ATWIHOS%3E2.0.CO%3B2), URL [http://journals.ametsoc.org/doi/abs/10.1175/1520-0493\(1919\)47%](http://journals.ametsoc.org/doi/abs/10.1175/1520-0493(1919)47%3C717%3ATWIHOS%3E2.0.CO%3B2)
1821 [3C717%3ATWIHOS%3E2.0.CO%3B2](http://journals.ametsoc.org/doi/abs/10.1175/1520-0493(1919)47%3C717%3ATWIHOS%3E2.0.CO%3B2).
- 1822 Willoughby, H. E., F. D. Marks, and R. J. Feinberg, 1984: Stationary and moving convective bands
1823 in hurricanes. *J. Atmos. Sci.*, **41** (22), 3189–3211, [https://doi.org/10.1175/1520-0469\(1984\)](https://doi.org/10.1175/1520-0469(1984)041<3189:samcbi>2.0.co;2)
1824 [041<3189:samcbi>2.0.co;2](https://doi.org/10.1175/1520-0469(1984)041<3189:samcbi>2.0.co;2), URL [https://doi.org/10.1175/1520-0469\(1984\)041<3189:samcbi>](https://doi.org/10.1175/1520-0469(1984)041<3189:samcbi>2.0.co;2)
1825 [2.0.co;2](https://doi.org/10.1175/1520-0469(1984)041<3189:samcbi>2.0.co;2).
- 1826 Wingo, M. T., and D. J. Cecil, 2010: Effects of Vertical Wind Shear on Tropical Cyclone Pre-
1827 cipitation. *Mon. Wea. Rev.*, **138** (3), 645–662, <https://doi.org/10.1175/2009MWR2921.1>, URL
1828 <http://journals.ametsoc.org/doi/abs/10.1175/2009MWR2921.1>.
- 1829 Wong, M. L. M., and J. C. L. Chan, 2004: Tropical Cyclone Intensity in Vertical Wind
1830 Shear. *J. Atmos. Sci.*, **61** (15), 1859–1876, [https://doi.org/10.1175/1520-0469\(2004\)061<1859:](https://doi.org/10.1175/1520-0469(2004)061<1859:TCHVW>2.0.CO;2)
1831 [TCHVW>2.0.CO;2](https://doi.org/10.1175/1520-0469(2004)061<1859:TCHVW>2.0.CO;2), URL [http://journals.ametsoc.org/doi/abs/10.1175/1520-0469%282004%](http://journals.ametsoc.org/doi/abs/10.1175/1520-0469%282004%29061%3C1859%3ATCHVW%3E2.0.CO%3B2)
1832 [29061%3C1859%3ATCHVW%3E2.0.CO%3B2](http://journals.ametsoc.org/doi/abs/10.1175/1520-0469%282004%29061%3C1859%3ATCHVW%3E2.0.CO%3B2).
- 1833 Xu, Y., and Y. Wang, 2013: On the initial development of asymmetric vertical motion and
1834 horizontal relative flow in a mature tropical cyclone embedded in environmental vertical shear.
1835 *J. Atmos. Sci.*, **70** (11), 3471–3491, <https://doi.org/10.1175/jas-d-12-0335.1>, URL [https://doi.](https://doi.org/10.1175/jas-d-12-0335.1)
1836 [org/10.1175/jas-d-12-0335.1](https://doi.org/10.1175/jas-d-12-0335.1).
- 1837 Yu, C.-L., B. Tang, and R. G. Fovell, 2023: Tropical cyclone tilt and precession in moderate shear:
1838 Precession hiatus in a critical shear regime. *J. Atmos. Sci.*, **80** (3), 909 – 932, [https://doi.org/](https://doi.org/https://doi.org/10.1175/JAS-D-22-0200.1)
1839 <https://doi.org/10.1175/JAS-D-22-0200.1>.

- 1840 Zagrodnik, J. P., and H. Jiang, 2014: Rainfall, Convection, and Latent Heating Distributions
1841 in Rapidly Intensifying Tropical Cyclones. *J. Atmos. Sci.*, **71** (8), 2789–2809, [https://doi.org/](https://doi.org/10.1175/JAS-D-13-0314.1)
1842 10.1175/JAS-D-13-0314.1.
- 1843 Zawislak, J., H. Jiang, G. R. Alvey, E. J. Zipser, R. F. Rogers, J. A. Zhang, and S. N. Stevenson,
1844 2016: Observations of the Structure and Evolution of Hurricane Edouard (2014) during Intensity
1845 Change. Part I: Relationship between the Thermodynamic Structure and Precipitation. *Mon. Wea.*
1846 *Rev.*, **144** (9), 3333–3354, <https://doi.org/10.1175/MWR-D-16-0018.1>, URL [http://journals.](http://journals.ametsoc.org/doi/10.1175/MWR-D-16-0018.1)
1847 [ametsoc.org/doi/10.1175/MWR-D-16-0018.1](http://journals.ametsoc.org/doi/10.1175/MWR-D-16-0018.1).
- 1848 Zawislak, J., and E. J. Zipser, 2014: Analysis of the thermodynamic properties of developing and
1849 nondeveloping tropical disturbances using a comprehensive dropsonde dataset. *Mon. Wea. Rev.*,
1850 **142**, 1250–1264, <https://doi.org/10.1175/mwr-d-13-00253.1>.
- 1851 Zeng, Z., Y. Wang, and L. Chen, 2010: A Statistical Analysis of Vertical Shear Effect
1852 on Tropical Cyclone Intensity Change in the North Atlantic. *Geophys. Res. Lett.*, **37** (2),
1853 L02 802, <https://doi.org/10.1029/2009GL041788>, URL [http://onlinelibrary.wiley.com/doi/10.](http://onlinelibrary.wiley.com/doi/10.1029/2009GL041788/abstract)
1854 [1029/2009GL041788/abstract](http://onlinelibrary.wiley.com/doi/10.1029/2009GL041788/abstract).
- 1855 Zhang, F., and D. Tao, 2013: Effects of Vertical Wind Shear on the Predictability of Tropical
1856 Cyclones. *J. Atmos. Sci.*, **70** (3), 975–983, <https://doi.org/10.1175/JAS-D-12-0133.1>.
- 1857 Zhang, F., D. Tao, Y. Q. Sun, and J. D. Kepert, 2017: Dynamics and predictability of secondary
1858 eyewall formation in sheared tropical cyclones. *J. Adv. Mod. Earth Systems*, **9** (1), 89–112,
1859 <https://doi.org/10.1002/2016MS000729>.
- 1860 Zhang, J. A., and R. F. Rogers, 2019: Effects of parameterized boundary layer structure on
1861 hurricane rapid intensification in shear. *Mon. Wea. Rev.*, **147** (3), 853–871, [https://doi.org/](https://doi.org/10.1175/mwr-d-18-0010.1)
1862 [10.1175/mwr-d-18-0010.1](https://doi.org/10.1175/mwr-d-18-0010.1), URL <https://doi.org/10.1175/mwr-d-18-0010.1>.
- 1863 Zhang, J. A., R. F. Rogers, P. D. Reasor, and J. Gamache, 2023: The mean kinematic structure
1864 of the tropical cyclone boundary layer and its relationship to intensity change. *Mon. Wea.*
1865 *Rev.*, **151** (1), 63–84, <https://doi.org/10.1175/mwr-d-21-0335.1>, URL [https://doi.org/10.1175/](https://doi.org/10.1175/mwr-d-21-0335.1)
1866 [mwr-d-21-0335.1](https://doi.org/10.1175/mwr-d-21-0335.1).

1867 Zhang, J. A., R. F. Rogers, P. D. Reasor, E. W. Uhlhorn, and F. D. Marks, 2013: Asym-
1868 metric hurricane boundary layer structure from dropsonde composites in relation to the
1869 environmental vertical wind shear. *Mon. Wea. Rev.*, **141** (11), 3968–3984, [https://doi.org/](https://doi.org/10.1175/mwr-d-12-00335.1)
1870 [10.1175/mwr-d-12-00335.1](https://doi.org/10.1175/mwr-d-12-00335.1), URL <https://doi.org/10.1175/mwr-d-12-00335.1>.